CHARACTERIZATION OF FLAVONOID REACTIVITIES AND DEGRADATION PRODUCTS USING ONLINE CONTINUOUS FLOW KINETIC MEASUREMENTS AND HIGHER ORDER MASS SPECTROMETRY

by

JEREMY S. BARNES

Presented to the Faculty of the Graduate School of

The University of Texas at Arlington in Partial Fulfillment

of the Requirements

for the Degree of

DOCTOR OF PHILOSOPHY

THE UNIVERSITY OF TEXAS AT ARLINGTON

DECEMBER 2013

Acknowledgements

I must acknowledge my research mentor, Dr. Kevin Schug, who I have had the honor to work with so many years. I've thoroughly enjoyed the journey, thank you for the opportunities. Also, to the professors who serve on my committee, Dr. Frank Foss and Dr. Purnendu Dasgupta, I would like to thank them for the time and effort they have given me.

I cannot express thanks enough to my loving wife, who has carried me through the majority of my hardships. She inspires me to do my best at everything I do. And finally, to my father, thank you for making me so strong, and to my mother, my angel, who has always watched over me.

November 21, 2013

Abstract

CHARACTERIZATION OF FLAVONOID METABOLITE STRUCTURES AND REACTIVITIES USING ONLINE CONTINUOUS FLOW KINETIC MEASUREMENTS AND HIGHER ORDER MASS SPECTROMETRY

Jeremy S. Barnes, PhD

The University of Texas at Arlington, 2013

Supervising Professor: Kevin A. Schug

Epidemiological studies offer strong evidence that diets rich in fruits and vegetables provide a defense against cardiovascular disease, cancer and other physiological disorders. One theory suggests that these hazards are due in part to an imbalance of the body's oxidative load, caused by an increase in biologically-relevant free radicals, such as reactive oxygen species (ROS). Flavonoids, a family of plant metabolites, are associated with an antioxidant capacity which could reduce oxidative stress and aging. Quercetin, a flavonol with one of the highest rated antioxidant characteristic, was used as a model system to evaluate the reactivity of flavonoids in the presence of ROS under physiological conditions.

Degradation pathways induced by thermal degradation, reaction with hydrogen peroxide and reaction with azo-initiated free radicals were followed using continuous flow kinetics and mass spectrometry (MS). An in-house built online continuous flow device, constructed of concentric capillary tubes and modified to fit the inlet of a photodiode array (PDA) and MS detector, provided time-resolved measurements of degradation of quercetin and the ability to track formation of intermediate degradation products. Reactant concentrations and reaction time could be varied by adjustments to the flow speeds and to the volume of the reaction chamber. Identification and structural

elucidation of intermediates and degradation products were aided by high mass accuracy and the use of multi-dimensional tandem mass spectrometry(up to MS^3). Computational modeling was used to investigate the reactive sites of quercetin.

Based on the findings herein, a few conclusions regarding oxidative degradation of quercetin, which have been established in previous literature, were confirmed. First, it was concluded that regardless of the oxidant source, oxidative degradation of quercetin followed first order kinetics. Second, the oxidative pathway involved formation of *o*-quinones and semiquinones through electron transfer steps, followed by solvent adducts generated by nucleophilic attack. Lastly, the end products of oxidative degradation were smaller weight phenolic acids.

Adding to that, this work demonstrated that oxidative degradation of quercetin was quite complex and that numerous species (>20) were observed in aqueous solutions. Depending on the oxidant source, different solvent adducts were formed. These solvent adducts were intermediates which lead to different smaller weight phenolic acids. Under autoxidative conditions, a chalcantrione species was formed, which lead to 2,4,6-trihydroxymandelate and 2,4,6-trihydroxyglyoxylate, while, in the presence of hydrogen peroxide, a cyclic peroxidation adduct was formed, which lead to a depside intermediate followed by formation of 2,4,6-trihydroxybenzoate. Furthermore, in the presence of azo-initiated free radicals, a peroxyl adduct was observed, as well as phenolic acids that were common to autoxidation and hydrogen peroxide-induced oxidation. However, use of the azo-compounds also generated numerous unrelated side reactions.

Table of Contents

List of Illustrations

List of Tables

Chapter 1

Introduction

Antioxidant flavonoids protect biological cells from damage induced by reactive oxygen species (ROS), adding to the human body's antioxidant defense system, made up of other antioxidant plant compounds, enzymes and vitamins [1,2]. Reactive oxygen species, such as singlet oxygen, hydrogen peroxide, superoxide, hydroxyl radicals, peroxyl radicals, and peroxynitrile, are a product of numerous metabolic pathways and can be generated from environmental stress [3-5]. Considering the multitude of flavonoid species, their subtle differences and their interaction with the numerous types of ROS, there is still a large gap in the understanding of the fundamental mechanisms by which the equilibrium in biological redox states can be maintained [6].

A variety of test methods have been developed to determine the antioxidant capacity (AOC) of substances and natural products. Test methods use different radical sources and can represent various reaction mechanisms for neutralizing oxidants. For example, the oxygen radical absorbance method (ORAC) relies on an azo-initiator 2,2'-Azobis(2-amidinopropane) dihydrochloride (AAPH) to create peroxyl radicals, and involves a hydrogen atom transfer (HAT) mechanism, while diphenyl picyrlhydrazyl (DPPH) assay uses an organic nitrogen radical and a single electron transfer (SET) method [7]. In addition, the interaction of antioxidants with certain oxidants can occur by more than one mechanism and antioxidants may respond differently to different oxidant sources [8]. Complicating matters more, extracts of natural products and food sources often contain an assortment of different antioxidants that introduce a layer of synergistic complexities. For these reasons, no single assay can universally characterize the AOC of a substance.

Proper understanding of the results generated by AOC assays requires insight into the reactivity of the antioxidants being evaluated, which is often not the case. Targeted analysis of flavonoid antioxidants is hindered by the limited long-term stability, availability and related costs of high purity polyphenolic standards. Of the limited studies available, many only provide the degradative end products, and lack the crucial intermediate species needed to establish the degradation pathways, which help to justify the mechanisms by which antioxidants interact with reactive compounds. Further impeding academic advances is the fact that flavonoid species and their degradation products are composed of

only carbon, hydrogen and oxygen, sometimes differing by only one atom and many differing by only their related constitutional and stereochemical isomers, which makes definitive identification problematic [9].

To overcome these hurdles, a compilation of complementary techniques can be used. An online continuous flow method can provide a straightforward and effective means by which reaction kinetics can be monitored and formation of intermediates can be tracked [10]. First, mixing can initiate a chemical reaction and then would flow towards downstream detectors. Monitoring the degradation of the analyte can be achieved using inline non-destructive detectors, such as a photodiode array (PDA) and a fluorescence detector (FLD). The flow can then be diverted into the inlet of a mass spectrometer, where qualitative identification of degradation products can then be achieved using tools offered by technological advancements, such as the soft ionization ability of electrospray ionization (ESI), the selective fragmentation ability of an ion trap (IT), and the high resolution ability of time-of-flight (TOF) mass spectrometry detection [9]. Further, structural characterization of degradation products can be elucidated through higher order multi-dimensional fragmentation (MS^n). These empirical results can further be interpreted through the use of computational modeling.

The focus of this work was to advance the understanding of the reactive nature of flavonoids under physiological conditions, using quercetin as a model analyte. To achieve this, an in-house built online continuous flow device with adjustable reactor chamber volume was constructed of concentric capillary tubes and coupled to an inline PDA detector and a ESI-IT-TOF MS. Degradation pathways of quercetin were proposed based on the effects of pH, heat, and reaction with oxidants. Determination of the degradation products and intermediates was accomplished without the use of rare and expensive standards.

The degradation of quercetin in aqueous solution with dissolved oxygen was first established and evaluated in both acidic and physiological conditions, pH 5.9 and 7.4 [11]. Degradation was thermally accelerated by flowing quercetin solutions through the continuous flow device which was placed in a water bath, controlled between 65-85 °C. The heating time was adjusted from 2 to 21 minutes by varying the reaction chamber of the flow device. Time-resolved mass spectral measurements were collected in the negative mode, allowing for an evaluation of the degradation rates of the deprotonated quercetin ion, [Q-H]-, as well as determination of intermediate degradation products, aided by higher order

fragmentation (up to MS^3) and high mass accuracy. Based on time of appearance and signal intensity of ions, the preferred degradation pathways were proposed.

Next, the time-dependent hydrogen peroxide-induced oxidative degradation of aqueous quercetin at pH 7.4 was measured. Varying amounts of hydrogen peroxide [2-4 mM] were mixed with aqueous solutions of quercetin, and allowed to react at room temperature within the time range of 3 to 21 minutes using the continuous flow device. For comprehensive kinetic measurements, the flow was then directed into a photodiode array (PDA) detector and a ESI-IT-TOF-MS. As the reaction time or concentration of hydrogen peroxide was increased, the deprotonated quercetin ion signal, $[Q-H]^-$, decreased and formation of degradation product ions were observed. Structural elucidation of degradation product ions was proposed using higher order tandem mass spectrometry (up to MS^3) and high mass accuracy. A computational study using density functional theory (DFT) was performed to further deduce the reactive mechanisms and structures of intermediates.

Finally, the time-contingent interaction of quercetin with peroxyl radicals was evaluated. The peroxyl radicals were generated using the azo-initiator 2,2'-Azobis(2-amidinopropane) dihydrochloride, (AAPH), which is commonly used in the ORAC assay and other bulk antioxidant capacity measurements. In order to mimic typical reaction conditions used in the ORAC assay (and of physiological conditions) solutions were prepared in a pH 7.4 buffer solution and the continuous flow device was placed in a water bath controlled at 37°C. Time-resolved measurements were made within a range of 5 to 22 minutes by adjusting the reaction chamber volume and directing the eluent flow into a PDA and a ESI-IT-TOF-MS. In addition to evaluating the degradation products of quercetin, the degradation products of AAPH were also assessed.

There are many choices available for evaluating the antioxidant capacity of substances. Each of these methods vary greatly in terms of the needed resources, such as time, cost and instrumentation. It is not feasible to conduct multiple tests to cover all of the possible aspects of the antioxidant characteristics of natural product extracts. A better understanding of the antioxidants present and their reactivity with known oxidant sources will help guide which assay is most appropriate and will provide the most valid results for comparison to similar substances.

Chapter 2

General Background

2.1 Oxidative Stress and Reactive Oxygen Species

Some prominent theories suggest that many physiological disorders and the gradual decline in organ function from aging, are due to damage caused by reactive oxygen species (ROS) and free radicals [12]. Reactive oxygen species (ROS) include reactive molecules that contain oxygen. ROS not only include free-radicals, such as the hydroxyl ($^{\bullet}OH$), peroxyl ($^{\bullet}OOR$), superoxide ($^{\bullet}O_2^-$), and nitric oxide($^{\bullet}ON$) radicals, but they also include non-radical species, like singlet oxygen ($^1O_2$), hydrogen peroxide (H_2O_2), hypochlorite (HOCl), nitroxyl anion (NO^-) and the hydroxyl ion (^-OH).

As humans have evolved under an oxygen-rich environment, an elaborate defense network of enzymatic and non-enzymatic antioxidants has been developed to help protect the body from ROS. It should also be noted that ROS are needed for many cellular metabolic and signaling pathways and, thus, their production is required to maintain internal equilibrium. Overproduction of ROS and/or a lack of antioxidants lead to an imbalance which is defined as oxidative stress (Figure 2.1) [13].

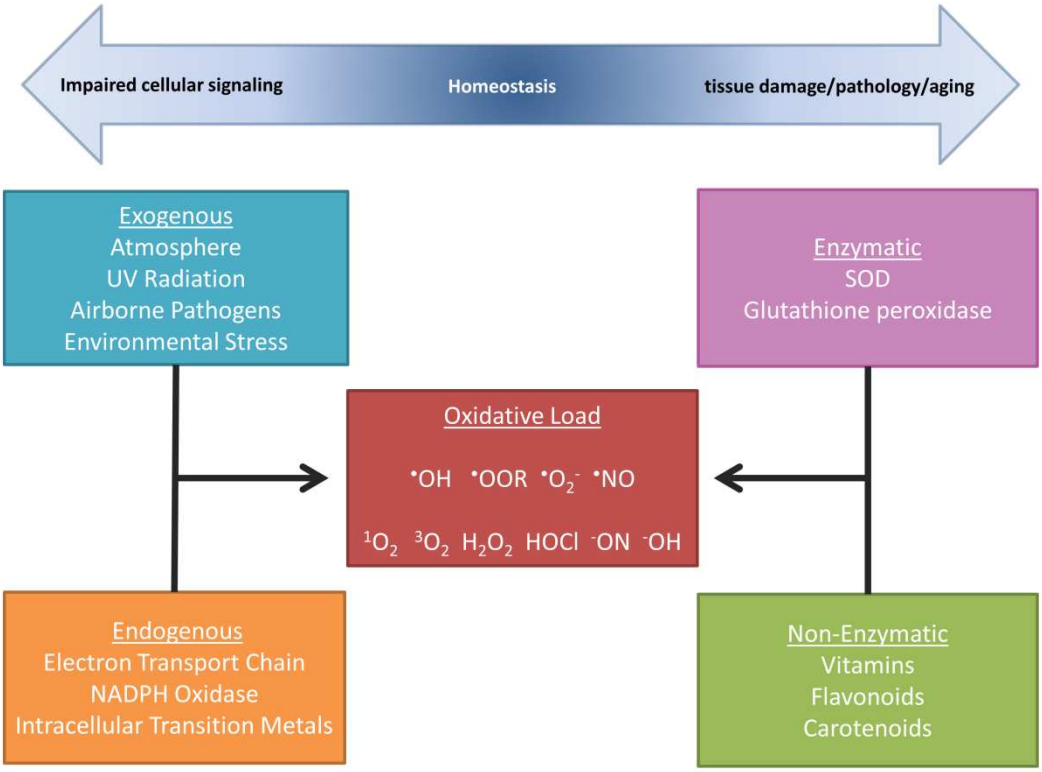

Figure 2.1: An antioxidant defense system is needed to maintain the oxidative load within the body.

2.1.1 Endogenous Sources of ROS

ROS are generated through a multitude of metabolic processes within the body. One estimate is that the body is exposed to 0.15 moles of endogenous ROS [14,15]. The majority of ROS are believed to be generated within the mitochondria, a metabolic powerhouse where consumed oxygen is reduced to H_2O through the electron transport chain [16]. During this reduction, up to 1-2% of electron leakage can occur, which leads to the formation of superoxide and hydroxyl radical from partial reduction of O_2 [17]. Superoxide can then be further dismutated into H_2O_2 via the enzyme superoxide dismutase. Endogenous ROS can also be produced through non-mitochondrial respiration, such as in phagocytic vacuoles where NADPH oxidases pull electrons across the wall of the phagocytic vacuole and form superoxide and hydrogen peroxide [18]. Some staggering estimates would result in concentration of about 0.5–2.0 M H_2O_2 within the vacuole [19,20]. In addition, low levels of ROS are produced by numerous enzymes through poorly coupled redox processes.

2.1.2 Exogenous Sources of ROS

Interactions with the environment also contribute to a steady supply of ROS. Along with constant inhalation of molecular oxygen, ROS can be introduced through the airways from inhalation of environmental pollutants, such as cigarette smoke and automobile exhaust. Particles, viruses and bacteria can also be inhaled, which further simulate phagocytic and inflammatory responses, leading to an increase in ROS as described above. In areas bathed in light, such as the skin and eyes, ground state triplet oxygen ($^3O_2$) can be converted into reactive singlet oxygen ($^1O_2$) by UV rays [21]. In plants, stresses from the environment such as reduction in oxygen levels and increase in heat can also lead to an increase in metabolic production of ROS [22].

2.1.3 ROS-related Physiology and Pathophysiology

Numerous studies have demonstrated that ROS are involved with cellular signaling. To maintain homeostasis, this “oxidative interface” is tightly regulated through redox mechanisms by proteins. As discussed above, under conditions of stress, cells may have evolved adaptive mechanisms through ROS signaling. Cytosolic ROS may be used to signal cells to undergo cellular proliferation and growth for survival, as well as signal apoptosis to help preserve energy and rid the host from damaged cells [23]. One study linked ROS signaling with mitochondrial glucose metabolism, providing a mechanism for

sensing glucose levels [24]. There is also some evidence that ROS may signal senescent pathways, which further support the correlation of oxidative stress and aging [25].

Biological macromolecules such as cell membranes, lipoproteins, proteins, and DNA can undergo damage from ROS. Lipid peroxidation occurs when a hydrogen atom ($H^{\bullet}$) is abstracted from an unsaturated fatty acid bond. This creates a free radical which reacts with O_2 forming a lipid peroxyl radical and a chain reaction that can continue forming many more lipid peroxyls [14]. Direct oxidation of amino-acid side chains and oxidative cleavage of proteins can create carbonylation of proteins. Some diseases associated with protein carbonylation include Alzheimer's disease, chronic lung disease, chronic renal failure, diabetes, and sepsis [26]. DNA is also damaged from interaction with ROS and one source estimates that DNA can undergo up to 1000 oxidative hits a day [13]. This damage leads directly to genetic mutations and pathogenesis, if unrepaired.

2.2 Flavonoids in Nature

Epidemiological studies link plant-rich diets to improved health conditions, such as decreased risk of cardiovascular disease [27]. Numerous *in vitro* experiments suggest that compounds from the flavonoid class, a class of phytochemicals found in plants, may be partly responsible for a number of physiological phenomena, such as cancer cell disruption, anti-inflammation, and diabetic cataract inhibition[28-30]. This may be due to their antioxidant ability to neutralize reactive oxygen species (ROS).

Flavonoids are one of the largest classes of polyphenolic plant metabolites, with currently over 10,000 reported species [31]. They are found in nearly every plant type and tissue type and are ingested in diets on a daily basis [32]. Their synthesis in plants typically begins through a series of condensation reactions between hydroxycinnamic acid and malonyl residues which generates a 15 carbon core that is common for all flavonoids [31]. This 15 carbon-core is made up of two phenyl rings, commonly labeled as the A-ring and B-ring, which are bridged by 3 carbons (Figure 2.2).

The flavonoid class can be further divided into 12 different subclasses which are classified by the degree of oxidation, conjugation or substitution of the inner bridging carbons and if the inner carbons have been cyclized into a pyran or furan ring (Figure 2.2) [33]. The inner heterocyclic ring is labeled as the C-ring. The uniqueness of individual species is further defined by variations in substituents, glycosylation and acylation.

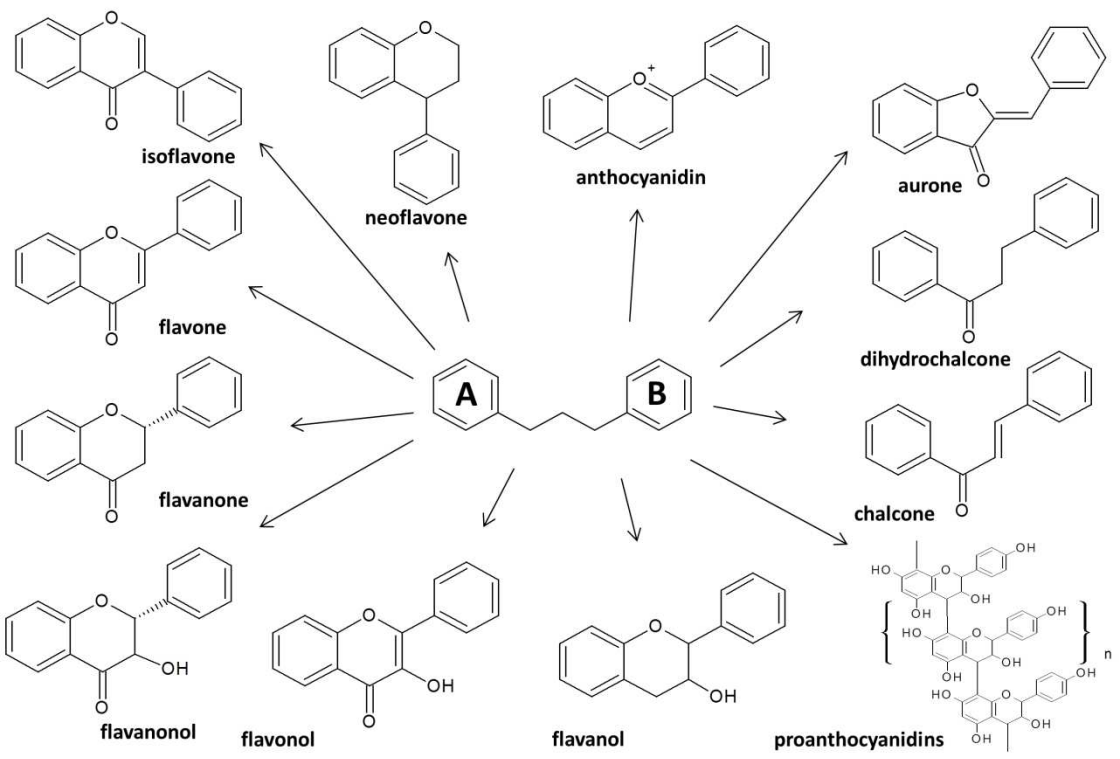

Figure 2.2: The different subclasses of flavonoids.

2.2.1 Quercetin Derivatives

One of the more widely distributed subclasses is the flavonol. Between the years 1986-2003, more than 410 new flavonol species were identified [34,35,37]. Quercetin is probably the most studied species of the flavonol subclass and its biochemical activity has been well documented. The name comes from *quercetum* meaning “oak forest”. As with all flavonol aglycones, quercetin has a hydroxyl group at the C3 position, a ketone group at the C4 position and a double bond between C2 and C3. Four other hydroxyl groups are located at C5, C7, C3’, and C4’ (Figure 2.3).

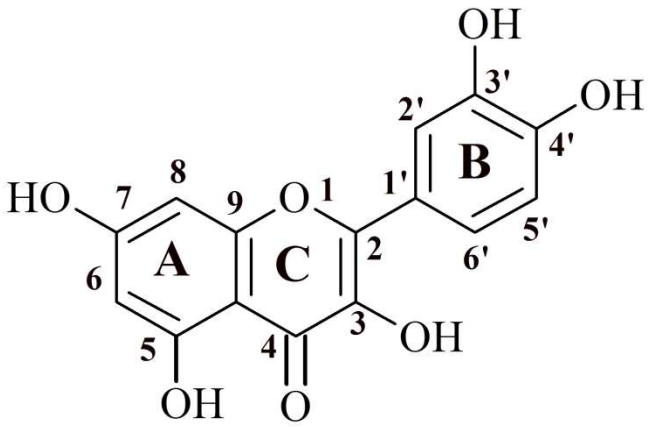

Figure 2.3: The chemical structure for quercetin, a member of the flavonol subclass.

In nature, quercetin is predominantly found glycosylated. Ether linkages can also be formed between the hydroxyl groups of quercetin and an alcohol, primarily methanol. The majority of quercetin derivatives exist as mono-glycosides, which are connected with a O-linkage at the C3 site. Other glycosylation sites include the 7 and 4' position. Commonly found sugars include glucose, rhamnose, galactose and xylose. Disaccharide linkages are also observed. Many other derivatives can be formed by acylation of the glycosides with groups such as aliphatic and aromatic acids [38]. There may be hundreds of quercetin derivatives in the plant kingdom. In one study of blueberries alone, fourteen different quercetin derivatives were identified [36].

Besides berries, major dietary sources of quercetin can be found in onions, apples, mangos, lettuce, beans, buckwheat, tea, and honey (Table 2.1) [37,38]. Quercetin derivatives are typically found accumulated in the outer areas of the plant that are closest to light, such as in the skin, leaves and bark. One notable exception is in onions, in which quercetin glucosides are the predominant flavonoid observed, yet the plant develops below the soil protected from light [39]. Other famed quercetin derivatives include rutin (quercetin-3-O-rutinoside), found in apples, and quercetrin (quercetin-3-O-rhamnose) found in berries [37,40].

Table 2.1: Various quercetin derivatives found in nature. Adapted from [38] and [39].

Quercetin Derivative Type	**Name**	**Food Source**
Monoglycoside	Quercetin-3-glucoside	Sage, Mango
	Quercetin-3-galactoside	Mango Plums, Berries
	Quercetin-3-xyloside	Mango
	Quercetin-3-rhamonside	Spinach
	Quercetin-3-glucuronide	St. John's Wort, Green beans, Lettuce
	Quercetin-7-glucoside	Beans
	Quercetin-4'-glucoside	Onions
Disaccharide	Quercetin-3-rutinoside	Blueberries, tea, buckwheat, apples
	Quercetin-3-diglucoside	Beans
Diglycoside	Quercetin-3,4'-diglucoside	Onions
	Quercetin-3-rhamnoside-7-glucoside	Peppers
Triglycoside	Quercetin 3,7,4'-triglucopyranoside	Onions
Acylated	Quercetin-3-6"-acetylglucoside	Beans
Ether	Quercetin-3-methyl ether	Honey
	Quercetin-3,3'-dimethyl ether	Honey

The substitution of the quercetin derivative affects the compound's hydrophilicity. Although quercetin has five hydroxyl groups, as an aglycone it is relatively lipophilic and has poor solubility in water. Addition of glycosides makes it become more hydrophilic. This chemical characteristic also affects how it is absorbed into the body. The aglycone's lipophilic nature allows for absorption in the stomach, however, glycosylated quercetin may not be hydrolyzed in the stomach due to the β-glycosidic linkage and will pass into the small intestines were it is deglycosyated and metabolized [41]. Within the

small intestine quercetin glucosides can be efficiently absorbed due to the hydrolyzing activity of cells in this area. Hydrolysis of the glucose accelerates absorption. This location has also been associated with metabolic conversion of flavonoids by glucuronidation and sulfation [42].

Many studies have shown that the quercetin aglycone is absorbed into the blood at a lower percentage than its glucosylated counterparts [43-45]. One study showed that quercetin metabolites in the plasma were made entirely of glucoronides and sulfoglucoronides of quercetin and 3'-O-methyl quercetin [46,47]. With continued eating, quercetin can build up in the blood stream due to a long half-life of elimination, estimated by one study at 28 hours based on consumption of onions [37]. Regardless of how it enters the body and is metabolized, an understanding of the chemistry of the quercetin nucleus for these derivatives is crucial in understanding how it may interact within food and at a cellular level.

2.3 Flavonoid Reactivity

2.3.1 Biological Antioxidants

There are many different biological antioxidants, including both enzymatic and non-enzymatic varieties. Some enzymatic antioxidants include superoxide dismutase, catalase, and the family of glutathione peroxidases. Examples of non-enzymatic antioxidants include vitamins (A, C and E), melatonin, carotenoids and low molecular weight polyphenolics such as flavonoids [48]. As there are many different sources of oxidants and antioxidants, all which have a wide array of interactions, a review of the antioxidant qualities of flavonoids is warranted as well as the mechanisms by which they inactivate oxidants, specifically quercetin, since it is regarded as one of the most effective flavonoid antioxidants.

An antioxidant is defined as a compound that delays or prevents oxidative damage to a target. Evaluation of the quality of an antioxidant should include the degree and rate of oxidant neutralization and the ability for the antioxidant to reach the location where oxidants are being generated. The potential for an antioxidant to generate secondary reactions should also be considered, since when an antioxidant neutralizes a free radical, it inherently becomes a free radical in the process, and depending on the newly formed reactivity could become a prooxidant and be as deleterious as the ROS which was neutralized.

2.3.2 Flavonoids as Antioxidants

First, it should be considered that flavonoids are effective at donating their phenolic hydrogens and reducing ROS. In a study by Javonivic *et al.*, researchers demonstrated that thermodynamically,

many flavonoids have the potential to reduce most ROS due to their low redox potentials [49-51]. For example, the calculated redox potential for catechin, quercetin, rutin and hesperidin were E_7 = 0.57, 0.6, 0.6 and 0.72V, respectively, compared to Trolox (6-hydroxy-2,5,7,8-tetramethylchroman-2-carboxylic acid; a vitamin E analog) at 0.48V. While the estimated redox potentials for alkylperoxyl and superoxide/hydroperoxyl radicals were E_7 = 1.05 and 0.94, respectively. Further evaluation of the changes in redox potential shows that these potentials are significantly affected by the electron donating properties of the B-ring substituents, as can be seen with the lower potential in quercetin due to its 3'-OH and 4'-OH groups compared to the higher potential of hesperidin, in which the 3'-OH group is replaced by a methoxy group.

Correlations can also be made between the antioxidant capacity and the number and position of hydroxyl groups on the B-ring. Comparison of kaempferol, a monohydroxy flavonol, and quercetin, a dihydroxy flavonol, reveals reduction potentials of 0.75V and 0.33V, respectively, and antioxidant capacities in Trolox Equivalents (TE) of 1.3 and 4.7, respectively, demonstrating a significant advantage for dihydroxy flavonols to inactivate ROS. Addition of a third hydroxyl substituent to the B-ring, as is the case in myricetin, showed no additional antioxidant benefit. Finally, when the position of the hydroxyl groups lead to increased resonance, an increase in antioxidant capacity was observed. This was the case when comparing quercetin, a 3',4'-dihdydroxy flavonol, with morin, a 2',4'-dihydroxy flavonol [51,52].

Two mechanisms identified by which flavonoids neutralize ROS include hydrogen atom transfer (HAT) and single electron transfer (SET) (Figure 2.4). The HAT mechanism involves a one-step transfer of both a proton and an electron, while the SET mechanism involves a two-step process in which an electron is transferred first, followed by proton transfer. It is generally considered that most flavonoid systems are involved with both these mechanisms and they occur in parallel in solution; however, the contribution of one may be greater than the other depending on the pH of the solution and the properties of the antioxidant, and influences from the system. Both mechanisms end with the same result though, transfer of a hydrogen atom, but they can differ based on kinetics and secondary reactions.

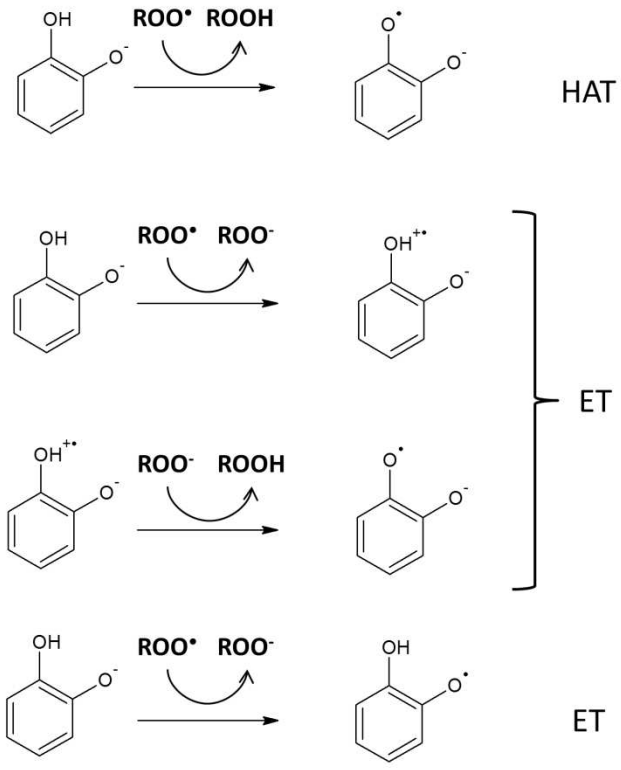

Figure 2.4: Flavonoid can neutralize free radicals by a one-step hydrogen atom transfer (HAT) or by a two-step process in which an electron is transferred first, followed by a proton transfer.

Compounds with low bond dissociation energy (BDE) of the group providing the hydrogen atom typically follow the HAT mechanism. This mechanism is described as occurring rapidly (complete in seconds or minutes) and as being pH and solvent independent [7]. Due to the two-step process, flavonoid interactions that involve the SET mechanism require longer reaction times, which contribute to generation of secondary reactions. The mechanism is pH dependent, therefore, the charge of the flavonoid species must be considered.

At high pH, flavonoids are deprotonated and only the electron transfer mechanism is possible [49]. It is interesting to note that the deprotonated ion would theoretically have a lower redox potential and therefore make it a more optimum free radical scavenger. However, as noted by Javonovic *et al.*, due to electrostatic repulsion, increased charge states reduced the ability of some flavonoids to inactivate

the superoxide radical [50]. For quercetin at physiological pH (7.4), most species are deprotonated, with a small fraction being doubly-deprotonated [53].

Transfer of a hydrogen atom from the flavonoid propagates the formation of an aroxyl radical. As noted, the ability of an antioxidant to stabilize the unpaired electron is essential to reduce the reactivity of the free radical and reducing further damaging prooxidant activity. The polyphenolic flavonoid can delocalize the orphaned electron as described by π-resonance stabilization. For flavonols and other flavonoids with desaturation in the C-ring, this delocalization can be extended across all three rings, maximizing resonance energy from multiple mesomeric structures [54]. In some cases the aroxyl radicals can react again with another ROS, thus terminating the radical chain reaction.

Transient spectra collected through use of pulsed radiolysis showed formation of B-ring semiquinone radicals in flavonoids with saturated C-rings. For flavonols, with desaturated C-rings, the radicals were unstable and delocalized over the entire ring system [55,56]. Quercetin aroxyl radicals can undergo a second electron transfer to form a quinone, potentially creating prooxidant superoxide radicals from molecular oxygen through a redox reaction [57]. Quercetin flavonoid quinones can lead to quinone methides which are prone to nucleophilic attack [58].

Considering the discussed structure-activity relationships and through observation of empirical data, researchers have determined that there are three essential criteria for effective flavonoid free radical scavenging: 1.) *o*-dihydroxy group in the B-ring, 2.) a double bond at the 2-3 position, and 3.) 3-OH and 5-OH groups in order to form quinonic structures upon oxidation. Bearing in mind that the structure of quercetin has all of these noted criteria, it is no surprise that it is one of the most effective flavonoid antioxidants [49].

2.4 Methods of Flavonoid Analysis

2.4.1 UV/Vis Absorptivity and Flavonoid Content

Many methods can be employed to characterize the content of flavonoids in plants and food. Due to their polyphenolic structure, flavonoid can be easily detected spectrophotometrically, with intense absorptions in the UV spectra. In this region, flavonoids have two distinguishable maxima. The band with a longer wavelength is commonly attributed to the B-ring and the shorter wavelength to the A-ring. This is easy to imagine by considering flavones and flavonols as an example. The B-ring, with extended

conjugations through the C-ring and 4-oxo group, establishes a cinnamoyl function which can be correlated to the lower energy band. The A-ring and the 4-oxo group in the C-ring form a benzoyl function, which represents a system with less delocalization and thus a higher energy absorption band [59].

Within the food and wine industry, as well as in biological testing, one common method used to evaluate the total phenolic content of substances is the Folin-Ciocalteu (F-C) method [60]. In this method, total phenolic content is quantified based on the total reducing capacity of a solution. The reaction proceeds in an alkali solution where the phenolics are ionized. The resulting phenolates donate an electron to a polymeric complex of phosphomolybdic and phosphotungstate compounds (F-C Reagent). This SET reaction causes a reduction of the valence of the complex from +6 to +5, resulting in a blue color which can be measured spectrophotometrically. Gallic acid or Trolox (a water soluble vitamin E derivative), is used as a reference standard. One drawback of this method for testing natural product extracts is interference from other potentially present reducing agents, such as metals and enzymes.

2.4.2 Antioxidant Capacity

There has also been extensive development of methods to evaluate the reactivity and antioxidant capacity of flavonoids. These methods feature many different sources, types of radicals, and reducing agents that interact with the antioxidant sample. The antioxidant sample, in turn, protects a sensitive marker, such as fluorescein. Depending on the combination of free radical/reducing agent, antioxidant sample and marker, the reaction mechanism is either HAT, SET, or a combination [7].

There are a couple of ways to generate free radicals. They can be created enzymatically or with biological components, with transition metals, such as Fe and Cu in the presence of reducing agents (H_2O_2), with stable free radical small molecules or thermally labile azo-initiators. Azo-initiators are used in many common methods such as oxygen radical absorbance capacity (ORAC) and trolox equivalence absorbance capacity (TEAC), which uses 2,2'-azobis(2-amidino-propane) dihydrochloride (AAPH also known as ABAP) and 2,2'-azinobis(3-ethylbenzothiazoline-6-sulfonic acid) also known as $ABTS^{\bullet+}$. AAPH is often used to estimate how flavonoid antioxidants protect against lipid peroxidation. With little kinetic energy N_2 is freed from the center of the azo initiator compound, creating two methyl radicals. These undergo a quick reaction with molecular oxygen to create a peroxyl radical [61]. Azo-initiators are well

suited for antioxidant assays since they are water soluble, create biologically relevant peroxyl radicals and radical generation can be predictably quantitated. However, some groups have shown that carbon radicals could also be formed due to β-cission, and they could compete with the peroxyl radicals as hydrogen atom acceptors [62].

Another advantage of the ORAC method is that the reaction goes to completion allowing for a more complete kinetic observation, including secondary reactions. At the beginning of the interaction of free radicals with a substrate, the state can be described as being in a lag phase in which little oxidation occurs. This phase is followed by a rapid increase in radicals through chain-propagating intermediates. Then, at some point the rate of oxidation declines. Addition of an antioxidant can extend the lag phase by neutralizing free radicals and protecting the substrate. Quantification of AOC by determining the area under the decay curve (AUC) for the sample *vs* a blank provides a measurement in which both the time and degree of free radical inhibition can be assessed [63,64].

Due to frequent misuse of ORAC values in advertisements by the food and dietary supplement industry, as well as a growing consumer belief, the USDA's Nutrient Data Laboratory removed the USDA ORAC Database for Selected Foods from their website in 2010. The USDA stated there was "no evidence that the beneficial effects of polyphenol-rich foods can be attributed to the antioxidant properties of these foods" [65]. Additionally, these methods characterize the bulk antioxidant capacity or the degradation rate of substances, but do not offer insight into the degradative mechanism or the production of associated reaction products.

2.4.3 Flavonoid Analysis Using Mass Spectrometry

One major problem associated with natural product research is the high costs and limited availability of flavonoid standards, which when available typically do not have long-term stability. Many standards for degradant and metabolite compounds are simply not available. In terms of identifying unknowns, MS is a powerful tool and is much more sensitive than nuclear magnetic resonance (NMR). In addition to sensitivity, it provides elemental formula and structural determination and is easily hyphenated with non-destructive techniques such as UV/Vis, allowing for identification of trace degradants and metabolites, which makes it well suited for flavonoid analysis. Adding to this, MS is becoming increasingly more affordable and available in academic and industrial settings.

2.4.3.1 Ionization

Many types of ionization have been used for the analysis of flavonoids. Electron impact (EI) and fast atom bombardment (FAB) have been used previously to differentiate between structurally similar and isomeric flavonoid aglycones [66,67]. Flavonoids can also be detected by chemical ionization (CI) as well, but due to their nonvolatile nature first requires derivitization by methylation or trimethylsilylation. With development of atmospheric chemical ionization (APCI) and ESI, flavonoid analysis has become increasingly easier and as a result, they are currently the most commonly used ionization techniques. The advantage of ESI is that it is soft enough to avoid fragmentation of the molecular ion, providing the molecular mass of the analyte without destroying the thermally labile glycosides, unlike in EI or FAB. ESI analysis also allows for analysis of samples in liquid solutions compared to EI or FAB which requires compounds to be volatile. This allows for a more relevant observation of flavonoids under physiological conditions.

During ESI, a solution is directed into a capillary upon which a charge is applied. The charged liquid leaves the capillary at a tip, which nebulizes the liquid and disperses it into a fine aerosol. The solvent evaporates from the charged droplets, making them smaller and smaller, eventually delivering the charged analyte to the gas phase. At this point the ion can enter the mass spectrometer. Electrospray uses high voltages and the source is operated at atmospheric pressure. ESI analysis of flavonoids can be conducted in both positive and negative mode. Most flavonoids are acidic, which causes them to have low ionization efficiencies as protonated species, $[M+H]^+$. Flavonols, such as quercetin, are easily deprotonated allowing for facile ionization and strong signals at trace amounts in the negative mode [68].

2.4.3.2 Collision Induced Dissociation

Isomeric and structurally similar compounds can be differentiated by fragmentation using multistage tandem mass spectrometry, which provides the capability of producing unique fragment substructures. Precursor compounds can be isolated by their mass/charge (m/z) ratio and be further fragmented by way of collisionally-induced dissociation (CID). This can be achieved through the use of ion-trap (IT) and triple quadrupole (QqQ) instruments. Within the ion trap, analyte ions are repeatedly collided by the He bath gas until they reach a high enough internal energy to dissociate into fragments [69,70].

Fragmentation mass spectrometry allows for the definitive identification of ions as well as unknown ions. Identification can be accomplished by matching product ion spectra to other spectra previously collected within a spectral library. The structures of ion species without previously recorded library spectra can be deduced and mapped out, such as in the use of fragmentation trees, in which structural similar precursor ions with similar fragmentation patterns can be clustered with other ions with similar fragmentation patterns aided by computationally-derived algorithms [71,72].

Controlled fragmentation of flavonoids adds an extra degree of species confirmation allowing for identification of the nature, number and order of attached sugars, and acyl groups [73,74]. Flavonoid O-glycosides are easily fragmented due to the fairly weak O-glycosidic bond which is easily cleaved by low energy CID, with neutral loss of the sugar. The nature of the glycoside can be determined by monitoring the mass of the neutral loss, although differentiation of diasteroisomeric sugars is a known problem [75].

Tandem MS has been used extensively for identification of flavonoid aglycones [67]. Due to differences in the substituents of the B-ring, fragmentation of flavonoid aglycones can result in diagnostic product ions, by which species can be identified. Further, flavonoid subclasses can be differentiated based on the fragmentation pathways observed in cross-ring cleavage of the C-ring. For instance, cross-ring cleavage of flavones, flavonols, and flavanones occur between the following C-ring bonds: (0,4), (1,2), (1,3), and (1,4), while anthocyanidins were observed to fragment at (0,2) and (0,3) bonds (Figure 2.5) [66,76,77].

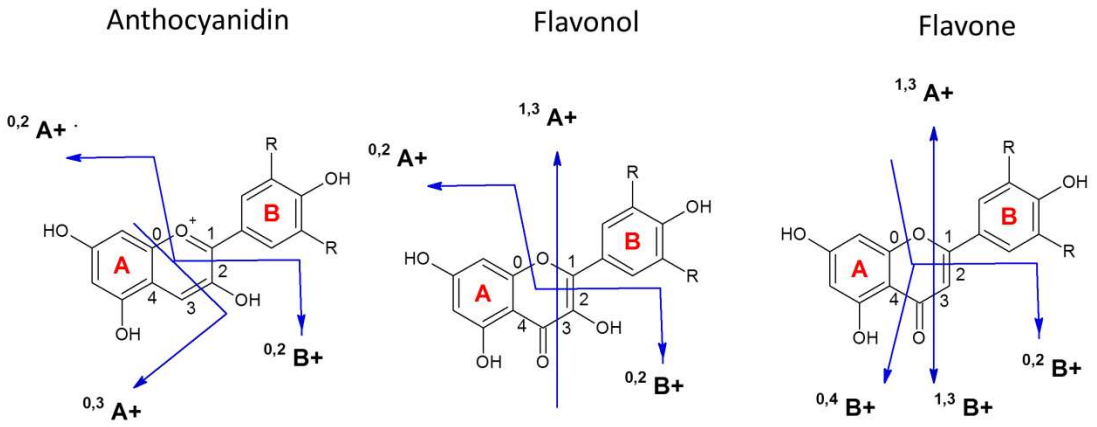

Figure 2.5: Diagnostic signals produced by low energy CID of different flavonoid classes. Adapted from [66].

2.4.3.3 Higher Order Tandem Mass Spectrometry (MS^n (n≥3)) and High Mass Resolution

In many instances, with low resolution tandem MS, identification of unknown signals is inconclusive due to limited fragmentation information and the possibility of multiple formulaic possibilities. With nominal masses, an observed ion may be fit to multiple elemental formula possibilities, particularly with organic compounds, which only contain carbon, hydrogen, and oxygen, as in the case of flavonoids. Advances in hyphenated mass detectors, such as ion trap-time of flight (IT-TOF), provide a means to overcome these setbacks.

Within the IT-TOF, trapped and fragmented ions are ejected from the ion trap and accelerated by an electric field towards a detector at the end of a flight tube. Due to differences in the mass and charge of the ions, they will travel at different speeds down the flight tube, considering they all were accelerated with the same kinetic energy. Therefore, based on their flight time, their mass-to-charge ratio (m/z) can be determined with great accuracy (<5 ppm). By increasing the resolution with higher mass accuracy, erroneous elemental formulaic choices can be discarded, providing a higher degree of confidence for assigning exact elemental formulas. By applying some heuristic rules, setting the element choices to C, H and O and limiting the mass accuracy to <5 ppm, the number of possible elemental formulae for compounds with masses from 100 to 600 Da, can be narrowed to one [78].

Since definitive elemental formulas and structural characterization can be obtained, these powerful instruments are well suited for flavonoid and flavonoid metabolite analysis. Multiple studies have been previously conducted on anthocyanins, isoflavones, kaempferol, mixtures of flavonoids from natural product extracts and many other polyphenolics [77,79-86].

2.4.3.4 Online continuous flow kinetic MS

In order to more fully evaluate the kinetic aspects of flavonoid degradation, it may be beneficial to conduct continuous-flow online kinetic ESI-MS studies. The inlet of an ESI allows for direct injection, therefore, solutions can be mixed or reacted and directly flown into the inlet with minimal dwell time. This combined technique allows the user to monitor the relative concentration of multiple ionizable species as a function of time, and can be done so with significant selectivity and high sensitivity. In addition no quenching additives are needed to control the reaction times.

Konermann *et al*. have demonstrated numerous continuous-flow time resolved ESI-MS studies from which they developed a capillary mixer with an adjustable reaction chamber volume for rapid time-resolved studies, which could be fitted to the inlet of an ESI-MS. The device was used in a variety of demonstration, in which millisecond time-resolved kinetic measurements were made, like demetalation of chlorophyll, refolding of ubiquitin, and the enzymatic hydrolysis of p-nitrophenyl acetate[87-91]. A noteworthy advantage of this apparatus is the ability to operate in two modes. In the "kinetic mode", specific ion abundances can be monitored while continuously increasing the distance between the mixer and the ion source. Transient intermediates can be monitored in a "spectral mode" by scanning the entire spectra at designated time points by selecting a fixed reaction volume. An apparatus such as this has not been previously applied to studies focused on assessing antioxidant capacity.

2.4.4 Computational Analysis

Ab initio and semi-empirical computational studies of flavonoids can provide insight into their reactivity with oxidants. Through computational evaluation of ionization potentials (IP), bond dissociation energies (BDE), and reaction energies, many have proposed that flavonoids reacts with free radical ROS through hydrogen atom transfer (HAT) and that the activity is focused in the B and C-ring [92-96]. Computations of spin densities, charge distributions, and HOMO/LUMO states have consistently shown that the favored site for nucleophilic attack by nucleophilic species are carbons in the C-ring [92,96,97,98].

Computational studies have also supported the elucidation of fragmentation pathways for polyphenolic natural products ions and prediction of structures of gas phase fragment ions, which otherwise are difficult to structurally characterize. March *et al*. used density functional theory (DFT) to evaluate bond energies and fragmentation events of flavones based on the energy states of computed product ions [99], while Barnes and Schug used DFT calculations to propose which cross-ring cleavage pathway was favored for anthocyanidins using estimations of the lowest energy configurations of product ions [100]. Tedmon *et al*. also used DFT calculations to explore differences in the fragmentation pathways of isobaric polyphenolic estrogen compounds [83]. Similar studies could be used to evaluate degradation pathways and structures of flavonoid degradants.

2.5 Flavonol Degradation

In general, through empirical observations, a few trends for flavonol stability have been established. First, as the number of hydroxylation sites in the B-ring increases, the stability of the flavonol decreases [101]. Second increased methylation and increased glycosylation also increases stability [102]. In addition, to the commonly accepted redox reactions of flavonols which involve hydrogen atom transfer, degradation of flavonoids also involves C-ring opening and cross-ring cleavage, which leads to formation of lower molecular weight phenolic carboxylic acids. Studies of some common degradation pathways for quercetin, including thermal, ROS, and free radical-induced degradation are expanded below.

2.5.1 Thermal Processing

Thermal processing of foods has been shown to have a direct effect on the flavonoid content in foods. Depending on the type of processing, such as microwaving, roasting, blanching or other, flavonoid content can be increased due to improved extraction or degraded, such as in deglycosylation [103]. The effects of heat drying on fruit was demonstrated by evaluating the total anthocyanin content of treated and untreated blueberries. A significant decrease in total anthocyanin response between the pre- and post-processed samples was observed [79]. In a study on rose extracts using UV/Vis spectroscopy, thermal degradation was observed to follow first order kinetics (Figure 2.6, J. S. Barnes, 2011, work not published). Understanding the effects of thermal processing on food may not be easily understood considering the complexities and interactions that could be created by the numerous chemical constituents within food matrices.

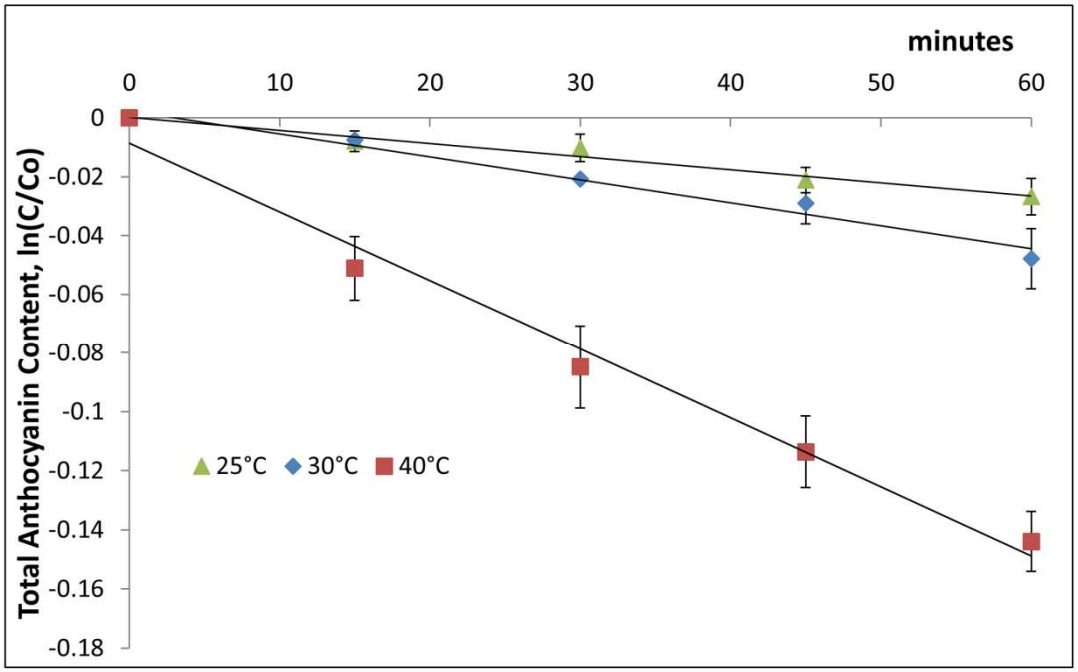

Figure 2.6:The thermal degradation of rose petal extracts under varying temperatures.

A few other groups have demonstrated that in the presence of oxygen, thermal degradation of aqueous solutions of quercetin and rutin followed first order degradation [104-106]. Rutin was demonstrated to be significantly more thermally stable, presumably due to the C3 group being blocked by a rutinoside, which suggests this site may be involved in degradation. These studies also demonstrated that thermal degradation was also significantly reduced when oxygen was removed from solution by sparging with nitrogen, suggesting that ROS species may be involved with degradation.

Buchner *et al*. showed that changes in pH affect the thermal degradation rates. In their study, weakly acidic solutions (pH 5) increased thermal stability [106]. They also used LC-ESI-MS^n to show that the major thermal degradation product of quercetin was protocatechuic acid. Other smaller degradation products were also noted and which they believed had a greater polar character than quercetin based on chromatographic elution order. They proposed that some of these degradation products were formed from solvent adducts, including a hydroxylated quercetin structure, and that these adducts formed after quercetin was oxidized by ROS into a quercetin quinone.

2.5.2 Oxidative Degradation

Oxidation of flavonols, specifically species with a 3-hydroxyl group such as quercetin, have been studied using a host of complementary techniques, including separation with liquid and gas chromatography (LC and GC) and detection with UV-vis spectroscopy, electrochemical, NMR and MS. A variety of oxidizing sources have been used. These include aerobic autoxidation [107,108], electrochemical [109,110], free radical oxidation [108,111-113] and enzymatic degradation [108,114].

These studies also evaluated differences in solvent conditions. Researchers have demonstrated that differences in nucleophiles present in solvents can effect intermediate solvent adduct products. One group proposed that within a non-polar system the oxidation occurred through hydrogen atom donation while in aqueous systems, oxidation occurred through electron donation [115]. Regardless of the oxidation source or solvent, the end products of flavon-3-ol oxidation were smaller molecular weight phenolic acids, such as protocatechuic acid (PA) and phloroglucinol carboxylic acid (PCA) in quercetin degradation.

2.5.2.1 Autoxidation under Aerobic Conditions

A. Zhou *et al.* demonstrated that under room temperature in the presence of oxygen quercetin undergoes oxidation, and that degradation of quercetin follows first order kinetics. This indicated that the rate determining step is a one-electron oxidation of quercetin anions and formation of a semiquinone radical, which was then followed by two fast steps, 1.) radical disproportionation and formation of an o-quinone, and 2.) solvent addition at C2 [131]. An isotope labeling study using $^{18}O_2$ demonstrated that a depside intermediate is formed after a peroxide adduct is formed [116]. In a headspace analysis, Zenkevich *et al*. demonstrated that CO_2 is produced through oxidation which they proposed is formed through a decarboxylation mechanism and not decarbonylation [107].

2.5.2.2 Electrochemical Oxidation

Through bulk electrolysis of quercetin under physiological conditions Zhou *et al*. showed that oxidation was a complicated process that involved both electrochemical and chemical steps [110]. The electrochemical steps involved a two electron oxidation of quercetin. First a one-electron loss formed a semi-quinone, followed by a second one-electron loss to form the *o*-quinone. The *o*-quinone could

tautomerize into a quinone methide. In the chemical step, water attacked at C2, influenced by the quinone methide. The addition of water is unstable and leads to the C-ring opening (Figure 2.7).

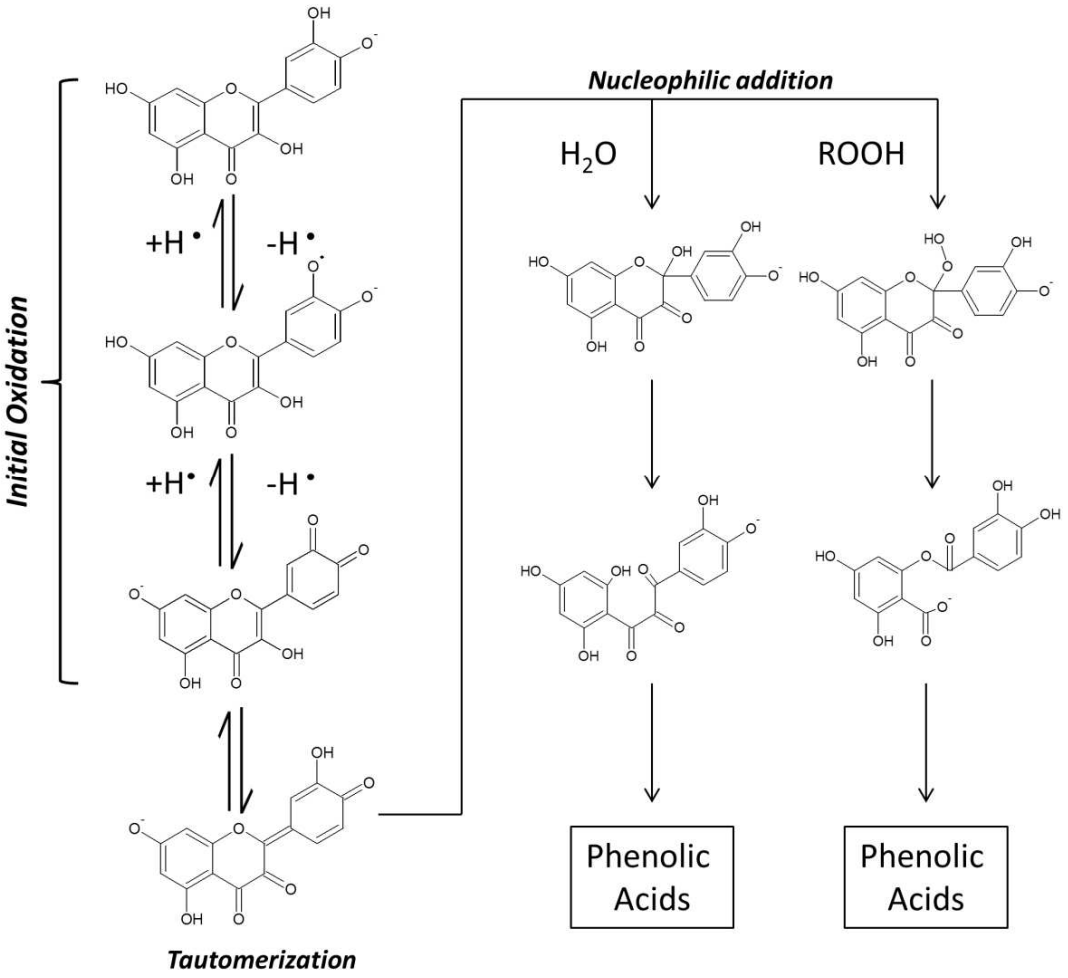

Figure 2.7: The oxidative degradation pathways of quercetin in mildly basic aqueous conditions.

2.5.2.3 Free Radical Initiated Oxidation

Using a Cu_2SO_4/H_2O_2 system, Makris and Rossiter generated hydroxyl free radicals which were used to degrade quercetin and morin. Their results also supported a quinone methide mediated water addition at C2, which lead to ring opening and formation of a propanetrione. They proposed that the observed PA and PCA end products where from cleavage generated by hydroxyl free radical attack of the propanetrione ketone groups [117].

A study of quercetin degradation with the DPPH free radical demonstrated that quercetin donates two H atoms, which leads to solvent adduct products, presumably at C2 [113]. In a study using an azo-

initiator to produce peroxyl radicals, the principle sites for ROS scavenging by quercetin occurred in the B and C-rings. By varying the pH and the solvent they demonstrated that solvent nucleophiles competed with peroxides for attack of the C2-centered carbocation. Depending on which nucleophile was present, a benzofuranone or depside was generated. They also suggested that the initial oxidation of quercetin formed an *o*-quinone or a *p*-quinone by successive abstraction of two H atoms at 3' and 4' or 3 and 4', respectively, and that the *o*- and *p*- quinones could interconvert [112]. This argument would explain the increased stability of rutin, since the 3-hydroxyl is blocked by a glycosyl group.

2.5.2.4 Enzymatic Oxidation

Makris and Rossiter used plant enzymes involved in flavonoid degradation to study flavonol degradation. The study confirmed that *o*-diphenols were transformed into *o*-quinones [115]. In a study using tyrosinase, Zhou *et al*. demonstrated that enzyme degradation followed the same oxidative paths as those described above, however, one difference was that *o*-quinone formation may occur from a spontaneous two electron transfer [108].

2.6 Conclusion

Considering the complex process of oxidation, it can become clear that one analysis method alone is not enough to adequately define the total antioxidant capacity of a substance. Each antioxidant capacity assay has been demonstrated to rely on specific mechanisms and have associated limitations, and results generated from these assays can be easily misinterpreted. Therefore, in order to more fully realize the power and efficiency of some of these cheap and simple methods, it is essential that the complex interactions between specific flavonoid classes and varying oxidative sources are better understood. To do this, complementary techniques must be used that provide quantitative kinetic measurements, while providing the ability to definitively qualitatively identify intermediates and end products.

Chapter 3

Thermally Accelerated Oxidative Degradation Of Quercetin Using Continuous Flow Kinetic Electrospray-Ion Trap-Time Of Flight Mass Spectrometry

3.1 Abstract

Thermally accelerated oxidative degradation of aqueous quercetin at pH 5.9 and 7.4 was kinetically measured using an in-house built online continuous flow device made of concentric capillary tubes, modified to fit to the inlet of an electrospray ionization – ion trap – time-of-flight – mass spectrometer (ESI-IT-TOF-MS). Time-resolved mass spectral measurements ranging from 2 to 21 minutes were performed in the negative mode to track intermediate degradation products and to evaluate the degradation rate of the deprotonated quercetin ion, $[Q-H]^-$. Upon heating solutions in the presence of dissolved oxygen, degradation of $[Q-H]^-$ was observed and was accelerated by an increase in pH and temperature. Regardless of the condition, the same degradation pathways were observed. Degradation mechanisms and structures were determined using higher order tandem mass spectrometry (up to MS^3) and high mass accuracy. The observed degradation mechanisms included oxidation, hydroxylation and ring-cleavage by nucleophilic attack. A chalcan-trione structure formed by C-ring opening after hydroxylation at C3 was believed to be a precursor for other degradation products, formed by hydroxylation at the C2, C3, and C4 carbons from attack by nucleophilic species. This resulted in A-type and B-type ions after cross-ring cleavage of the C-ring. Based on time of appearance and signal intensity, nucleophilic attack at C3 was the preferred degradation pathway, which generated 2,4,6-trihydroxymandelate and 2,4,6-trihydroxyphenylglyoxylate ions. Overall, 23 quercetin-related ions were observed.

3.2 Introduction

Plant cells produce a diverse array of metabolites, many of which are bioactive and nutritionally beneficial. Polyphenolic compounds are one such division of secondary plant metabolites which include the flavonoid group and other phytochemicals. The reactive nature of the flavonoids may partially contribute to some therapeutic phenomena. It is still unclear, though, by what mechanism and to what extent flavonoids participate. Studies of diets that are rich in flavonoids have been shown to reduce coronary heart disease, while others have shown no significant correlation [118-121].

Continued medical research on flavonoids, along with growing interest from the food and dietary supplement markets, have fueled further study into reactive flavonoid chemistry. Attention to the antioxidant content in foods and supplements is growing in the mainstream media and is being advertised on packaging. Flavonoids may also contribute to the visual quality and color in plants and plant-based foods. Degradation of these compounds by enzymatic and non-enzymatic browning is a major concern and the decrease of flavonoid content due to thermal processing has been well documented [79,105,106,122-124].

Being a major constituent in tea, red wine and onions, quercetin is one of the most commonly ingested flavonols. The antioxidant capacity (oxidative degradation) of quercetin, can be associated to its chemical structure (Figure 3.1). The B-ring contains an *o*-dihydroxy structure which allows for proton donation and free radical neutralization. The combination of the double bond located between C2 and C3, the hydroxyl group at C3 and the keto group at C4 in the C-ring provides electron delocalization and radical stabilization. Additional catechol-like structures can be formed between the hydroxyl group at C5 and the C4 keto group and between the hydroxyl group at C3 and the C4 keto group, which impart further ability for radical scavenging [106,117].

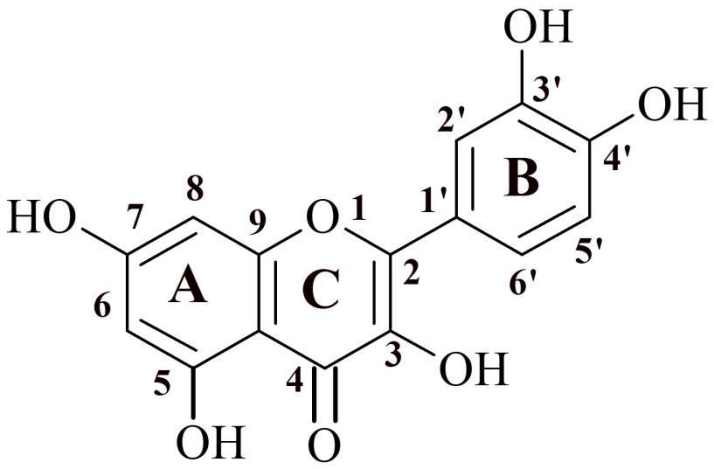

Figure 3.1: The chemical structure of quercetin.

Measurement of the total content, reactivity and antioxidant capacity of quercetin and other flavonoids are typically assessed using non-specific techniques which exploit the UV/Vis absorptivity of flavonoids, or the ability to protect fluorescent markers from oxidative degradation [63,104,125,126].

These traditional methods characterize the bulk antioxidant character or the degradation rate, but do not offer insight into the degradative mechanism or the production of associated reaction products [127].

Quercetin degrades at ambient temperatures in aqueous solutions and is susceptible to oxidation. Previous kinetic studies have demonstrated that the rate of oxidative degradation can be accelerated upon heating and/or the addition of metal catalysts [105,106,104,114]. In addition to proton abstraction, one accepted oxidative degradative mechanism involves C-ring opening, which leads to formation of lower molecular weight phenolic carboxylic acids, the common reported end products being 3,4-hydroxybenzoic acid (protocatechuic acid) and 2,4,6-trihydroxybenzoic acid (phloroglucinol carboxylic acid) [117,111,107,128]. Based on the location of the hydroxyl substituents of quercetin, these end products represent both an A-ring type degradant and a B-ring type degradant. Most of these studies do not consider intermediate structures and only a few have attempted to identify additional degradation products [110,108].

Kinetic mass spectrometry (MS) studies which use electrospray ionization (ESI) have been conducted in a variety of applications and have allowed the determination of rates of degradation and production of chemical species; from these, the mechanisms associated with degradation can be gleaned. Clarke *et al*. used a quench-flow method to study the mechanisms of enzymatic reactions [129]. Many stopped-flow MS methods have been utilized to evaluate chemical reactions in solutions [130-133]. Konermann *et al*. have demonstrated numerous continuous-flow time resolved ESI-MS studies [87, 89, 90, 91].

There are many difficulties associated with natural product research using mass spectrometry. Plant sample matrices have an assortment of compounds that are similar in structure and character which makes identification problematic since high purity polyphenolic standards are hard to obtain or keep in supply due to their limited long-term stability, limited selection, and associated costs. Identification may be deduced through reduction of formulaic possibilities with the nominal mass of the parent ion and structural information using collision induced fragmentation. However, many polyphenolic metabolites have the same formula and similar MS/MS patterns, making them indistinguishable by tandem mass spectrometry. The hybrid technique of ESI-IT-TOF-MS, which includes higher order ion-trap

fragmentation and high mass accuracy, is a means to address these limitations, providing efficient structural elucidation and definitive identification of analytes [83, 89].

In this work, an online capillary device inspired by Wilson and Konnermann [87] with an adjustable reactor volume was modified to fit an electrospray inlet of a mass spectrometer. Using the device, the oxidative degradation of quercetin in aqueous solutions, unbuffered and at physiological pH, was studied. Degradation was thermally accelerated by placing the device into a water bath heated from 65 ℃ to 85 ℃. The reaction time (1.8-20.6 min) c ould be controlled by making adjustments to the device. Incorporation of MS^n with high mass accuracy on a hybrid ion trap – time-of-flight (IT-TOF) MS system with this device allowed for an in-depth continuous flow kinetic study of the mechanisms and pathways by which thermally accelerated oxidative degradation of quercetin degradation and mechanisms occurs. To our knowledge, this type of combined on-line and mass spectrometry-based degradation study has not been performed before on quercetin or other flavonoid compounds.

3.3 Methods and Equipment

3.3.1 Reagents and Solution

Stock solutions of quercetin where prepared by dissolving quercetin (100 mg, Sigma-Aldrich, St. Louis, MO, USA) into dimethyl sulfoxide (100 mL, Sigma-Aldrich, St. Louis, MO, USA). This solution was noted to be extremely stable over a period of months. Aqueous solutions of quercetin (65 µM) were prepared by diluting the stock solution with LCMS-grade water (Burdick and Jackson, Muskegon, MI, USA). The pH of the aqueous solution in unbuffered water was measured to be 5.9 using a UB-10 pH meter (Denver Instrument, Denver, CO, USA) equipped with an Orion pH electrode (Thermo Fisher Scientific, Waltham, MA, USA). The aqueous solution was adjusted to 7.4 by addition of sodium hydroxide (~150 µM, J.T. Baker, Phillipsburg, NJ, USA). Fresh solutions were prepared at each measured time point.

3.3.2 Kinetic Device

Kinetic measurements were performed using a continuous-flow device which was built in-house (Figure 3.2) and consisted of two concentric capillary tubes. A 2.5 mL glass syringe (7.284 mm internal diameter (I.D.); Hamilton, Reno, Nevada, USA) was connected to a five foot length of polyetheretherketone (PEEK) tubing (100 µm I.D.; 360 µm outer diameter (O.D.)). The downstream end

of the PEEK tubing was inserted into a five foot length of fluorinated ethylene propylene (FEP) tubing (400 µm I.D.; 1000 µm O.D.). A stainless steel union (0.052" thru-hole) was slid over the FEP tubing 5 cm from the upstream end of the outer capillary and tightened with a fitting and a ferrule to seal any leaks. The downstream outlet end of the FEP tubing (outer capillary) was connected to the inlet of the ESI. The syringe was driven by a syringe pump (NE-1010, New Era Pump Systems, Farmingdale, NY, USA).

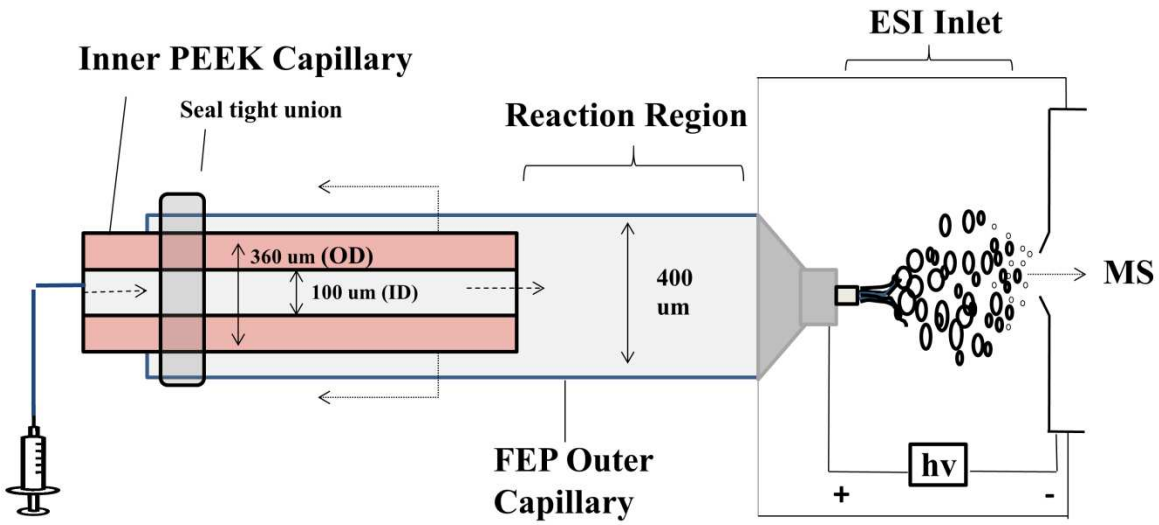

Figure 3.2: An online kinetic continuous flow device made from two concentric capillary tubes used to interface to the inlet of an ESI.

By moving the inner capillary, the volume of the reaction region was controlled, which allowed the user to regulate the amount of time the solution was heated. A flow rate of 10.0 µl/min was used to pump the solution through the tubing and directly infused into the ESI inlet. At this flow rate, the dwell time of the system was 1.8 minutes based on total system volume of 18 µL from 5 feet of inner tubing and 2 inches of outer tubing (seal union overlap). Kinetic measurements were made by pulling the inner PEEK tubing out at 1 foot intervals, allowing for measurements ranging from 1.8 to 20.6 minutes of reaction time. Thermally-accelerated degradation was performed by submerging the coiled tubing into a heated, wide-mouth beaker, which had been filled with water. The temperature was controlled between 65-85 ℃.

3.3.3 Instrumentation

Negative ion MS spectra were acquired using an ion trap–time of flight mass spectrometer (IT-TOF-MS, Shimadzu Scientific Instruments, Inc., Kyoto, Japan) equipped with a conventional electrospray

ionization (ESI) source. Analytical parameters for ionization, fragmentation, and detection were: interface voltage, -3.5 kV; nebulizing gas (N_2), 1.5 L/min; drying gas (N_2), 10 L/min; curved desolvation line, 200 ℃; detector voltage, 1.92 kV; ion accumulation tim e, 10 ms; precursor ion isolation width, 0.1 amu; collision gas (Ar), 50%; and frequency constant (q), 0.251. The estimated resolution of the instrument is 10,000 at m/z 1000. A scanning rate of 100 ms was used. The estimated duty cycle at MS^3 with these settings was < 0.5 seconds. The collision energy during collision-induced dissociation (CID) was adjusted at each tandem MS stage to determine the optimum parameters at which a maximum amount of signal information would be obtained. The IT-TOF was calibrated to < 5 ppm mass accuracy using a solution of sodium trifluoroacetate.

Data collection and analysis was carried out using *LCMS Solutions* version 3.4 software. The *Accurate Mass Calculator* and *Formula Predictor* software tools were used to support determination of theoretical *m/z* values and elemental formulas of observed fragments. The software was configured to eliminate formulaic possibilities based on the following requirements: 1-15 Carbons, 0-10 Oxygens, 0-15 Hydrogens, and within 25 ppm error. Isotopic ratios were also evaluated.

3.4 Results

Overall, aqueous solutions of quercetin at pH 5.9 and pH 7.4 were observed to be relatively stable at room temperature for periods of up to 24 hours. Quercetin solubility was noticeably improved at the mildly basic physiological pH compared to unbuffered acidic quercetin solutions. The color of the solution changed from a dull pale yellow at pH 5.9 to a bright fluorescent yellow at pH 7.4; however, the color would fade within 2-3 hours at room temperature. Numerous charged species could be monitored in the negative mode and although some quercetin-related ions were observed in the positive mode, they were not observed at significant intensity levels for informative analysis during any of the test conditions, and therefore, are not discussed in this assessment.

The base peak observed in the spectra at room temperature was of $[Q\text{-}H]^-$ (m/z 301.0361), and was larger by an exponential degree at the mildly basic pH of 7.4, as expected, based on the spontaneous deprotonation of quercetin; the 4' hydroxyl group has a pKa ~7 [50,53,134]. In general, over 23 quercetin-related ions were observed in aqueous solution. These ions were classified into four types: 1) Simple deprotonated quercetin-like; 2) solvent and/or oxidized adducts of quercetin; 3) cross-ring

cleavage products of quercetin; and 4) compounds formed by small molecule loss. The signal intensity of $[Q\text{-}H]^-$ was monitored as a function of reaction time and was observed to decrease. The rate of decrease in the intensity of this ion was greater with increasing temperature and when increasing the pH, from weakly acidic to weakly basic (Figure 3.3). Similarly the doubly-deprotonated ion $[Q\text{-}2H]^{2-}$ (m/z 150.0148) was observed to decrease over time; however, it was observed at a much smaller quantity. Other deprotonated ions of quercetin appeared to be sensitive to pH conditions and higher mass oxidated ions appeared to reach equilibrium and were less affected by heat. Over time, growth in intensity of low molecular weight cross-ring cleavage ions were observed (Figure 3.4), and in general, appeared at significant levels at earlier time points with increasing heat and pH.

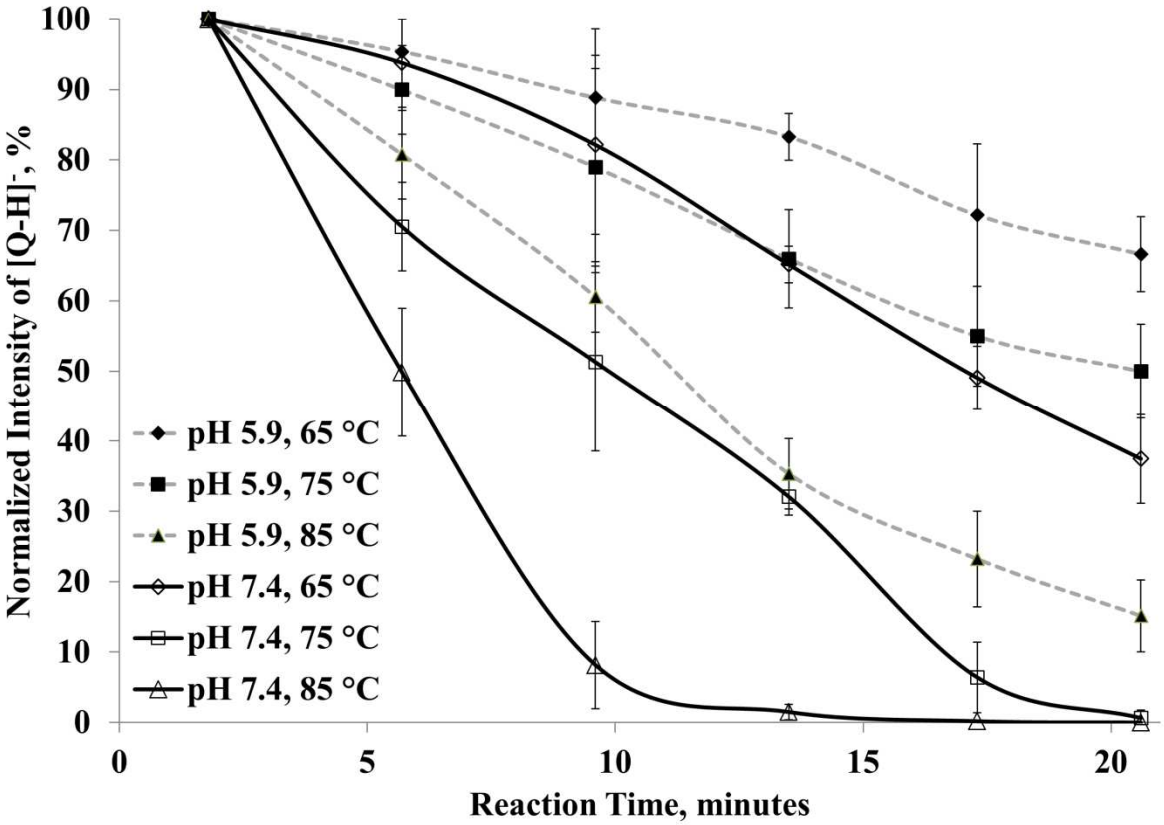

Figure 3.3: A plot of the thermally accelerated oxidative degradation of [Q-H]– (m/z 301.0354) ion intensity over time, with n=2. Solutions at pH 5.9 and 7.4 were heated over a range of 65, 75, and 85 ℃. The ion intensity was normalized against the signal intensity observed at the dwell time (1.8 min)

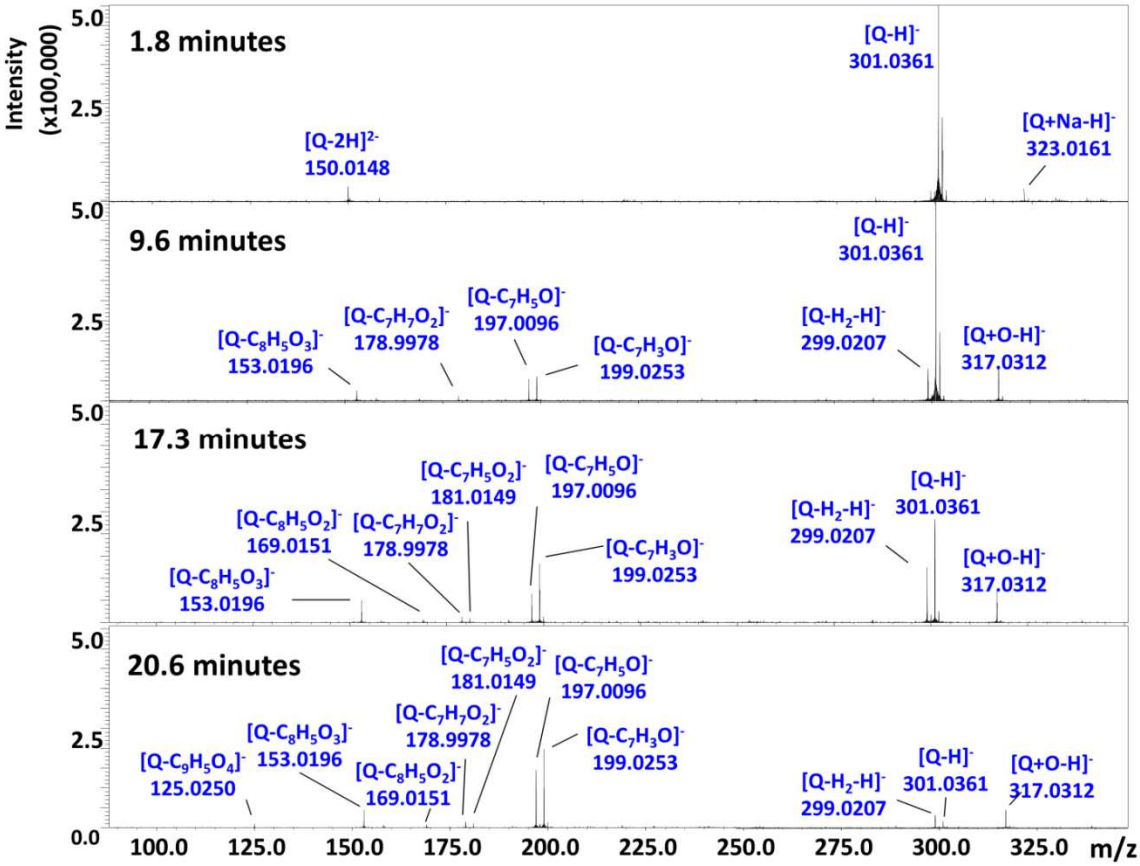

Figure 3.4: Comparative time-resolved spectra in the negative mode of 20 ppm aqueous solutions of quercetin at pH 7.4 heated at 75 ℃

3.4.1 Time-Resolved Observations

All of the ions reported in Table 1 were observable in solutions of quercetin at room temperature, however, most of these signals were observed in trace amounts and were difficult to distinguish from baseline noise. As time and temperature increased, all of the reported ions had been observed at a 1% relative intensity or greater. At this intensity, ion signals could be sufficiently identified from the baseline and provided high mass accuracy measurements (<10 ppm). Ions at or above this threshold and ions that had grown larger than the 1% threshold were considered significant and are discussed below.

Table 3.1: The Degradation and Fragment Ions Observed in Aqueous Solutions of Quercetin

Deprotonated and Simple Oxidated Ions					
Ion Identity	**Proposed Identity**	**Formula**	**Theoretical Mass, m/z**	**Observed Mass, m/z**	**Error, ppm**
[Q]	quercetin	$C_{15}H_{10}O_7$	302.0427	------	-----
$[Q-H]^-$	quercetin monoanion	$C_{15}H_9O_7$	301.0354	301.0361	2.4
$[Q-2H]^{\bullet-}$	quercetin radical anion	$C_{15}H_8O_7$	300.0262	300.0262	0.0
$[Q-2H]^{2-}$	quercetin dianion	$C_{15}H_8O_7$	150.0141	150.0148	5.0
$[Q-H_2-H]^-$	quercetin *o*-quinone anion	$C_{15}H_7O_7$	299.0197	299.0207	3.3
$[Q-H_2-2H]^{2-}$	quercetin *o*-quinone dianion	$C_{15}H_6O_7$	149.0062	149.0071	5.9
$[Q+O-H]^-$	2,3,4-chalcan-trione monoanion	$C_{15}H_9O_8$	317.0303	317.0312	2.9
$[Q+O-2H]^{2-}$	2,3,4-chalcan-trione dianion	$C_{15}H_8O_8$	158.0115	158.0118	1.9
$[Q+O-H_2-H]^-$	*o*-quinone 2,3,4-chalcan-trione anion	$C_{15}H_7O_8$	315.0460	315.0456	-1.3
$[Q+Na-H]^-$	Sodiated quercetin anion	$C_{15}H_9O_7Na$	323.0154	323.0161	2.2
$[Q+Na+O]^-$	sodiated 2,3,4-chalcan-trione anion	$C_{15}H_8NaO_8$	339.0122	339.0128	1.7
Degradation Products Ions					
Ion Identity	**Proposed Identity**	**Formula**	**Theoretical Mass, m/z**	**Observed Mass, m/z**	**Error, ppm**
$[Q-C_7H_3O]^-$	2,4,6-trihydroxymandelate	$C_8H_7O_6$	199.0248	199.0253	2.5
$[Q-C_7H_5O]^-$	2,4,6-trihydroxyphenylglyoxylate	$C_8H_5O_6$	197.0092	197.0096	2.2
$[Q-C_7H_5O_2]^-$	3,4,-dihydroxyphenylgloxylate	$C_8H_5O_5$	181.0142	181.0149	3.6
$[Q-C_7H_7O_2]^-$	2-oxo-2-(3,4-quinone)acetate	$C_8H_3O_5$	178.9966	178.9978	6.7
$[Q-C_8H_5O_2]^-$	2,4,6-trihydroxybenzoate	$C_7H_5O_5$	169.0142	169.0151	5.0
$[Q-C_8H_5O_3]^-$	3,4-dihydroxybenzoate	$C_7H_5O_4$	153.0193	153.0196	1.8
$[Q-C_8H_7O_3]^-$	*o*-quinone-4-carboxylate	$C_7H_3O_4$	151.0044	151.0040	-2.6
$[Q-C_8H_5O_4]^-$	4-carbaldehyde-2-hydroxyphenolate	$C_7H_5O_3$	137.0244	137.0242	-1.6
$[Q-C_9H_5O_4]^-$	3,5-dihydroxyphenolate	$C_6H_5O_3$	125.0244	125.0250	4.7
$[Q-C_9H_5O_5]^-$	3-hydroxyphenolate	$C_6H_5O_2$	109.0295	109.0301	5.5
Small Molecule Loss Ions					
Ion Identity	**Proposed Identity**	**Formula**	**Theoretical Mass, m/z**	**Observed Mass, m/z**	**Error, ppm**
$[Q-O-H]^-$	-----	$C_{15}H_9O_6$	285.0375	285.0379	1.4
$[Q-CO-H]^-$	-----	$C_{14}H_9O_6$	273.0361	273.0373	4.4
$[Q-CO-H_2-H]^-$	-----	$C_{14}H_7O_6$	271.0229	271.0237	3.0
$[Q-OH-CO-H_2]^-$	-----	$C_{14}H_7O_5$	255.0299	255.0309	3.9

3.4.1.1 Degradation of acidic unbuffered aqueous quercetin solution

At room temperature, very limited degradation could be observed in unbuffered acidic aqueous solutions of quercetin (65 µM, pH 5.9). At time zero, the only signals above a 1% relative intensity

compared to $[Q\text{-}H]^-$, were those for $[Q\text{-}2H]^{2-}$, $[Q\text{-}H_2\text{-}H]^-$ and $[Q\text{-}2H]^{\bullet-}$ (*m/z* 150.0148 (3% relative intensity), 299.0207 (3%) and 300.0262 (1%), respectively). Through 120 minutes, the signals for $[Q\text{-}2H]^{2-}$, $[Q\text{-}H_2\text{-}H]^-$ and $[Q\text{-}2H]^{\bullet-}$ increased slightly to 4%, 5% and 2% relative intensity, respectively. In addition, signals for $[Q\text{-}C_7H_5O]^-$ and $[Q+O\text{-}H]^-$ (m/z 197.0096 and 317.0312) could begin to be observed at the 1% threshold. Near the 240 minute mark, these signals remained consistent and the signals $[Q+O\text{-}H_2]^-$ and $[Q\text{-}C_7H_3O]^-$ (m/z 158.0118 and 199.0253) could begin to be observed above the 1% threshold. The $[Q\text{-}C_7H_5O]^-$ and $[Q\text{-}C_7H_3O]^-$ (m/z 197.0096 and 199.0253) could be observed at a 1:1 ratio which contrasted with the ~3:1 ratio (197:199) seen in trace amounts at time zero. After 240 minutes, only a 5% decrease in intensity of the $[Q\text{-}H]^-$ signal was observed.

The degradation of the $[Q\text{-}H]^-$ signal was notably accelerated by heating the solution in the range of 65 to 85 ℃ over a 20 minute interval (Figure 3. 3). After the minimum heating time which occurred due to the dwell time (~1.8 minutes), the total ion content increased ~10%. This increase is most likely due to improved desolvation and ionization. Heating at 65 to 85 ℃ for the minimum dwell time also affected the signal of $[Q\text{-}H_2\text{-}H]^-$, $[Q+O\text{-}2H]^{2-}$, and $[Q+O\text{-}H]^-$, (m/z 299.0207, 158.0118 and 317.0312). They were observed to increase to ~10%, 3% and ~10% relative intensity, respectively. The $[Q\text{-}2H]^{2-}$ signal (m/z 150.0148) decreased from 5% relative intensity and could not be distinguished from the noise after 21 minutes at 65 ℃. The $[Q+O\text{-}2H]^{2-}$ and $[Q+O\text{-}H]^-$ remained relatively constant throughout the twenty minute time period with heating.

After just 9.6 minutes at 65 ℃, the $[Q\text{-}C_7H_5O]^-$ (m/z 197.0096) was seen at a 1% relative intensity, much earlier than was observed at room temperature. This ion appeared to be the first charged cross-ring cleavage degradation species to form, and was closely followed by the appearance of $[Q\text{-}C_7H_3O]^-$ and $[Q\text{-}C_8H_5O_3]^-$ (m/z 199.0253 and 153.0196), signals for which were seen at 13.5 minutes at 65 ℃. These three ions were the only three cross-ri ng cleavage ions to appear above a 1% relative intensity compared to $[Q\text{-}H]^-$. Through the 16 and 19 minute time points at 65 °C, the $[Q\text{-}C_7H_3O]^-$ and $[Q\text{-}C_8H_5O_3]^-$ signal intensities increased, and reached a maximum relative intensity of ~7% and ~3% compared to the initial $[Q\text{-}H]^-$ intensity observed during the dwell condition. The $[Q\text{-}C_7H_5O]^-$ signal reached a maximum relative intensity of 6% at the 16 minute time point and slightly decreased at the 20.6 minutes time point and was observed at a 1:2 ratio compared to $[Q\text{-}C_7H_3O]^-$.

Measurements made at 75 ℃ and 85 ℃ showed increas ed degradation rates of $[Q-H]^-$ and showed the same degradative ion signals as observed at 65 ℃, but at earlier time points. After just 5.7 minutes at 85 ℃, the $[Q-C_7H_5O]^-$ was seen at a 1% relative intensity compared to the initial dwell time signal of $[Q-H]^-$, and it reached a maximum of 7% relative intensity at 17.3 minutes. The $[Q-C_7H_3O]^-$ and $[Q-C_8H_5O_3]^-$ could all be seen above the 1% relative intensity at 9.6 minutes at 85 ℃ and reached a maximum relative intensity of 8% and 5%.

3.4.1.2 Oxidative Degradation of aqueous quercetin solution at pH 7.4

At room temperature, more oxidative degradation could be observed in aqueous solutions of quercetin adjusted to physiological pH (65 µM, pH 7.4) as compared to solutions at pH 5.9. At time zero, ion signals observed above a 1% relative intensity compared to $[Q-H]^-$ were for $[Q-2H]^{2-}$ (12%), $[Q-2H]^{\bullet-}$ (5%), $[Q-H_2-H]^-$ (3%), $[Q-H_2-2H]^{2-}$ (1%), $[Q+O-H]^{2-}$ (1%) and $[Q+Na-H]^-$ (2%). After 45 minutes at room temperature, the signals for $[Q+O-H]^-$ and $[Q+Na+O-H]^-$ (m/z 317.0312 and 339.0128) began to appear consistently at the 1% threshold in the mass spectra. After 120 minutes, the three cross-ring cleavage products, $[Q-C_7H_5O]^-$, $[Q-C_7H_3O]^-$, and $[Q-C_8H_5O_3]^-$ (m/z 199.0253, 197.0096 and 153.0196) appeared near 1% relative intensity. After 240 minutes, the relative intensities of the $[Q-2H]^{2-}$, $[Q-H_2-H]^-$, $[Q-H_2-2H]^{2-}$, $[Q+Na-H]^-$ and $[Q+Na+O-H]^-$ signals remained consistent with the relative intensities observed at time zero value, while the signals for $[Q-2H]^{\bullet-}$ (9%), $[Q+O-H]^-$ (14%), $[Q+O-H_2-H]^-$ (5%), $[Q+O-2H]^{2-}$ (8%), $[Q-C_8H_5O_3]^-$ (1%), $[Q-C_8H_5O_2]^-$ (1%), $[Q-C_7H_5O]^-$ (4%) and $[Q-C_7H_3O]^-$ (1%) increased. The $[Q-H]^-$ signal intensity was observed to decrease by an absolute amount of 15%.

There was a considerable difference noted in the degradation rate of the $[Q-H]^-$ signal and the overall increase in intensity of degradation products when the solution at physiological pH was heated (Figure 3.3 and 3.4). Many degradation products observed were the same as those observed at pH 5.9, including a few additional lower mass cross-ring cleavage product ions; they followed the same trend of appearing earlier as the temperature was increased.

The trends of some of the simple deprotonated and oxidated signals were also in contrast when heated compared to at room temperature. The $[Q-H_2-2H]^{2-}$ ion which was observed at 1% relative intensity at room temperature, was not observed at a significant intensity at any time point when heated. The $[Q-2H]^{\bullet-}$ ion reached a maximum of 9% relative intensity at room temperature, but only reached a

maximum of 4% relative intensity after 1.8 minutes at 65 ℃ and decreased in intensity after that; it was not observed in significant intensity in the 75-85 ℃ temperature studies. The $[Q-2H]^{2-}$ ion signal was only seen in the first time point (1.8 minutes) of the 65 and 75 ℃ studies, and was not seen at all in the 85 ℃ study.

Similar to the solution at pH 5.9, the $[Q+O-H]^-$ appeared immediately upon heating (1.8 minutes; dwell time) but remained at a consistent intensity (~10%) throughout the heating range, and only decreased when the $[Q-H]^-$ intensity had become very low. The cleavage product ions $[Q-C_7H_3O]^-$, $[Q-C_7H_5O]^-$ and $[Q-C_8H_5O_3]^-$ (m/z 199.0253, 197.0096 and 153.0196) could be observed at the minimum dwell time at 65 ℃ at pH 7.4. These cleavage deg radation products grew significantly over time and were the dominant degradation products through 20.6 minutes, with the $[Q-C_7H_3O]^-$ ion being the overall largest degradation product observed at all temperatures.

The cross-ring cleavage degradation products $[Q-C_7H_5O_2]^-$, $[Q-C_7H_7O_2]^-$ and $[Q-C_8H_5O_2]^-$ (m/z 181.0149, 178.9978 and 169.0151), which were not observed at pH 5.9, appeared in low intensities after 17.3 minutes at 65 ℃ and pH 7.4. Finally, after h eating for 20.6 minutes at 75 ℃, the cross-ring cleavage degradation products $[Q-C_8H_5O_4]^-$, $[Q-C_9H_5O_4]^-$ and $[Q-C_9H_5O_5]^-$ (m/z 137.0242, 125.0250 and 109.0301) could be observed at low intensities. After 20.6 minutes at 85 ℃, the $[Q-H]^-$ was not detectable.

3.5 Discussion

3.5.1 Deprotonation, autoxidation, and chalcone formation

Governed by acid-base equilibrium, spontaneous deprotonation of quercetin in aqueous solutions within the tested pH ranges should lead to the formation of the $[Q-H]^-$ and $[Q-2H]^{2-}$ ions. Based on pKa's available in the literature, these protons would be lost from the 4' and 7 substituents [50,53,134]. The intensities of these ions observed in the mass spectra were in general agreement with those expected in solution. It should be noted, however, there are often discrepancies of ion intensities for species of charge state distributions in mass spectra compared to the actual equilibrium concentration of charged species in solution. During electrospray ionization, charged species formation may be potentially affected by coulombic interactions on a decreasing droplet surface, as well as contributions from the voltage and

temperature of the curved desolvation line (CDL) on the gas-phase disassociation of the neutral proton and anion pair [135,136].

Since the solutions were not sparged or prepared under evacuation of air, it was assumed that dissolved O_2 was present in the solutions. In addition, since the outer capillary was constructed of transparent FEP, it is reasonable to assume that trace amounts of reactive oxygen species (ROS) would form in the aqueous solutions, originating from light-induced excitation of O_2 and H_2O. One study observed 15 nM of H_2O_2 in distilled water saturated with dissolved oxygen in the presence of light [137]. Additionally, the auto-ionization of water would contribute 100-250 nM of hydroxyl ions, depending on the pH.

The presence of the $[Q\text{-}H_2\text{-}H]^-$ ion in fresh solutions at room temperature demonstrates that oxidation of quercetin (followed by ionization from the electrospray) occurs rapidly within these pH ranges. Formation of the $[Q\text{-}2H]^{\bullet-}$ radical anion appeared to be pH-dependent since it was only observed in the pH 7.4 solutions. This radical may be an intermediate during oxidation of the catechol substituent and could generate a superoxide radical [135]. It may also act as a reducing agent in solution.

The oxidative adduct $[Q+O\text{-}H]^-$ also appeared to form rapidly in aqueous solution at pH 5.9 and above without thermal acceleration. The $[Q+O\text{-}2H]^{2-}$ ion was not seen in fresh solutions at either pH, but was seen in solution at pH 7.4 at room temperature after 30 minutes and in the thermally accelerated pH 5.9 solution. In addition, the ratio of ion intensity of these two signals were close to 1, in stark contrast to the $[Q\text{-}H]^-$ and $[Q\text{-}2H]^{2-}$ ion intensity ratio. Previous studies suggested that hydroxylation can occur at the C2 position to form a 2-hydroxy-3,4-flavonedione [111,138]. Differences in the $[Q+O\text{-}H]^-$ and $[Q+O\text{-}2H]^{2-}$ ion intensity ratio compared to $[Q\text{-}H]^-$ and $[Q\text{-}2H]^{2-}$ further supports hydroxylation at this site since this loss of the C2-C3 double bond would disrupt the resonance stabilization by 4-oxo, causing a negative shift in the pKa of the 3' and 4' diol hydrogens.

Besides the 2-hydroxy-3,4-flavonedione anion, two other structures with hydroxylation at C2 and a m/z of 317.0312 are possible. One possible structure would be the 2,3,4-chalcan-trione anion formed by C-ring opening of the 2-hydroxy-3,4-flavonedione at the O1-C2 bond and formation of a double bonded oxygen at C2 (Figure 3.5). The latter structure seems more likely to be present based on the tested pH range. Anthocyanins also form a chalcone-type structure starting above pH 6 [10]. The chalcone

structure was also supported by product ions observed by higher order fragmentation of the $[Q+O-H]^-$ ion (Figure 3.6). A depside-type structure formed by C-ring opening of the 2-hydroxy-3,4-flavonedione at C2-C3 and formation of a double bonded oxygen at C2 could also have been responsible for the $[Q+O-H]^-$ ion; however, this structure was not supported by the fragmentation ions. Regardless of the structure, the ion intensity of this signal stays relatively constant when heated over time, which suggests that this structure may be an intermediate that leads to further degradation.

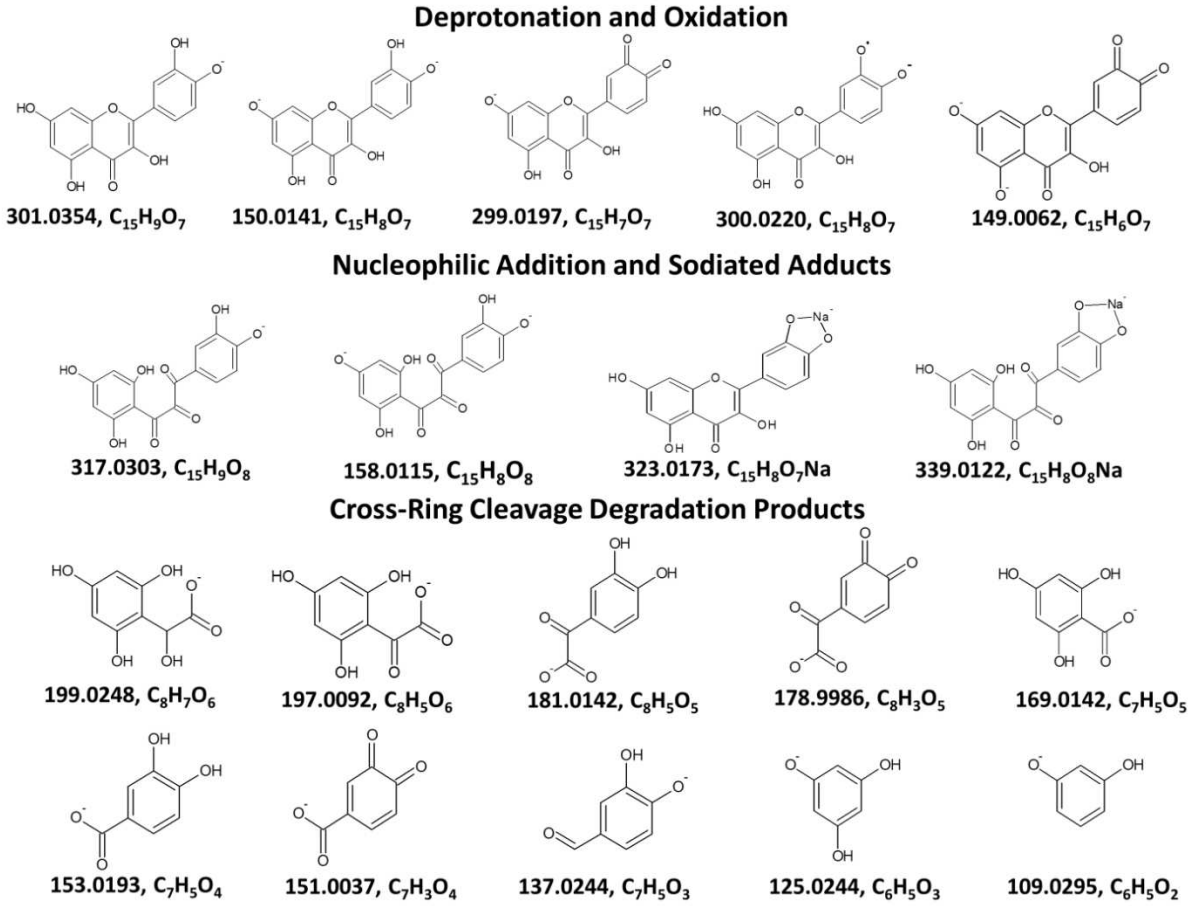

Figure 3.5: Proposed structures of ion signals observed during analysis of 20 ppm aqueous quercetin solutions

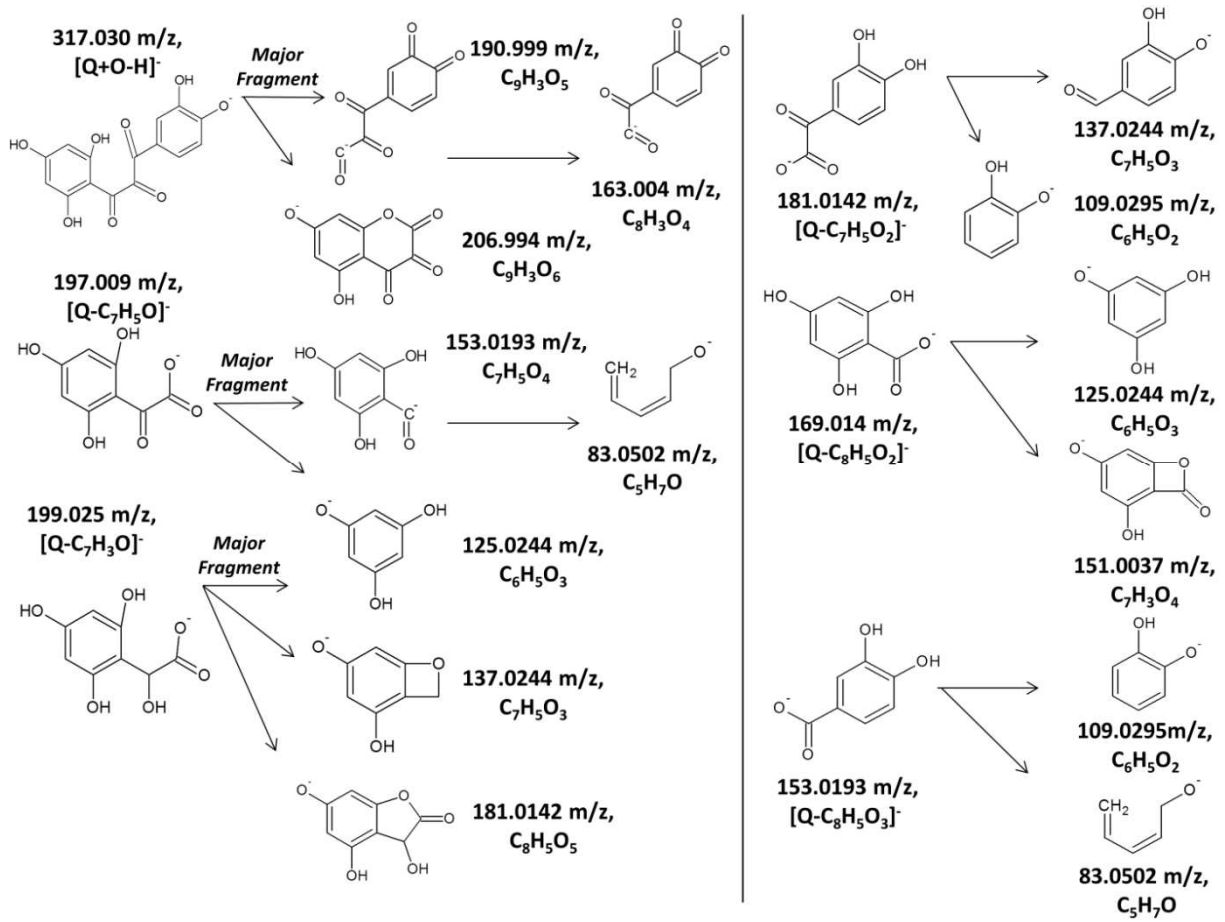

Figure 3.6: Proposed structures of ion signals observed during analysis of 20 ppm aqueous quercetin solutions

3.5.2 Cross-Ring Cleavage Pathways

Additional interaction of the 2,3,4-chalcan-trione with ROS could result in different degradants. Degradant ion signals observed suggest that three pathways were followed, which involved nucleophilic attack at the C2, C3, and C4 position, and caused hydroxylation at the site and a neutral loss (Figure 3.7). Opening of the C-ring may allow the structure to unfold, decreasing steric hindrance for nucleophilic attack along the chain of carbonyl groups. The C2, C3 and C4 carbons should have a partial positive charge due to the electron withdrawing effects of the ketone groups. The C3 carbon would appear to have the largest partial charge of the groups, since the ketones at C2 and C4 could be further withdrawing electron density from it. The central ketones of vicinal tricarbonyl compounds are known to be highly electrophilic due to the neighboring carbonyl groups, which would increase its reactivity with reactive oxygen species and promote hydroxylation and C-C cleavage [139-141].

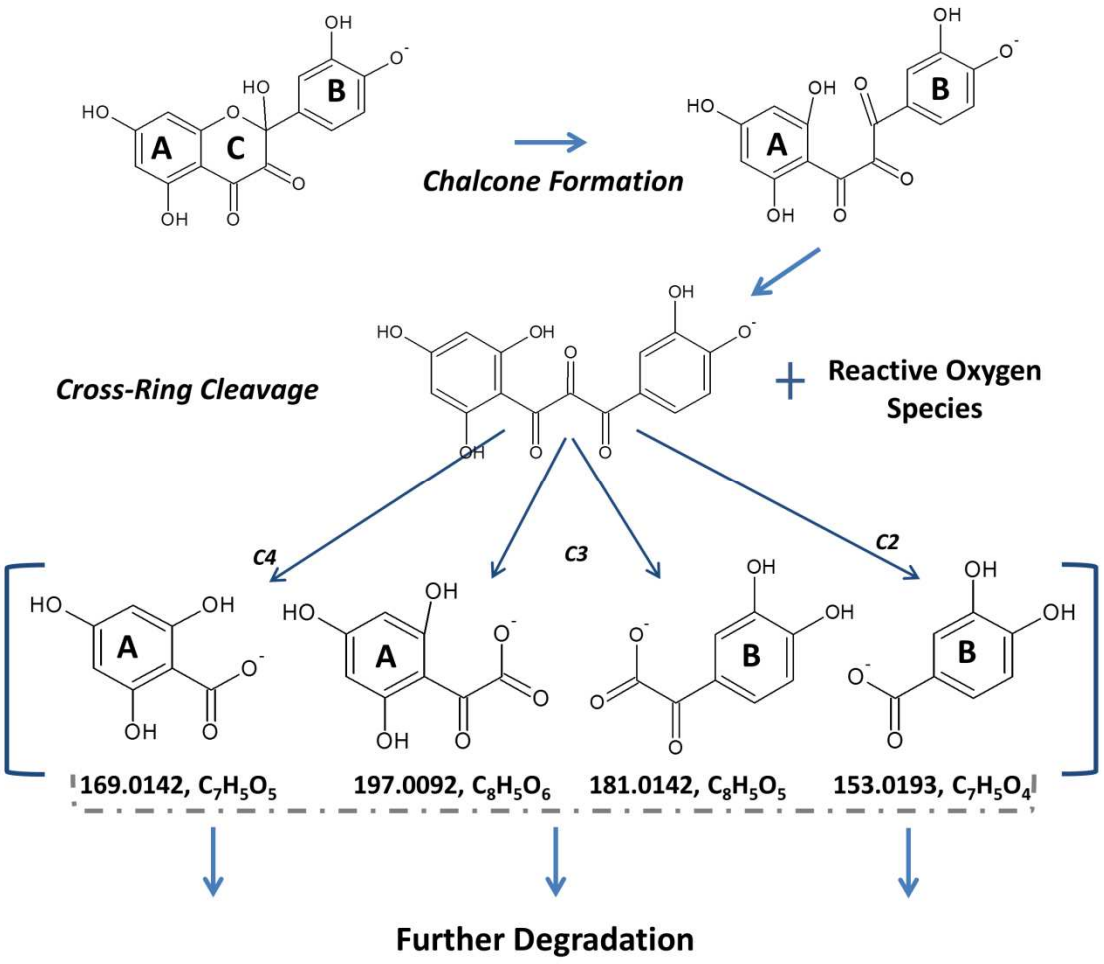

Figure 3.7: Proposed mechanism of the oxidative degradation pathways of quercetin aqueous solutions due to the nucleophilic attack by water and reactive oxygen species (ROS)

The appearance of ion signals at m/z 197.0096 and 199.0253 were the first time-resolved lower molecular weight degradants of quercetin, and since they are the most abundant degradant ion signals observed, this suggests that the degradation pathway which leads to these structures is the most favored, assuming that electrospray ionization efficiency does not vary significantly between the different species. Based on the mass difference, the m/z 199.0253 signal appears to be a reduced form of the structure responsible for the m/z 197.0096 signal. This reduction may be formed by radical anions in solution, like $[Q\text{-}2H]^{\bullet-}$. High mass accuracy predicts that these ions have the molecular formulas $C_8H_5O_6$ and $C_8H_7O_6$ (2.5 and 2.2 ppm error, respectively). Six carbons are found in both the A and B rings of the chalcone structure and three carbons lie in between the rings at the C2, C3, and C4 positions. Thus, cleavage to

form these ions would have to occur at C3, which is the center carbon in the carbon linkage between the rings, to maintain eight carbons. Additionally, the degradant ions would have to be formed from cleavage on the A-ring side in order to have six oxygens, since 3 oxygens are present on the A-ring and only 2 oxygens are present on the B-ring. This suggests that oxidation at C3 leads to a loss of the C2 carbonyl and the B-ring, and with charge retention, forms 2,4,6-trihydroxymandelate or 2,4,6-trihydroxyphenylglyoxylate. Higher order fragmentation of the $[Q\text{-}C_7H_3O]^-$ and $[Q\text{-}C_7H_5O]^-$ ions revealed product ion spectra, which contained a signal at m/z 125.0250 (loss of OH+CO+CO). The observed fragment ion at m/z 125.0250 (a diol phenolate) also suggests that the parent ions are A-type ions (Figure 3.6). 2,4,6-trihydroxyphenylglyoxylate has been reported in other oxidative degradation studies and has been reported with similar tandem MS fragmentation signals [108, 110].

If the leaving group would retain the charge or be ionized, it would be $[Q\text{-}C_8H_5O_4]^-$ (m/z 137.0242), which was observed, but not at significant relative intensities (>1%) until heated at 85 ℃ for 20.6 minutes in the pH 7.4 solution. If hydroxylation at C3 resulted in loss of the A-ring and the C4 carbonyl, the ion would have only 5 oxygens. The presence of the ions at 181.0149 and m/z 178.9978 predicts ion structures with formulas of $C_8H_5O_5$ and $C_8H_3O_5$, with the latter being a quinone structure, and fragmentation of the ion further supported that the ions are B-type ions. Their proposed structures are consistent with 3,4,-dihydroxyphenylglyoxylate and 2-oxo-2-(3,4-quinone)acetate.

If nucleophilic attack were to occur at the C2 carbon and the A-ring was the leaving group, the charged hydroxylated degradant would be $[Q\text{-}C_8H_5O_3]^-$ (m/z 153.0196). This ion appears after the appearance of $[Q\text{-}C_7H_3O]^-$ and $[Q\text{-}C_7H_5O]^-$ and in significant quantities, suggesting that this pathway is also favored at the physiological pH. If the B-ring was the leaving group of nucleophilic attack at C2, then the hydroxylated degradant ion would be $[Q\text{-}C_6H_5]^-$ (m/z 225.0041); however, this ion was not observed during any tested conditions.

The fragmentation of $[Q\text{-}C_8H_5O_3]^-$ resulted in the product ion of m/z 109.0301, a hydroxylated phenolate. Because this ion, and not m/z 125.0250, was seen in the fragmentation pattern of $[Q\text{-}C_8H_5O_3]^-$, it seems to be more likely generated from the B-ring. Tournaire *et al*. reported that 3,4-dihydroxybenzoic acid and 2,4,6-trihydroxybenzaldehyde (both anions would be $[Q\text{-}C_8H_5O_3]^-$) were the endpoints of quercetin degradation [142]. An anion of 3,4-dihdryoxybenzoic acid could be derived from the C-ring,

while 2,4,6-trihydroxybenzaldehyde could be derived from the A-ring by further degradation of the [Q-C_7H_5O]$^-$ structure, but this structure is not supported by the fragmentation of the [Q-$C_8H_5O_3$]$^-$ ion.

Lastly, if nucleophilic attack was to occur at the C4 carbon and the B-ring was the leaving group, then the charged hydroxylated degradant would be [Q-$C_8H_5O_2$]$^-$ (m/z 169.0142). Fragmentation of this ion also generates the m/z 125.0250 signal, which supports that this ion is an A-type ion. If nucleophilic attack were to be accompanied by the A-ring leaving, then the charged hydroxylated degradant would be [Q-C_6H_5O]$^-$ (m/z 209.0092); however, this ion was not observed during analysis.

High molecular weight degradation products (m/z 255.0309, 271.0237, 273.0373 and 285.0379) formed by small molecule loss were observed in trace amounts and did not appear to be significant players during degradation (Table 1).

3.6 Conclusion

At weakly acidic and at physiological pH, aqueous solutions of quercetin deprotonated spontaneously into [Q-H]$^-$ and followed similar oxidative degradation pathways within solution. Upon heating the solution, the increased kinetic energy provided a chance to accelerate the oxidative degradation process and the use of continuous flow kinetic MS allowed the ability to monitor the degradation products and provided some insight into the degradative mechanisms.

In addition to oxidation and autoxidation, cross-ring cleavage products were observed and increased over time with heating, as the [Q-H]$^-$ and [Q-2H]$^{2-}$ signals decreased. Cross-ring cleavage degradant ions were proposed to be formed from oxidation of a 2,3,4-chalcantrione, which resulted in two A-type and two B-type like ions. The most favored degradant products within the twenty minute time frame were proposed to be 2,4,6-trihydroxymandelate and 2,4,6-trihydroxyphenylgloxylate. Considering the reported endpoints of quercetin are 3,4-dihydroxybenzoic acid and 2,4,6-trihydroxybenzaldehyde, these ions may be intermediate structures which lead to further degradation with time.

3.7 Acknowledgements

The authors gratefully acknowledge Shimadzu Scientific Instruments, Inc. for their support of instrumentation through the Shimadzu Equipment Grants for Research Program.

Chapter 4

Oxidative Degradation Of Quercetin With Hydrogen Peroxide Using Continuous Flow Kinetic Electrospray-Ion Trap-Time Of Flight Mass Spectrometry

4.1 Abstract

The time-dependent hydrogen peroxide-induced oxidative degradation of aqueous quercetin at pH 7.4 was measured using an in-house built on-line continuous flow device made of concentric capillary tubes, modified to fit a photodiode array (PDA) detector and the inlet of an electrospray ionization – ion trap – time-of-flight – mass spectrometer (ESI-IT-TOF-MS). Comprehensive time-resolved measurements were made on mixed solutions of quercetin and varying amounts of hydrogen peroxide (2-4 mM), which were allowed to react within the time range of 3 to 21 minutes. As the reaction time or concentration of hydrogen peroxide was increased, the deprotonated quercetin ion signal, $[Q\text{-}H]^-$, decreased and formation of degradation product ions were observed. Structures for degradation product ions were proposed using higher order tandem mass spectrometry (up to MS^3) and high mass accuracy. The determined degradation pathways included oxidation, hydroxylation, cyclic peroxidation, ring-cleavage, and small molecule loss. The most intense degradation product observed was 2,4,6-trihydroxybenzoate. It was proposed that this structure was the endpoint of the peroxidation pathway and that it was the favored pathway under these conditions. This pathway is believed to be the result of nucleophilic attack by hydrogen peroxide at the C2 position of quercetin. This was followed by a cross ring cyclic peroxidation event at C2-C4, which resulted in an intermediate depside that was defined by C-ring opening due to loss of C3-OH and cleavage of the peroxy bond. Further cleavage of the depside resulted in the 2,4,6-trihydroxybenzoate. A sodiated pseudo adduct of the dimerized trihydroxybenzoate was believed to be induced under electrospray conditions. Overall, 22 quercetin-related ions were observed. A computational study using density functional theory (DFT) was performed to further justify the position within the C-ring for both the attack by nucleophilic oxidants and the cyclic peroxidated intermediate structure.

4.2 Introduction

Quercetin is one of the most abundant dietary flavonols and can be found in significant quantities as a glycoside in teas, red wine and onions [143]. In addition to its promising potential to reduce the risk

of cancer, quercetin has been shown to be a natural histamine reducer and an effective anti-inflammatory agent [144-146]. Some theories suggest that the quercetin aglycone may be involved in several signal transduction pathways and has been shown to interact with key receptors involved with development of cancers, inflammation and carcinogenesis [147]. Although it has been linked as being bioactive in some *in vivo* studies, the mechanisms of quercetin's physiological chemistry are still unproven.

Of all the flavonoid compounds, quercetin has been shown to be the most effective at scavenging reactive oxygen species (ROS) *in vitro* [148]. Because of this antioxidant characteristic, it is no surprise that quercetin has drawn significant interest in the supplement market and food industry. A recent study of improving nutrients in vegetables has even shown organic tomatoes to have a 79% increase in quercetin compared to tomatoes grown conventionally [149]. The protective nature of the compound may be a primary reason behind some of the related therapeutic benefits of organic vegetables.

The antioxidant characteristics of quercetin can be correlated to the many pharmacophores of its chemical structure (Figure 4.1). The catechol-like structures that can be formed between the hydroxyl group at C5 and the C4 keto group and between the hydroxyl group at C3 and the C4 keto group, as well as the o-dihydroxy structure located on the B-ring, allows for free radical neutralization via hydrogen atom donation. Quercetin becomes a free radical during the process, but due to electron delocalization, a characteristic of phenoxy radicals, the species is too low in energy to react [150,151]. These attributes provide multiple facets for quercetin to contribute to the body's antioxidant shield, providing balance against the oxidative attack of ROS.

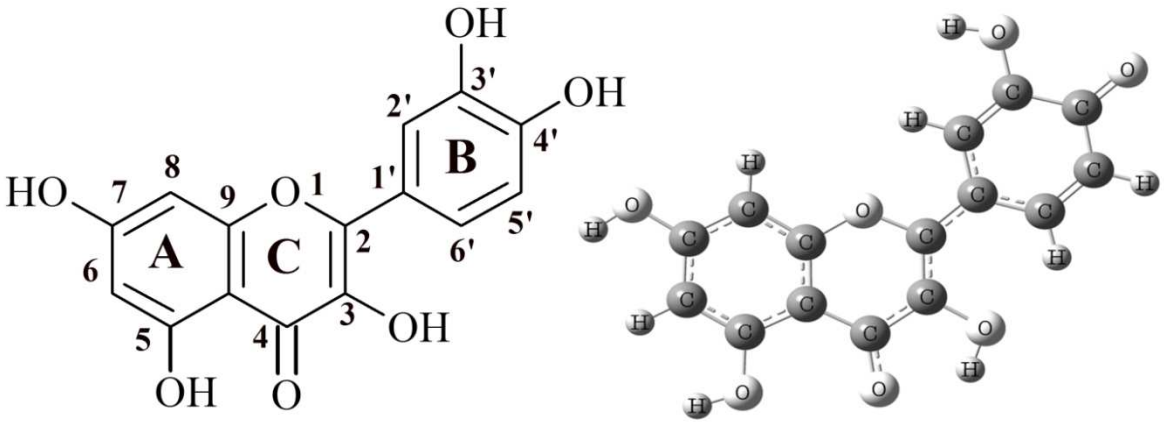

Figure 4.1: The generic resonance structure of quercetin and the deprotonated quercetin anion $[Q\text{-}H]^-$ in its lowest energy configuration (LEC) using Gaussian 03 and optimized with DFT/B3LYP and a 6-31G basis set.

One of the most common ROS in the body is hydrogen peroxide (H_2O_2). In addition to hydrogen peroxide being a non-radical ROS, decomposition of hydrogen peroxide in aqueous solution leads to formation of hydroxyl and hydroperoxyl radicals [152]**.**

$H_2O_2 \rightarrow 2\ ^{\bullet}OH$ <*UV Photolysis*>

$^{\bullet}OH + H_2O_2 \quad \bullet HO_2 + H_2O$

Although it may have some protective function in the urinary system, H_2O_2 has been commonly considered a cytotoxin [153]. Despite the fact it is commonly used around households to clean wounds, H_2O_2 may lead to further tissue injury [154]. This sterilizing agent is often used in aseptic packaging techniques and is commonly employed in wine production to oxidize sulfites, reducing allergic reactions. Hydrogen peroxide may also be used to decontaminate apples infected with *E. coli* [155].

Many studies have focused on quercetin's ability to shield against H_2O_2-induced DNA damage, even in trace amounts above 10 μM, by presumably scavenging the generated free radicals [156-159]. Lipid peroxidation may also be slowed by quercetin through scavenging of hydroxyl radicals spawned by UV photolysis of hydrogen peroxide [160]. In contrast, quercetin was suggested to combat lipid peroxidation by generation of hydrogen peroxide by donating protons from its hydroxyl groups to superoxide radicals [161]. This flavonol also plays a role in inhibiting platelet functions, such as platelet aggregation and platelet adhesion. These functions are believed to be driven by a signal pathway that

includes a burst of hydrogen peroxide, which may explain the link between red wine consumption and reduced risk of cardiovascular disease [162]. To fully understand how quercetin may provide health benefits, the study of quercetin's interaction with hydrogen peroxide and the nature of the resultant oxidative degradation products, should be considered a topic of substantial significance.

There are a few options for studying quercetin's degradation pathways. The polyphenolic structure has strong absorption of UV-A (λ_{max} = 365 nm) and UV-C light (λ_{max} = 256 nm), which may provide photoprotective mechanisms in plants. Small changes to the skeletal structure could disrupt electron delocalization, so that by monitoring the UV spectrum, kinetic information on degradation reaction can be obtained. Some quercetin degradation pathways studied in this fashion have included UV-induced, electrochemical, free-radical, enzymatic, metal catalyzed, and autoxidation degradation [163-165]. Unfortunately, the multitude of species generated (up to 22 in studies by Zhou *et al.* [163]), combined with secondary oxidation events, can make the data convoluted and difficult to interpret. Without proper hyphenation, the results are limited to determining bulk antioxidant character and degradation rates and do not offer clues for elucidating degradative mechanisms or specific structural details of related reaction products.

The polyphenolic structure of quercetin also provides facile ionization which makes electrospray ionization mass spectrometry and tandem mass spectrometry (ESI-MS^n) ideally suited to supplement UV data, allowing qualitative identification and structural characterization by fragmentation**.** A few studies have used this technique to characterize quercetin degradation pathways. Buchner *et al.* proposed thermal degradation of quercetin lead to cross-ring cleavage and solvent adducts formed by nucleophilic attack at C2 [150]. Along with solvent adducts, Hvattum *et al.* demonstrated degradation of quercetin by loss of CO at the C3 position when reacted with a free radical generator, 2,2-diphenyl-1-picrylhydrazyl (DPPH) [167]. Zhou *et al.* completed an extensive comparative study of quercetin degradation by electrochemical, air oxidation, enzymatic and the free radical generator, azobisisobutyronitrile (AIBN) [163,168]. They proposed that quercetin hydroxylated at the C2 position could lead to three separate pathways, one that follows the C-ring opening at the O1-C2 bond, one with C-ring opening at the C2-C3 bond, and one with C-ring opening at the C3-C4 bond.

Problems associated with natural product research and mass spectrometry include high costs of standard, indistinguishable tandem spectra between similar species, and multiple formulaic possibilities due to nominal mass. These issues can be overcome by using ion trap-time of flight (IT-TOF) mass detection, which provides the potential for definitive identification through structural characterization with higher order fragmentation and exact formula determination with high mass accuracy, and which has been demonstrated before for investigating polyphenolic compounds [169,170]. Previously, the authors combined ESI-IT-TOF-MS with an in-house built capillary mixer with an adjustable reactor volume (motivated by Wilson and Konnermann [171]) to collect time-resolved mass spectral measurements of thermal degradation of quercetin in weakly acidic aqueous media and at physiological conditions [172]. In that study, it was proposed that thermally accelerated degradation followed a pathway that included a hydroxylation event at C2, which was proposed to lead to ring-cleavage starting by C-ring opening at the O1-C2 bond. This led to a chalcan-trione intermediate structure. It was suggested that further nucleophilic attack of the chalcan-trione at the C2, C3, and C4 carbons resulted in A-type and B-type ions, of which the most preferred led to the A-type ions, 2,4,6-trihydroxy-2-oxo-2-phenylacetate and 2,4,6-trihydroxy-2-hydroxyl-2-phenylacetate ions.

Ab initio and semi-empirical computational studies of quercetin's reactivity can provide insight into degradation pathways and solidify the understanding of how it neutralizes free radicals. By evaluating bond dissociation energy (BDE) and reaction energies, it has been proposed that quercetin reacts with free radical ROS through hydrogen atom transfer (HAT) and that the activity is focused in the B and C-ring [173-177]. In addition, interpretation of spin densities and charge distributions have consistently shown the C2 position in the C-ring to be the favored site for nucleophilic attack by single and double oxygen species[165,174,177,178].

To witness the kinetic characteristics of the reactivity between aqueous quercetin and hydrogen peroxide, an in-house built online capillary mixing device with an adjustable reactor volume was connected to a photodiode array detector. The eluent then was led into the electrospray inlet of an ion trap – time-of-flight (IT-TOF) MS system. The reaction time (3.1 – 21.3 min) and hydrogen peroxide concentration (2-4 mM) could be controlled by making adjustments to the device. Incorporation of continuous flow kinetic measurements with UV/Vis, MS^n, and high mass accuracy allowed for a novel in-

depth study of the interaction between quercetin and free radical species associated with hydrogen peroxide degradation. This embodiment and application of a combined on-line and mass spectrometry-based degradation study has not been previously conducted.

4.3 Methods and Equipment

4.3.1 Reagents and Solution

Aqueous solutions of quercetin (65 µM) were adjusted to pH 7.4 with sodium hydroxide (0.1N) as described previously [172]. Fresh solutions were prepared at each measured time point. Hydrogen peroxide (0.1% v/v) was prepared by diluting hydrogen peroxide (3%; Walgreens, Deer Field, IL, USA) with LCMS-grade water (Burdick and Jackson, Muskegon, MI, USA).

4.3.2 Kinetic Device

Kinetic measurements were performed using a continuous-flow device which was built in-house (Figure 4.2) and consisted of two concentric capillary tubes. Two 2.5 mL glass syringe (7.284 mm internal diameter (I.D.); Hamilton, Reno, Nevada, USA) were connected to a micro-mixing tee (IDEX, Lake Forest, Illinois, USA) via one foot lengths of polyetheretherketone (PEEK) tubing (1/16” O.D.; 0.005” I.D.). A five foot length of flourinated ethylene propylene (FEP) tubing (400 µm I.D.; 1000 µm O.D.) was connected to the outlet end of the mixing tee. The downstream end of the FEP tubing was inserted over a five foot length of PEEK tubing (100 µm I.D.; 360 µm outer diameter (O.D.)). A stainless steel union (0.052” thru-hole) was slid over the FEP tubing 2 inches from the downstream end of the outer capillary and tightened with a fitting and a ferrule to seal any leaks. The downstream outlet end of the PEEK tubing (outer capillary) was connected to a PDA which in turn was connected to the inlet of the ESI. The syringes were driven by two syringe pumps (NE-1010, New Era Pump Systems, Farmingdale, NY, USA).

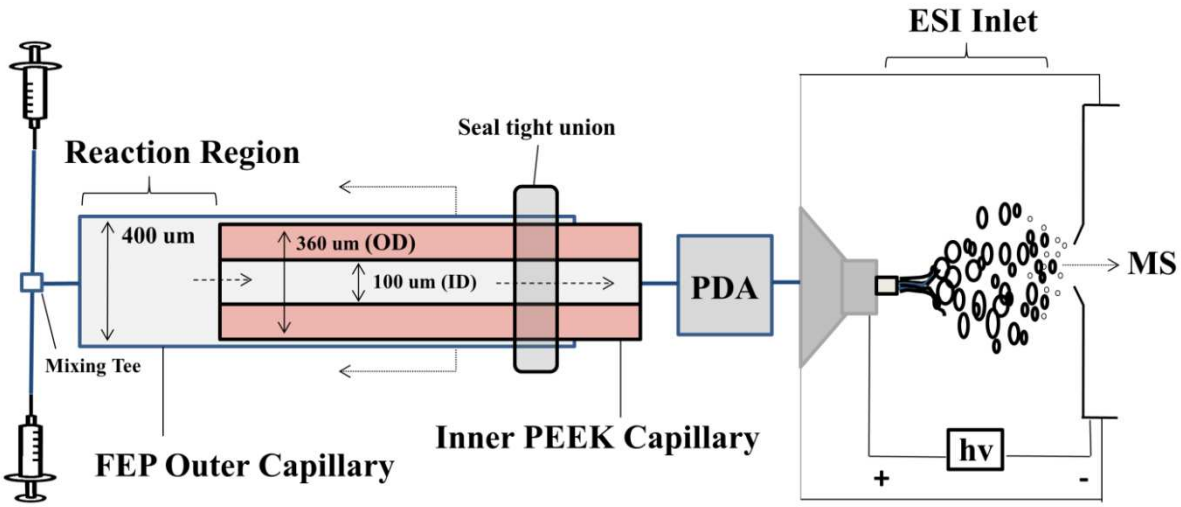

Figure 4.2: An online kinetic continuous flow device constructed from two concentric capillary tubes that interfaces with UV and MS detection.

By moving the inner capillary, the volume of the reaction region was controlled, which allowed the ability to regulate the amount of reaction time after mixing. The aqueous solution of quercetin was pumped through one syringe at a flow rate of 10.0 µl/min. Hydrogen peroxide was introduced using the other syringe and was pumped at flow rates of 0.5, 1.0 and 1.5 µl/min. These conditions resulted in solutions that contained quercetin concentrations of 57, 59 and 62 µM and hydrogen peroxide concentrations of ~ 2, 3 and 4 mM, respectively. Kinetic measurements were made by pulling the inner PEEK tubing out at 1 foot intervals. In the configuration in which the device had no extension (minimum dwell time), the total system volume was estimated to be 36 µL, based on 5 feet of inner tubing, 2 inches of outer tubing (seal union overlap), semi-micro flow cell with a 10 µl capacity and ~1 foot of PEEK tubing (0.005" ID) connecting the PDA to the ESI inlet, which made up the flow path downstream of the micro-mixer. At the combined flow rates of 10.0, 10.5, 11.0 and 11.5 µl/min, this allowed for measurements ranging from 3.6 to 22.4, 3.4 to 21.3, 3.3 to 20.3 and 3.1 to 19.4 minutes of reaction time, respectively.

4.3.3 Instrumentation

UV/Vis spectra were collected using a Prominence SPD-M20A diode array detector (Shimadzu Scientific Instruments, Inc., Kyoto, Japan) set to acquire between 200 and 800 nm. Negative ion MS spectra were obtained using an ion trap - time of flight mass spectrometer (IT-TOF-MS, Shimadzu Scientific Instruments, Inc., Kyoto, Japan) equipped with a conventional electrospray ionization (ESI)

source. Analytical parameters for ionization, fragmentation, and detection were: interface voltage, -3.5 kV; nebulizing gas (N_2), 1.5 L/min; drying gas (N_2), 10 L/min; curved desolvation line, 250 ℃; detector voltage, 1.92 kV; ion accumulation time, 10 ms; precursor ion isolation width, 0.1 amu; collision gas (Ar), 50%; and frequency constant (q), 0.251. The estimated resolution of the instrument is 10,000 at m/z 1000. A scanning rate of 100 ms was used. The estimated duty cycle at MS^3 with these settings was < 0.5 seconds. The collision energy during collision-induced dissociation (CID) was adjusted at each tandem MS stage to determine the optimum parameters at which a maximum amount of signal information would be obtained. The IT-TOF was calibrated to < 5 ppm error in mass accuracy using a solution of sodium trifluoroacetate.

Data collection and analysis were carried out using *LCMS Solutions* version 3.4 software. The *Accurate Mass Calculator* and *Formula Predictor* software tools were used to support determination of theoretical *m/z* values and elemental formulas of observed fragments. The software was configured to recommend formulaic possibilities based on the following requirements: 1-15 carbons, 0-10 oxygens, 0-15 hydrogens, 0-1 sodium, and within 25 ppm error. Isotopic ratios were also evaluated.

4.3.4 Computational Modeling

Three-dimensional Cartesian coordinates for structures of quercetin and related oxidated ions were submitted to Gaussian 03 [179] for optimization using DFT/B3LYP and a 6-31G basis set. The lowest energy conformation (LEC) was obtained by allowing the software to optimize the atoms in three dimensions.

4.4 Results

4.4.1 Time-Resolved Measurements of Aqueous Quercetin Mixed with Hydrogen Peroxide

Changes in the UV and mass spectra due to increasing reaction time were evaluated by maintaining the same flow of the syringe pumps and increasing the length of the reaction chamber. Since the most activity in terms of degradation of $[Q\text{-}H]^-$ and formation of degradation products was observed at the 1.5 µl/min flow rate for H_2O_2, the results described below are from that data set.

4.4.1.1 Changes in UV/Vis Spectra

The UV/Vis spectral profile of quercetin in water was characterized by three distinct bands (I, II, and III) that had maxima at 384, 322 and 270 nm, respectively (Figure 4.3). Absorbance of band I has

been associated with the cinnamoyl system of the B-ring and the absorbance of band II has been associated with the benzoyl system of the A-ring. Band III has been connected with quinonic structures [180,181]. As H_2O_2 began to be mixed with quercetin, a decrease in the absorbance of bands I and II was observed. As the reaction time was extended, the absorbance of band I further decreased and a hypochromic shift of the maximum of band I from 384 nm to 360 nm was noted. A further decrease in intensity was also noted in band II as the reaction time was extended. In contrast, after the initial addition of H_2O_2, the absorbance in band III increased at the 3.1 min and 6.5 min mark and then decreased at 9.9 and 16.6 min. Between 16.6 and 19.4 min, no change in band III was noted. A slight increase around 294 nm was seen at the 19.4 min mark. Two isosbestic points were noted at 285 nm and 364 nm.

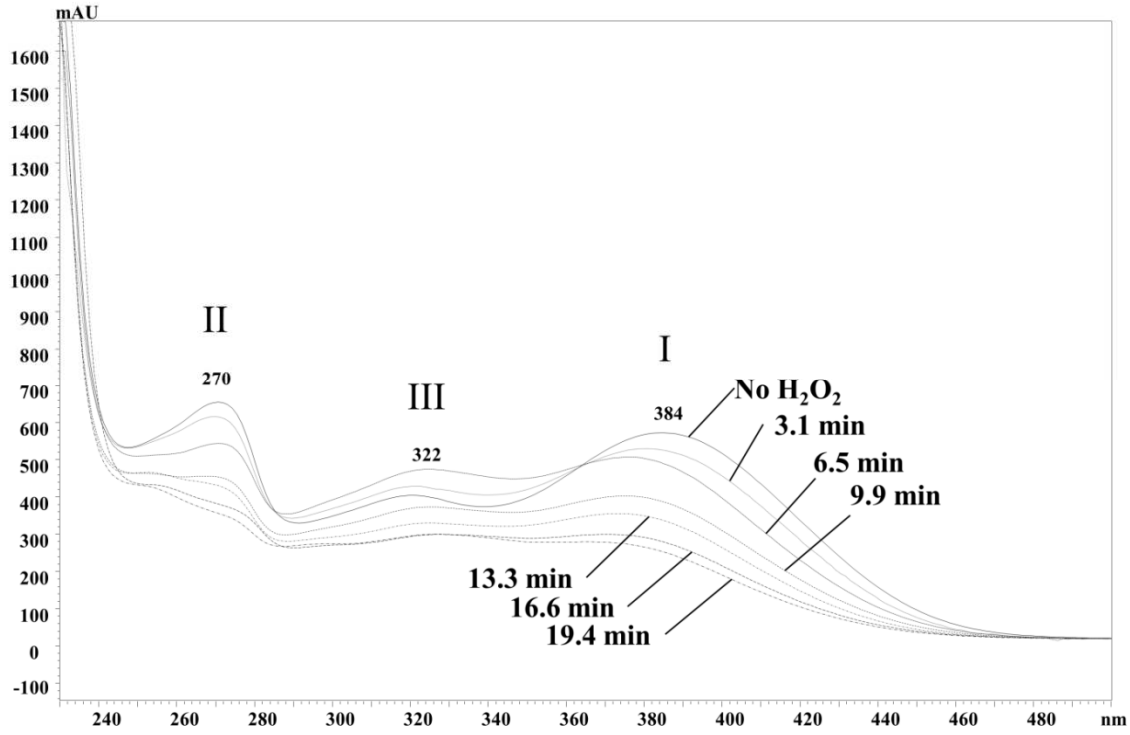

Figure 4.3: Changes to the UV/Vis spectral profile with increasing reaction time after mixing 65 µM quercetin (pH7.4) and 0.1% H_2O_2 at a ratio of 10:1.5 ul/min

4.4.1.2 Mass Spectral Analysis at Room Temperature

The signal for the deprotonated quercetin ion $[Q\text{-}H]^-$ (m/z 301.0343) has a significant intensity in the negative mode and can be easily observed at relatively low concentrations. This signal was the base

peak observed in the spectra at room temperature. Although some quercetin-related ions were observed in the positive mode, they were not observed at significant intensity levels for informative analysis during any of the test conditions, and therefore, are not discussed in this assessment.

Evaluation of the $[Q\text{-}H]^-$ signal intensity over long periods showed that aqueous solutions of quercetin at a concentration of 65 µM and at pH 7.4 were relatively stable for >6 hours at room temperature. In addition, a trace signal for $[Q\text{-}2H]^{2-}$ and $[2Q\text{-}H]^-$ (m/z 150.0135 and 603.0754) was observed at a level below 1% relative intensity. Other quercetin-related signals that could be observed at room temperature were classified into three categories: 1) simple oxidation events, 2) hydroxylated and peroxidated structures, 3) sodiated adducts, and 4) ions with small molecule loss (Table 1). The signals for $[Q\text{-}H_2\text{-}H]^-$ and $[Q\text{-}2H]^{\bullet-}$ at m/z 299.0189 and 300.0263, observed at 4% and 8% relative intensity, represent the initial oxidation events quercetin undergoes in aqueous solution. Two hydroxylated structures, $[Q+O\text{-}H]^-$ and $[Q+O\text{-}2H]^{2-}$ at m/z 317.0290 and 158.0108, were observed at 4% and <<1% relative intensity. Three sodiated structures, $[Q\text{-}H_2+Na]^-$ (<1% relative intensity), $[Q+O\text{-}H_2+Na]^-$ (<1%), and $[Q\text{-}H+2Na]^-$ (13%) at m/z 323.0141, 339.0117 and 347.0223, respectively, were observed and were believed to be formed due to influence from electrospray ionization [182,183]. Finally, trace amounts of signals at <1% relative intensity at m/z 273.0394 and 271.0239 were observed and were identified as $[Q\text{-}CO\text{-}H]^-$ and $[Q\text{-}CO\text{-}H_2\text{-}H]^-$ based on high mass accuracy.

Table 4.1: The adduct and degradant ions observed in aqueous solutions of quercetin at pH 7.4.

Deprotonated, Sodiated and Simple Oxidated Ions					
Ion Identity	**Proposed Identity**	**Formula**	**Theoretical m/z**	**Observed m/z**	**Error, ppm**
[Q]	quercetin	$C_{15}H_{10}O_7$	302.0427	------	-----
$[Q-H]^-$	quercetin monoanion	$C_{15}H_9O_7$	301.0354	301.0343	-3.7
$[2Q-H]^-$	quercetin dimer anion	$C_{30}H_{19}O_{14}$	603.0780	603.0754	-4.3
$[Q-2H]^{2-}$	quercetin dianion	$C_{15}H_8O_7$	150.0141	150.0135	-4.0
$[Q+2Na-H]^-$	disodiated quercetin anion	$C_{15}H_9O_7Na_2$	347.0149	347.0223	21.3
$[Q-2H]^{\bullet-}$	quercetin radical anion	$C_{15}H_8O_7$	300.0276	300.0263	-4.3
$[Q-H_2-H]^-$	quercetin *o*-quinone anion	$C_{15}H_7O_7$	299.0197	299.0189	-2.7
$[Q-H_2+Na]^-$	sodiated quercetin *o*-quinone anion	$C_{15}H_8O_7Na$	323.0154	323.0141	-4.0
Hydroxylated and Peroxidated Ions					
Ion Identity	**Proposed Identity**	**Formula**	**Theoretical m/z**	**Observed m/z**	**Error, ppm**
$[Q+O-H]^-$	2,3,4-chalcan-trione monoanion	$C_{15}H_9O_8$	317.0303	317.0290	-4.1
$[Q+O-H_2-H]^-$	*o*-quinone 2,3,4-chalcan-trione anion	$C_{15}H_7O_8$	315.0146	315.0131	-4.8
$[Q+O_2-H]^-$	2,4-peroxyl quercetin	$C_{15}H_9O_9$	333.0252	333.0242	-3.0
$[Q+O-2H]^{2-}$	2,3,4-chalcan-trione dianion	$C_{15}H_8O_8$	158.0115	158.0108	-4.4
$[Q+O-H_2+Na]^-$	sodiated 2,3,4-chalcan-trione anion	$C_{15}H_8O_8Na$	339.0122	339.0117	-1.5
$[Q+O_2-H_2+Na]^-$	sodiated 2,4-peroxyl quercetin anion	$C_{15}H_8O_9Na$	355.0072	355.0058	-3.9

Table 4.1 Continued

Degradation Products Ions					
Ion Identity	**Proposed Identity**	**Formula**	**Theoretical m/z**	**Observed m/z**	**Error, ppm**
$[Q\text{-}C_7H_5O]^-$	2,4,6-trihydroxy-2-oxo-2-phenylacetate	$C_8H_5O_6$	197.0092	197.0086	-3.0
$[Q\text{-}C_7H_7O_2]^-$	3,4-dione-2-oxo-2-phenylacetate	$C_8H_3O_5$	178.9986	178.9979	-3.9
$[Q\text{-}C_8H_5O_2]^-$	2,4,6-trihydroxybenzoate	$C_7H_5O_5$	169.0142	169.0140	-1.2
$[(Q\text{-}C_8H_5O_2)_2+Na]^-$	sodiated 2,4,6-trihydroxybenzoate dimer	$C_{14}H_{10}O_{10}Na$	361.0177	361.0168	-2.5
$[Q\text{-}C_8H_5O_3]^-$	3,4-dihydroxybenzoate	$C_7H_5O_4$	153.0193	153.0186	-4.6
$[Q\text{-}C_8H_7O_3]^-$	3,4-dione-benzoate	$C_7H_3O_4$	151.0037	151.0031	-4.0
Small Molecule Loss Ions					
Ion Identity	**Proposed Identity**	**Formula**	**Theoretical m/z**	**Observed m/z**	**Error, ppm**
$[Q\text{-}CO\text{-}H]^-$	4-(4,6-dihydroxy-oxo-2,3-dihydro-1-benzofuran-2-yl)-2-hydroxyphenolate	$C_{14}H_9O_6$	273.0405	273.0394	-4.0
$[Q\text{-}CO\text{-}H_2\text{-}H]^-$	2-(3,4-dioxocyclohexa-1,5-dien-1-yl)-6-hydroxy-3-oxo-2,3-dihydro-1-benzofuran-4-olate	$C_{14}H_7O_6$	271.0248	271.0239	-3.3
$[Q+O_2\text{-}CO\text{-}H]^-$	Quercetin depside anion	$C_{14}H_9O_8$	305.0303	305.0293	-3.3

4.4.1.3 Reaction with 3% Hydrogen Peroxide

Upon addition of 3% hydrogen peroxide with 65 µM quercetin (a post-mixed H_2O_2 concentration of 0.3%) at the minimum dwell time allowed by the device (3.1 minutes), the $[Q\text{-}H]^-$ signal disappeared immediately and two signals at m/z 169.0140 and 361.0168 were observed. Based on mass accuracy they were determined to be ions with an elemental formula of $C_7H_5O_5$ and $C_{14}H_{10}O_{10}Na$, respectively. The latter structure was proposed to be a sodiated dimer of the former (see Discussion), and would therefore make these two ions $[Q\text{-}C_8H_5O_2]^-$ and $[(Q\text{-}C_8H_5O_2)_2+Na]^-$, respectively. These two signals were seen in similar intensities and were the largest signals seen in the spectra. Numerous other quercetin-related signals could also be observed after addition of hydrogen peroxide that were not previously observed in unmixed quercetin solutions. The concentration of hydrogen peroxide being mixed was lowered

systematically until the signals for $[Q\text{-}C_8H_5O_2]^-$ and $[(Q\text{-}C_8H_5O_2)_2+Na]^-$ were no longer observed above 1% relative intensity and the intensity of the $[Q\text{-}H]^-$ was unaffected. The post-mixed concentration of hydrogen peroxide was 0.009% (~3 mM) when this was achieved. The ion signals forming from the simple oxidation events, $[Q\text{-}H_2\text{-}H]^-$ and $[Q\text{-}2H]^{\bullet-}$ appeared to also be unaffected at this concentration.

The presence of the hydrogen peroxide did appear to hinder the formation of some of the ions observed in the unreacted aqueous solutions, as the $[Q\text{-}2H]^{2-}$, $[2Q\text{-}H]^-$, and $[Q\text{-}H_2+Na]^-$ ions could no longer be discernible from the baseline after mixing quercetin with even low levels of H_2O_2. The hydroxylated ion signals $[Q+O\text{-}H]^-$ and $[Q+O+Na\text{-}H_2]^-$ increased significantly (10% and 2% relative intensity) and two peroxidated ion signals $[Q+O_2\text{-}H]^-$ and $[Q+O_2+ H_2\text{-}Na]^-$ could be observed at trace levels below 1% relative intensity, which were previously unidentifiable before mixing. Additionally, the small molecule loss signals $[Q\text{-}CO\text{-}H]^-$ and $[Q\text{-}CO\text{-}H_2\text{-}H]^-$ increased to 4% relative intensity.

4.4.1.4 Changes in MS Spectra Based on Increasing Reaction Time

To reduce the inherent variability of ion intensities observed over the course of many days and multiple preparations of reagents, quercetin, and product ions intensities were normalized as a percent of total ion intensity. As can be seen in Figures 4.4 and 4.5, as the reaction time was increased, the intensity of the $[Q\text{-}H]^-$ signal was observed to decrease, reaching 13% of the total ion intensity at 19.4 minutes. In contrast, the intensity of the ions $[Q\text{-}C_8H_5O_2]^-$ and $[(Q\text{-}C_8H_5O_2)_2+Na]^-$ grew as the reaction time was extended and reached a maximum of 7% and 28% of the total ion intensity, respectively. By 19.4 minutes, the signal for $[(Q\text{-}C_8H_5O_2)_2+Na]^-$ had become the base peak observed in the spectra. At the 13.3 min mark, trace signals below 0.5% total ion intensity of $[Q\text{-}C_7H_5O]^-$ and $[Q\text{-}C_7H_5O_2]^-$, m/z 197.0086 and 178.9979, respectively, could be observed. These signals increased slightly to a maximum of 0.9% and 0.6% total ion intensity by 19.4 min. At this time point, an ion at m/z 153.0186, $[Q\text{-}C_8H_5O_3]^-$, begun to be observed in trace amounts <0.5% total ion intensity.

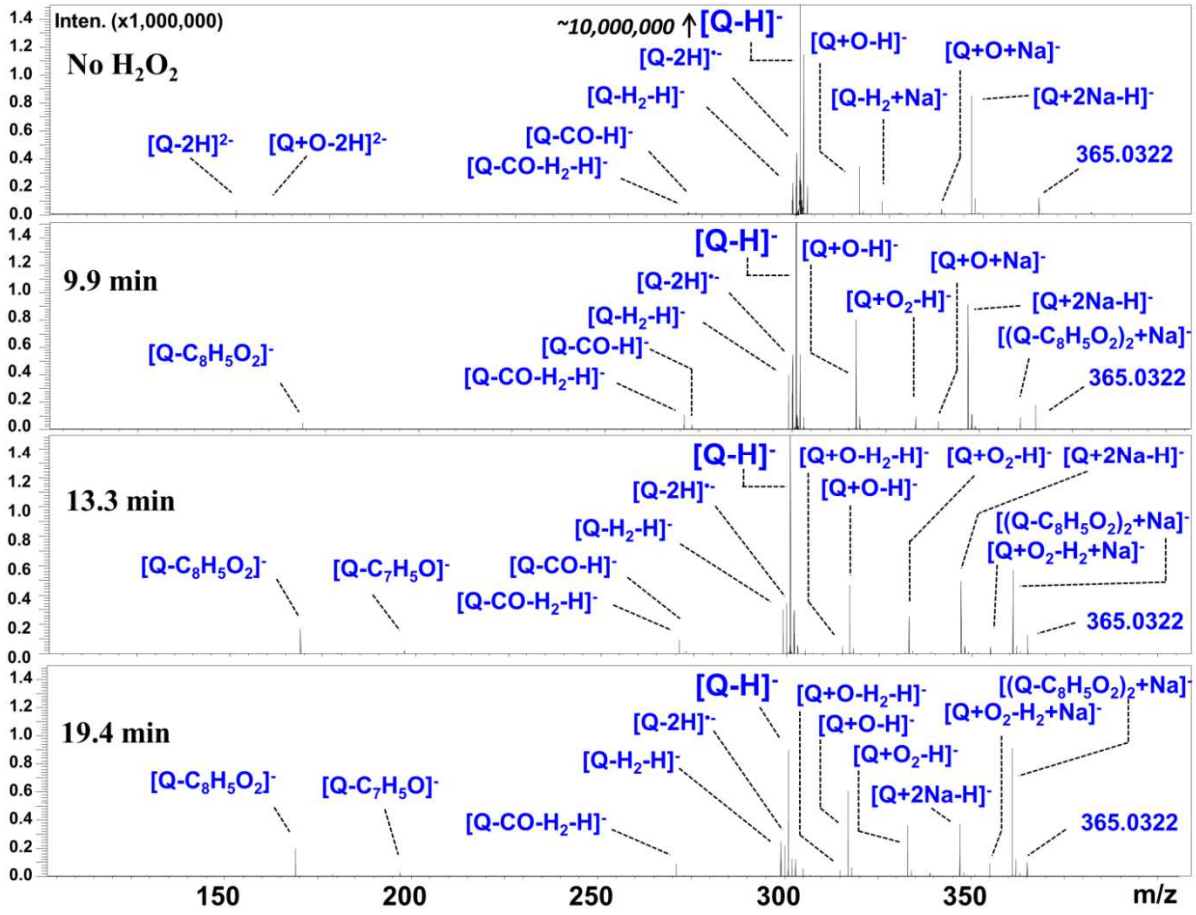

Figure 4.4: Comparative time-resolved spectra in the negative ionization mode after mixing 65 µM quercetin (pH7.4) and 0.1% H_2O_2 at a ratio of 10:1.5 ul/min.

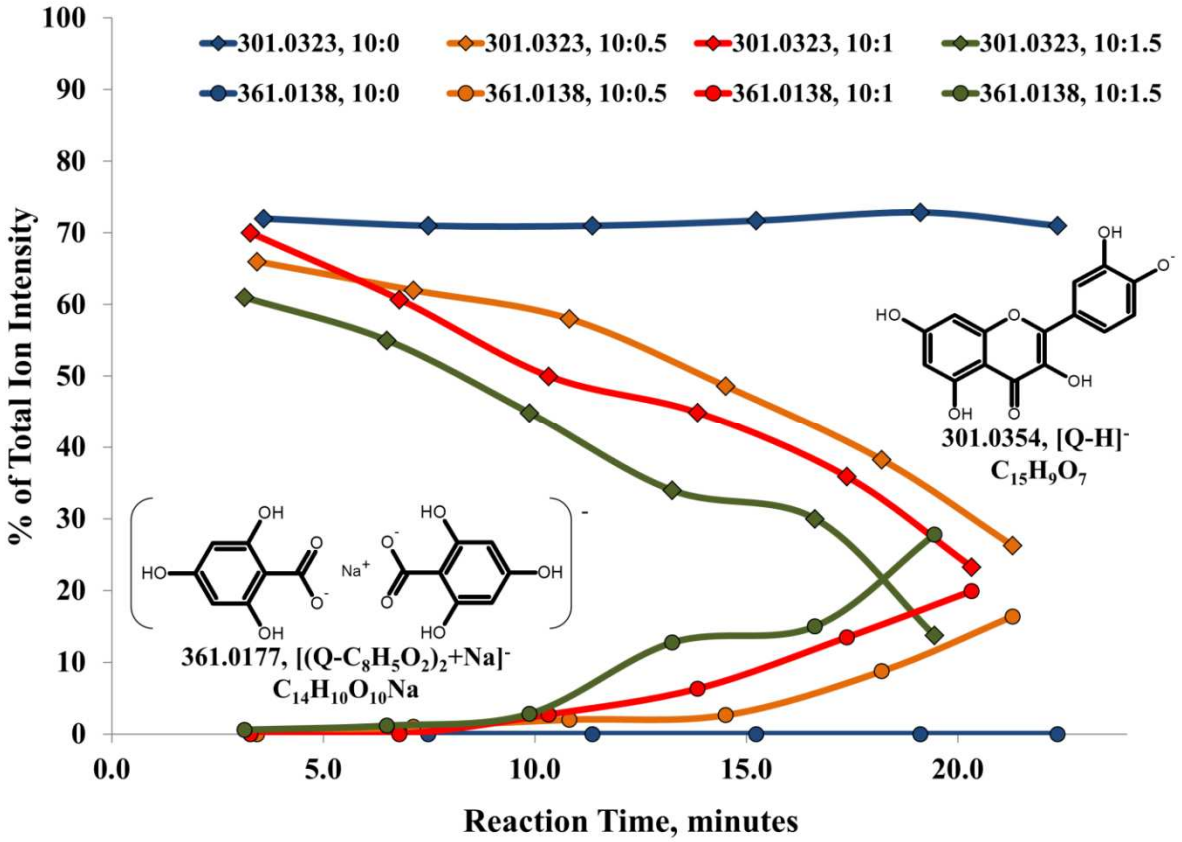

Figure 4.5: A plot of the H_2O_2-dependent oxidative degradation of $[Q-H]^-$ (m/z 301.0354) ion intensity (normalized against total ion intensity) over time. Formation of $[(Q-C_8H_5O_2)_2Na]^-$ (m/z 361.0177) was observed after addition of H_2O_2 and increased with increasing reaction time. The flow rate of quercetin (65 µM) was held constant at 10 µl/min, while the flow rate of the 0.1% H_2O_2 solution was increased from 0.0 µL, 0.5 µL/min, 1.0 µL/min and 1.5 µL/min

To further investigate the origin of the signal at m/z 361.0168, believed to be $[(Q-C_8H_5O_2)_2+Na]^-$, and to confirm it was a sodiated dimer of 2,4,6-trihydroxybenzoate (m/z 169.0142), quercetin solutions were prepared with KOH instead of NaOH and reacted with H_2O_2. The ion signal at m/z 169.0140 was observed, however, a signal near m/z 361.0177, $[(Q-C_8H_5O_2)_2+Na]^-$ was not observed (data not shown). A small ion with ~1% relative intensity at m/z 376.9917, which would correspond to the parent ion being $[(Q-C_8H_5O_2)_2+K]^-$, was observed. Fragmentation of this signal returned a product ion at m/z 169.0133 (Table 2).

Table 4.2: Higher order fragmentation of select quercetin degradation ions.

$[Q\text{-}C_8H_5O_2]^-$ 169.0140	**$[Q+O\text{-}H]^-$ 317.0290**	**$[Q+O_2\text{-}H]^-$ 333.0242**	**$[Q\text{-}H+2Na]^-$ 347.0223**	**$[(Q\text{-}C_8H_5O_2)_2+Na]^-$ 361.0168**	**$[(Q\text{-}C_8H_5O_2)_2+K]^-$ 376.9917**
125.0249	163.0068	169.0131	206.9941	125.0242	151.0025
151.0044	191.0010	181.0133	299.0204	151.0045	169.0133
	206.9952	194.9945	300.0257	169.0148*	190.9950
		271.0236	301.0314	343.0029	311.0129
		287.0179			329.0271
		289.0344			
		301.0117			
		305.0294			
*MS^3 of m/z 169.0148 resulted in ions at m/z 151.0032 and 125.0239					

The ion $[Q+O\text{-}H]^-$ increased slightly from 3.1 to 6.5 minutes and reached its maximum of 11% total ion intensity at the 6.5 min mark and then steadily decreased at each time point, reaching 5% total ion intensity at 19.4 min (Figure 4.6). The ion $[Q+O_2\text{-}H]^-$ also increased through 6.5 minutes and continued to increase at the 9.9 min mark reaching a maximum of 6% total ion intensity, and then was observed to decrease steadily at each time point thereafter, reaching 3% at 19.4 min. At the 13.3 min mark, signals for $[Q+O\text{-}H_2\text{-}H]^-$ and $[Q+O_2\text{-}H_2+Na]^-$ could be distinguished above baseline at 0.5% and 1.5% total ion intensity, respectively (Figure 4.4). These signals remained consistent at these levels through 19.4 minutes. A signal at m/z 305.0293 $[Q+O_2\text{-}CO\text{-}H]^-$ also appeared at the 13.3 min mark at 0.7% total ion intensity and remained consistent through 19.4 minutes.

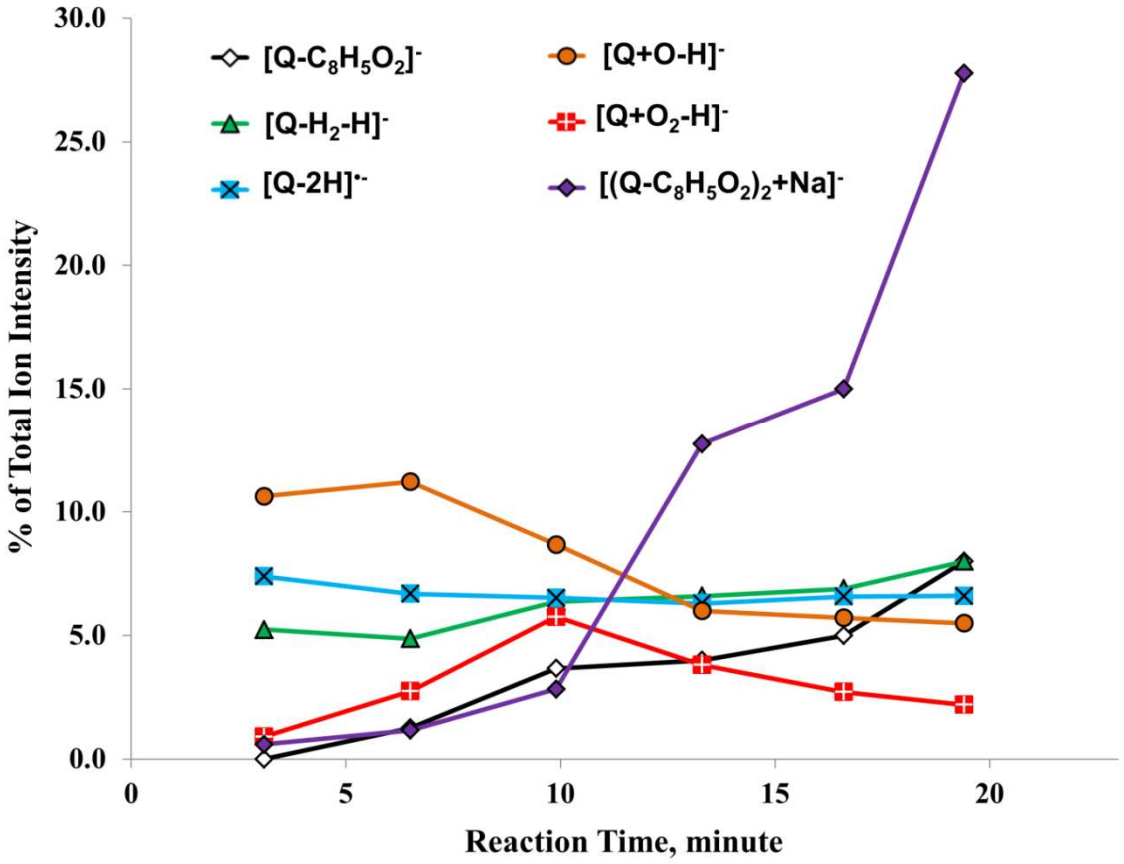

Figure 4.6: A plot of the H_2O_2-dependent oxidative degradation products of quercetin ion intensities (normalized against total ion intensity) over time. The flow rate of quercetin (65 µM) was held constant at 10 µl/min, while the flow rate of the 0.1% H_2O_2 solution was 1.5 µL/min

Many ions were either unaffected or had only a slight change. The intensity for the ions representing the simple oxidation events of quercetin, $[Q\text{-}H_2\text{-}H]^-$ and $[Q\text{-}2H]^{\bullet-}$, increased only slightly and reached a maximum of 6 and 7% total ion intensity for both ions. Ion signals at m/z 273.0394 ($[Q\text{-}CO\text{-}H]^-$) and 271.0239 ($[Q\text{-}CO\text{-}H_2\text{-}H]^-$) also remained at a consistent level compared to the dwell time as the reaction time increased. The ion at m/z 347.0223, tentatively identified as $[Q+2Na\text{-}H]^-$, was consistently near 10% total ion intensity regardless of condition. The identification of the ion as $[Q+2Na\text{-}H]^-$ was based on fragmentation ions (see Table 2); however, it was classified as tentative due to its poor mass accuracy (21 ppm error). Additionally an ion at m/z 365.0315 was observed near 1.5% total ion intensity in all conditions, but its identification was inconclusive.

4.5 Discussion

4.5.1 Acid-base equilibrium and simple oxidation ions

Interpretation of mass spectral intensities should be considered with caution since some inconsistencies in ion intensities may arise for species with multiple charge state distributions or ionization efficiency differences, as compared to what may be the actual concentration of charged species in solution. These inconsistencies may be explained by conditions inherent to the ionization process. In electrospray ionization, release of ions from the surface of highly charged droplets depends heavily on the chemical species present in the droplet and their relative abilities to both acquire a charge and compete for a limited number of sites at the droplet surface [182,184].

Considering the acid-base equilibrium of quercetin in the physiological environment, spontaneous deprotonation would lead to formation of $[Q\text{-}H]^-$ and $[Q\text{-}2H]^{2-}$ ions. Evaluation of the pKa's available in the literature, ion formation from deprotonation would be expected to form from a loss of a proton from the hydroxyl substituent at the C4' position (Figure 4.1). Further deprotonation would be expected at the hydroxyl group at C7 position, since the presence of a negative charge at the 4' position would further hinder another charge at the 3' position [185-187].

Since sample preparations were not sparged or prepared under evacuation of air, it should be assumed that aqueous quercetin would be in the presence of dissolved O_2 and ~250 nM of hydroxyl ions from auto-ionization of water (depending on the pH). In addition to electrospray ionization effects, the presence of trace ROS may contribute to the formation of the simple oxidated quercetin ion $[Q\text{-}H_2\text{-}H]^-$ and the radical ion $[Q\text{-}2H]^{\bullet-}$ in fresh solutions at room temperature. The radical ion $[Q\text{-}2H]^{\bullet-}$ which was observed to be pH-dependent in the previous evaluation of quercetin oxidation, was observed at ~2:1 higher intensities than the $[Q\text{-}H_2\text{-}H]^-$ ion and demonstrates the ability of the quercetin structure to stabilize a radical at ambient temperatures. As hydrogen peroxide is introduced, the levels of ROS would significantly increase, due to the decomposition of hydrogen peroxide into hydroxyl radicals, hydroxyl ions, peroxide radicals, and hydroperoxyl radicals. The notion that ROS promote simple oxidation of quercetin is further supported by the observed increase in the intensity of $[Q\text{-}H_2\text{-}H]^-$ and $[Q\text{-}2H]^{\bullet-}$ after addition of H_2O_2. These simple oxidated ions do not appear to be further affected as the reaction time

increases; only a slight increase in the $[Q\text{-}H_2\text{-}H]^-$ near 20 minutes of mixing was observed (Figures 4.4 and 4.6).

4.5.2 Hydroxylated and peroxidated ions

The hydroxylated adduct of quercetin, $[Q+O\text{-}H]^-$, was also observed at room temperature without the addition of hydrogen peroxide. In the previous kinetic study of thermal degradation of quercetin, the authors suggested that formation of this ion was due to first, hydroxylation at the C2 position to form a 2-hydroxy-3,4-flavonedione, then formation of a 2,3,4-chalcan-trione anion. This was presumably caused by C-ring opening of the 2-hydroxy-3,4-flavonedione at the O1-C2 bond and formation of a double bonded oxygen at C2 (Figure 4.7) [153]. Krishnamachari *et al.* suggested that this chalcan-trione structure would further stabilize into a benzofuran [188]. As H_2O_2 was mixed, the concentration of hydroxyl ions and hydroxyl radicals increased, which lead to increased hydroxylation of quercetin and a nearly two-fold increase in the intensity of this ion, as compared to unreacted solutions of quercetin.

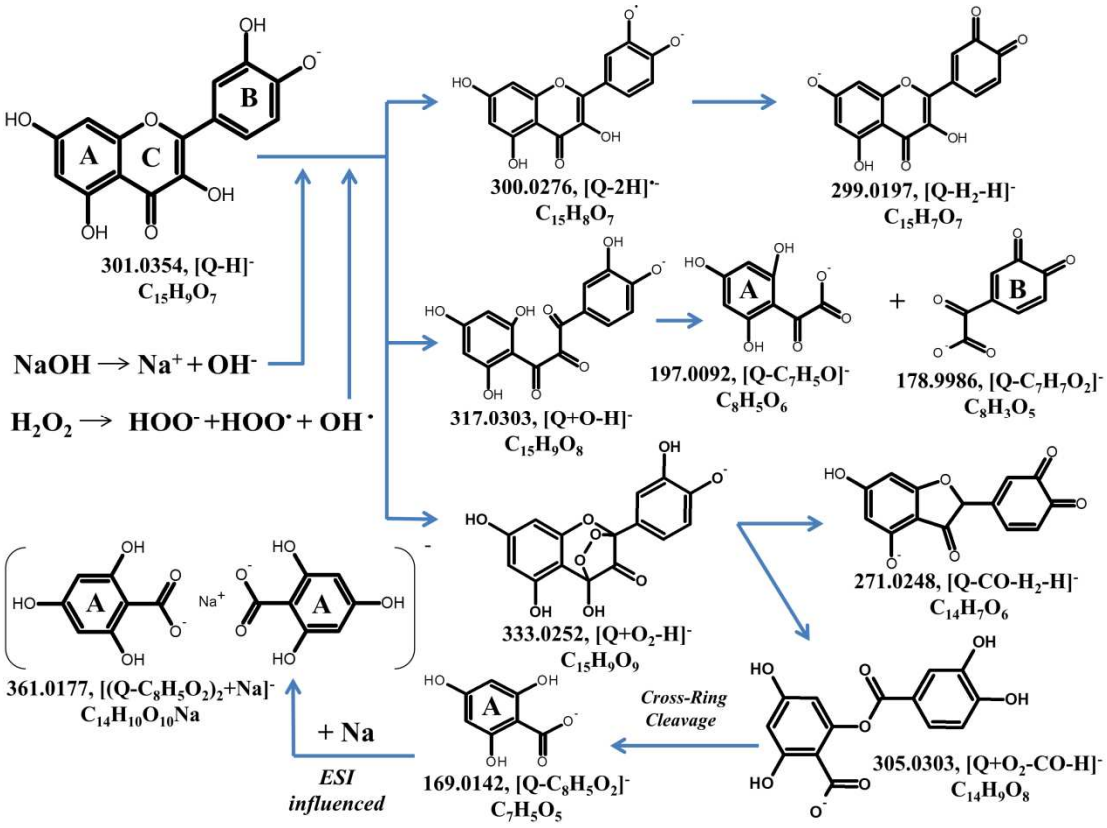

Figure 4.7: Proposed degradation pathways of quercetin in aqueous solutions in physiological conditions when mixed with hydrogen peroxide.

The peroxidated ion $[Q+O_2-H]^-$ was only observed after addition of H_2O_2. It can be assumed that the ion formation may be attributed to the reaction between quercetin and nucleophilic attack by hydrogen peroxide. Evaluation of the mulliken charges for the deprotonated quercetin $[Q-H]^-$ shows C2 as having the highest partial positive charge, and represents the carbon in the C-ring that has the most carbocation characteristics and reactivity (Figure 4.8 and Table 4.2). Additionally, many computational studies in the literature have demonstrated the charge distribution of the HOMO and LUMO located at this position [174-178]. Therefore, both hydroxylation and peroxidation would most likely occur at C2. The relationship between the increase in signal intensity for $[Q+O_2-H]^-$ within ten minutes and the decrease in the $[Q+O-H]^-$ after 6 minutes suggests competition between the individual ROS species for reactivity at this site on quercetin.

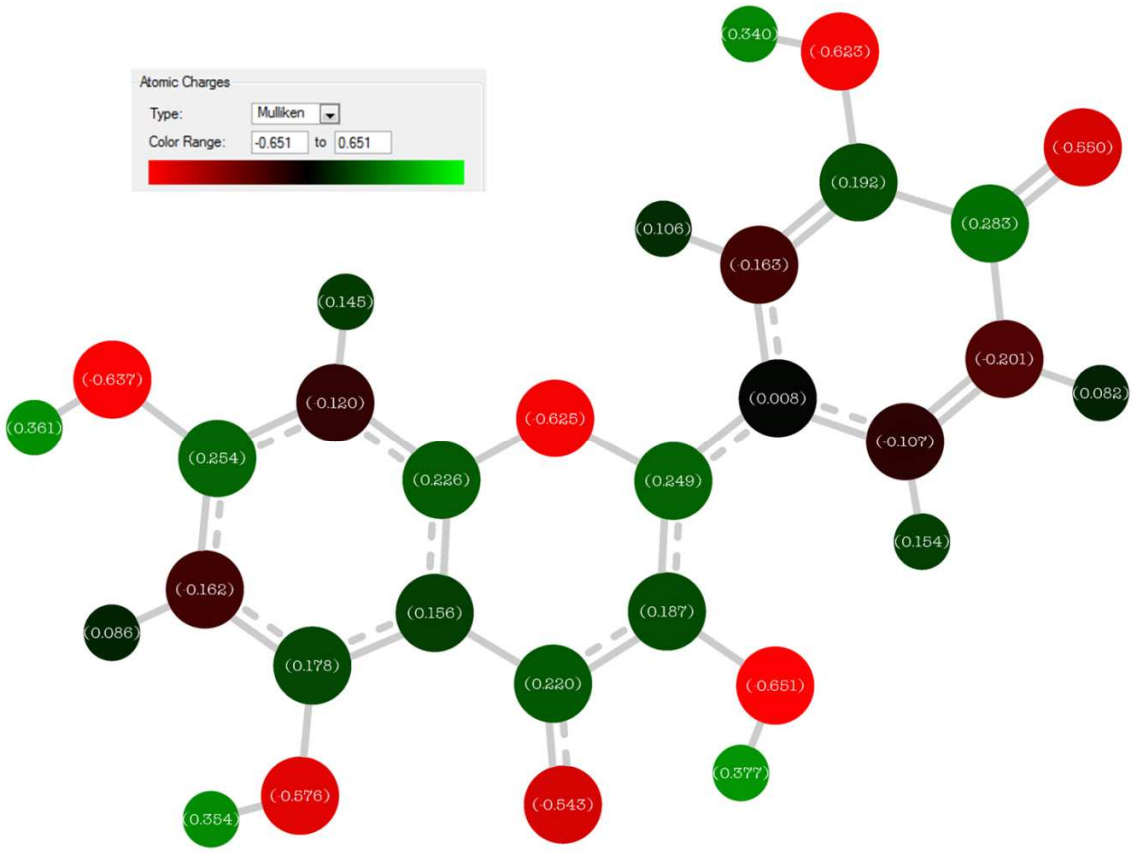

Figure 4.8: The estimated Mulliken charges of the deprotonated quercetin anion $[Q-H]^-$ in its lowest energy configuration (LEC) using Gaussian 03 and optimized with DFT/B3LYP and a 6-31G basis set.

Decrease in the intensity of both of these ions may also suggest that these ions are only intermediates in the degradation pathway of quercetin when mixed with ROS generated by hydrogen peroxide. Decrease in intensity may be due to further oxidation of the hydroxylated and peroxidated quercetin ions, such as $[Q+O-H_2-H]^-$ and $[Q+O_2-H_2+Na]^-$. However, $[Q+O-H_2-H]^-$ and $[Q+O_2-H_2+Na]^-$ could be formed by hydroxylation or by peroxidation of simple oxidated quercetin $[Q-H_2-H]^-$.

The structure for $[Q+O_2-H]^-$ could exist in many different configurations and may in fact exist in more than just one structure in solution. A few studies propose a cyclic peroxidated quercetin intermediate in which the peroxide reacts at the C2 position and forms a bridge across the C-ring by bonding with C4 [163,189]. The fragmentation product ions of m/z 333.0242 $[Q+O_2-H]^-$ further confirms this as a possible structure (Figure 4.9, Table 4.3). The major fragment product ion of $[Q+O_2-H]^-$ was m/z 271.0229 and represents an ion with an elemental formula $C_{14}H_7O_6$ (-4.4 ppm error). The neutral loss from fragmentation would be a loss of CH_2O and O_2. The loss of three oxygens and only one carbon suggest that the neutral loss involves the added peroxide as well as a carbonyl from either the C3 or C4 position.

Table 4.3: The estimated mulliken charges of the deprotonated quercetin anion $[Q-H]^-$, hydroxylated quercetin anion $[Q+O-H]^-$ and peroxidated quercetin anion $[Q+O_2-H]^-$ in their lowest energy configuration (LEC) using Gaussian 03 and optimized with DFT/B3LYP and a 6-31G basis set.

Ring	Atom	Q	$[Q-H]^-$	$[Q+O-H]^-$*	$[Q+O-H]^-$**	$[Q+O_2-H]^{-\ a}$	$[Q+O_2-H]^{-\ b\ C2-C4}$	$[Q+O_2-H]^{-\ b\ C2-C3}$
C-ring	C2	0.27	0.25	0.21	0.25	0.15	0.22	0.30
	C3	0.22	0.19	0.34	0.24	0.37	0.36	0.30
	C4	0.24	0.22	0.23	0.24	0.21	0.23	0.29
A-ring	C5	0.21	0.18	0.20	0.23	0.21	0.22	0.21
	C6	-0.14	-0.16	-0.16	-0.17	-0.16	-0.16	-0.17
	C7	0.27	0.25	0.26	0.26	0.27	0.25	0.26
	C8	-0.11	-0.12	-0.12	-0.12	-0.12	-0.12	-0.13
	C9	0.23	0.23	0.25	0.26	0.24	0.28	0.28
B-ring	C1'	0.04	0.01	0.01	0.05	0.02	0.08	0.07
	C2'	-0.15	-0.16	-0.13	-0.16	-0.16	-0.12	-0.13
	C3'	0.25	0.19	0.18	0.20	0.19	0.21	0.22
	C4'	0.27	0.28	0.28	0.29	0.29	0.28	0.29
	C5'	-0.16	-0.20	-0.20	-0.19	-0.21	-0.18	-0.18
	C6'	-0.12	-0.11	-0.12	-0.09	-0.09	-0.07	-0.04
			Energy, kJ/mol	3093.976	3094.082	3291.182	3291.168	3291.192

*C-ring intact; **C-ring opened; [a] C-ring intact and non-cyclic peroxidated; [b] C-ring intact and cyclic peroxide

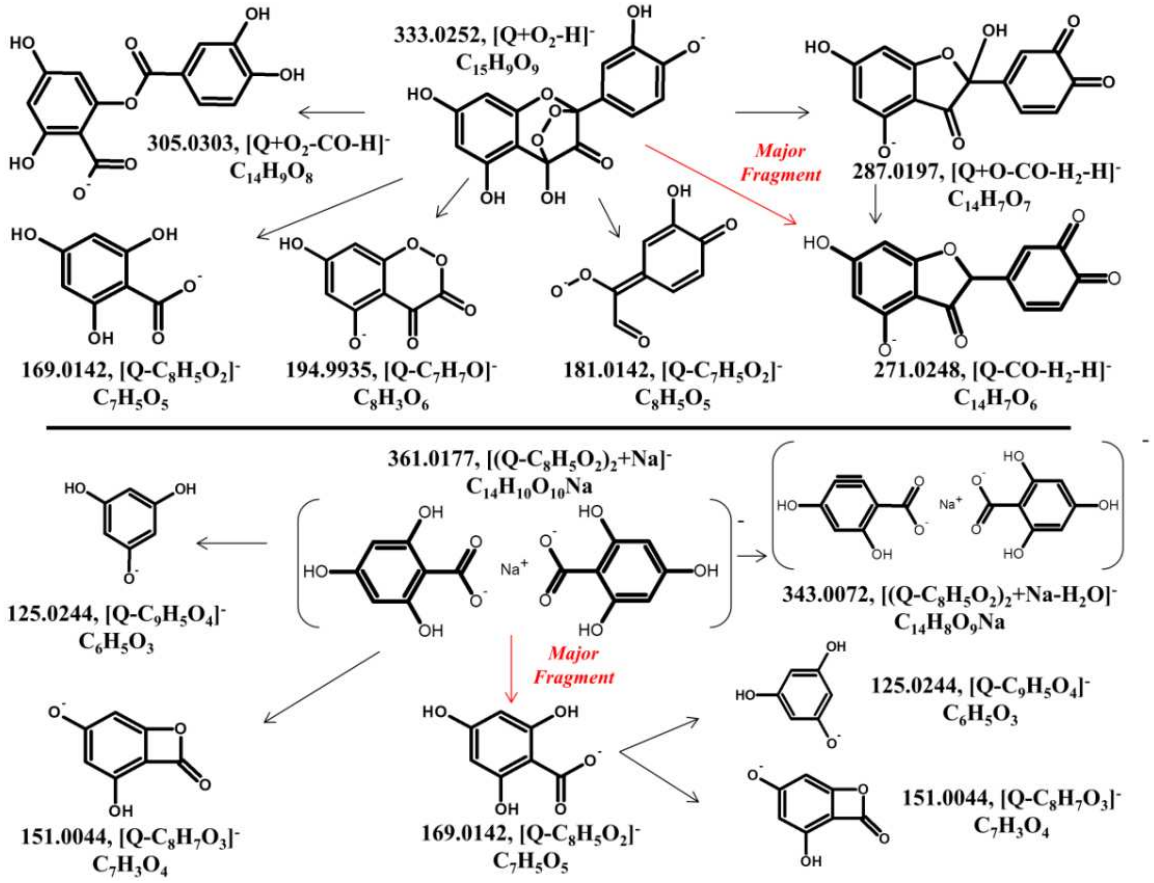

Figure 4.9: Proposed structures of product ions from higher order fragmentation (MS-MS and MS^3) of $[Q+O_2\text{-}H]^-$, m/z 333.0252 and $[(Q\text{-}C_8H_5O_2)_2Na]^-$, m/z 361.0177

Evaluation of the computationally-simulated structure in which peroxidation was only at C2 (and not bridged), suggested that bridging may also occur at C3, since C3 has a significantly higher estimated positive partial charge than C4 (Table 3). The C2 to C3 bridged peroxidated quercetin structure could also possibly lead to all of the fragmentation structures in Figure 4.8. The calculated total energies of the non-cyclic peroxidated quercetin, the 2,4-cyclic-peroxidated quercetin and the 2,3-cyclic peroxidated quercetin were similar (within ± 0.02 kJ/mol), however, the C2-C4 cyclic structure was slightly more energetically favorable than the other two (Table 3). Indeed, there may be a distribution of both the C2-C3 and C2-C4 bonded structures in solution. In a computational study of enzymatic oxygenolysis of quercetin, Fiorucci *et al.* concluded that the formation of cyclic peroxide would favor 1,3-cycloaddtion, instead of 1,2-cycloaddition [190].

Cleavage of the weak peroxide bond of the C2-C4 bond, followed by decarboxylation at the C3 site would give rise to a depside structure with a m/z of 305.0303, which was observed in the late kinetic time points (Figure 4.3 and 4.7) [166,167]. The computational analysis of the C2-C4 peroxidated quercetin confirms the potential reactivity and possibly decarboxylation at the C3 position based on its higher partial positive charge compared to the C2 and C4 positions (Table 3). The observed ions at m/z 273.0394 and 271.0239 also suggest decarboxylation from the C-ring. The fact that the major fragment product ion seen when fragmenting m/z 333.0242 was m/z 271.0236 supports the notion that the appearance of m/z 271.0239 and 273.0394 in the initial MS scan is related to the peroxidated quercetin pathway. These ions were also observed in the thermal degradation study of quercetin and a study of copper-catalyzed quercetin degradation [191].

4.5.3 Cross-Ring Cleavage Pathways

The structure for m/z 169.0140 and 361.0168 appear to be the preferred degradation products as they were observed to consistently increase as the reaction time was extended. Fragmentation of m/z 169.0140 resulted in m/z 125.0249 and 151.0044, which confirmed the precursor ion to be the A-type cross-ring cleavage product $[Q\text{-}C_8H_5O_2]^-$ (2,4,6-trihydroxybenzoate) observed in the thermal degradation study [172]. The major product ion that resulted from fragmentation of m/z 361.0168 was m/z 169.0148 and higher order fragmentation of the product ion m/z 169.0148 (MS^3) provided further product ion signals at m/z 151.0032 and 125.0239. Considering the fragmentation data and that m/z 361.0168 does not form when NaOH is replaced by KOH, the ion at m/z 361.0168 must be due to a 2,4,6-trihydroxybenzoate dimer bridged by a sodium ion. Previously, Schug and McNair demonstrated a similar phenomenon in which they observed pseudo-molecular ion formation of sodium-bridged dimers of aromatic carboxylic acids in the negative ionization mode by ESI [182,183].

The depside generated by degradation of the 2,4-cyclic peroxidated quercetin may be the intermediate that leads to formation of the 2,4,6-trihydroxybenzoate. Additional nucleophilic attack by ROS at the C2 position of this depside could cause cleavage of the O1-C2 bond. This would make 2,4,6-trihydroxybenzoate the charged leaving group. This preferred degradation product is different than the 2,4,6-trihydroxy-2-oxo-2-phenylacetate and 2,4,6-trihydroxy-2-hydroxyl-2-phenylacetate degradation

products (m/z 197.0092 and 199.0248) observed by the thermal degradation pathway [172]. The late kinetic time point of the hydrogen peroxide mixing study did show trace amounts of m/z 197.0086, along with two other A-type and B-type cross-ring cleavage product ions, m/z 153.0186 and 178.9979. Formation of these ions could be due to continued hydroxylation of the chalcan-trione, $[Q+O-H]^-$.

4.4.4 Interpretation of UV/Vis Spectral Profile

Details presented by the mass spectral data help to further explain the changes observed in the UV spectral profile. As expected, when the quercetin structure interacts with hydrogen peroxide at the C2 position and the hydroxylated and peroxidated structures are being formed, the cinnamoyl and benzoyl structures are interrupted, causing a decrease in the absorbance of bands I and II. As the reaction progresses, the quercetin continues to degrade causing further loss of absorbance. Shift of the maxima in band I from 380 nm (Figure 4.3) may also be in part due to simple oxidation events and disruption of C-ring aromaticity. Band III has been suggested to be influenced by the chalcone structure [192,193]. The increase in band III at the initial time points correlated with an increase in the $[Q+O-H]^-$ at the first two kinetic measurements, as well as the decrease in absorbance along with decrease in intensity. Further oxidation of the hydroxylated and peroxidated structures ($[Q+O-H_2-H]^-$ and $[Q+O_2-H_2+Na]^-$) may contribute to the hyperchromic shift of the maxima of band III. An HPLC-UV study by Zvezdanovic *et al.* identified 2,4,6-trihydroxybenzoate as a prominent quercetin degradant which had a UV profile that consisted of a single band with a maximum at 294 nm[51]. At the last time point, the influence of the 2,4,6-trihydroxybenzoate may have begun to be seen in band III with the slight increase in absorbance at 294 nm. The trihydroxybenzoate structure would maintain the benzoyl system from the A-ring side and an absorbance near band II [168,194].

4.6 Conclusion

The introduction of hydrogen peroxide into aqueous solutions dramatically increases the amount of hydroxyl and hydroperoxyl free radicals and polyphenolic flavonoids can combat the reactive nature of these compounds. Based on results presented in this study, quercetin neutralizes free radicals through more than one mechanism. First, quercetin can quench free radicals by donating a hydrogen atom from one of its hydroxyl groups. The generated radical would be stabilized by the polyphenolic structure.

Second, quercetin can capture reactive oxygen species upon nucleophilic attack at the carbocationic C2 position. Nucleophilic attack by water leads to an energetically favored C-ring opening at O1-C2, while attack by hydrogen peroxide leads to C-ring opening due to a cyclic addition of the peroxyl at C2-C4, followed by loss of C3-OH, and cleavage of the peroxy bond. Further interaction of these intermediates with ROS may lead to cross ring cleavage, and depending on the amount of oxygens captured, result in different simple phenolic acids, which are also known for their antioxidant characteristics. In addition, the degradative pathway may end in small molecule loss, without cross-ring cleavage. Sodiated pseudo adducts are expected when evaluating quercetin degradation in the presence of NaOH and ESI-MS.

4.7 Acknowledgements

The authors gratefully acknowledge Shimadzu Scientific Instruments, Inc. for their support of instrumentation through the Shimadzu Equipment Grants for Research Program.

Chapter 5

Oxidative Degradation Of Quercetin With Azo-initiated Peroxyl Radicals Using Continuous Flow Kinetic Electrospray-Ion Trap-Time Of Flight Mass Spectrometry

5.1 Abstract

The antioxidant capacity of polyphenolic plant metabolites is often measured using azo compounds to generate reactive oxygen species (ROS). Due to its widespread availability, ease of use and reliability, 2,2'-azobis(2-amidinopropane) dihydrochloride (AAPH) has been increasingly used as a model oxidant to replace hydrogen peroxide in oxidative studies. Nevertheless, common antioxidant capacity assays which have recently come under intense criticism and scrutiny, provide only a bulk antioxidant characteristic expressed in standard equivalents and do not provide any information on intermediates and degradation products. In this study, kinetic measurements of AAPH-generated peroxyl radical-induced oxidative degradation of quercetin were made using an in-house built online continuous flow device made of concentric capillary tubes, modified to fit to the inlet of an electrospray ionization-ion trap-time-of-flight-mass spectrometer (ESI-IT-TOF-MS). Time-resolved mass spectral measurements ranging from 5 to 22 min were performed in the positive and negative mode to track intermediate degradation products and to evaluate the degradation rate of the deprotonated quercetin ion, $[Q\text{-}H]^-$. Thermally degraded solutions of AAPH in the presence of dissolved oxygen, were also measured by ESI-MS to evaluate the degradation pathway and associated side reactions. The observed degradation mechanisms included oxidation, hydroxylation, and ring-cleavage by nucleophilic attack. The same smaller molecular weight phenolic acids were observed from cross-ring cleavage as was observed in previous studies on thermal and H_2O_2-induced degradation, although different intermediate structures were observed, including an azo-initiated peroxyl radical nucleophilic adduct.

5.2 Introduction

Reactive oxygen species (ROS) are highly reactive molecules that are well known for the deleterious effects of the body. ROS include molecules such as hydrogen peroxide, superoxide, hydroxyl, peroxyl and alkoxyl radicals. These species can be introduced to the body through interaction with the environment, such as in air pollution [195], but are also being constantly produced physiologically

through aerobic metabolism. The mitochondria are one of the primary places in which partially reduced and highly reactive metabolites of O_2 are generated. This is by way of a side product of the electron transport chain where molecular oxygen is reduced to H_2O [196]. ROS play a significant part in cellular signaling and regulation pathways, but build-up of these species above the cellular level of antioxidant capacity can lead to oxidative stress and pathology [197-198]. Contact between ROS and cellular components have been shown to cause DNA and tissue damage, as well as lipid peroxidation [199-201].

In addition to enzymatic antioxidants, dietary intake of plants and vegetables can supply nutritional antioxidants to the body, helping counterbalance oxidative stress. Flavonoids are a class of plant metabolites that are well studied for their ability to scavenge free radicals [202]. These species can break free radical chain reactions by either two mechanisms: electron transfer (ET) or a hydrogen atom transfer (HAT). Their polyphenolic structures allow for stabilization of the phenoxy radical formed through electron delocalization [49,203]. Quercetin is a flavonol species which has been established as having high antioxidant capability and can be found glycosylated in high quantities in teas, wine and wheat [204-205]. Quercetin's antioxidant character is enhanced due to the double bond found in the C-ring between C2 and C3, the *o*-dihydroxy structure located on the B-ring, and the catechol-like structures that can be formed between the hydroxyl group at C5 and the C4 keto group and between the hydroxyl group at C3 and the C4 keto group (Figure 5.1) [106,117].

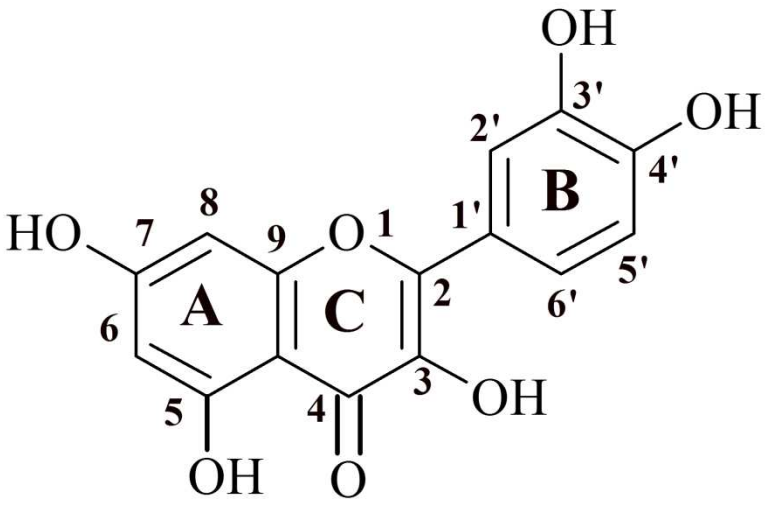

Figure 5.1: The chemical structure of quercetin.

A variety of test methods have been developed to determine the antioxidant quality of a substance. Common antioxidant capacity assays include trolox equivalence antioxidant capacity (TEAC), ferric ion reducing antioxidant capacity (FRAP) and oxygen radical absorbance capacity (ORAC). Although these assays are simple and straightforward, it is difficult to use one-dimensional methods to assess multifunctional food and biological antioxidants in a detailed fashion [206]. In addition, these assays use different radical or oxidant sources which results in unique reaction mechanisms. This makes comparison of values between studies difficult and current methods do not offer specific information such as the identity of the metabolites and degradation products formed.

Many antioxidants capacity assays, including ORAC, use azo compounds as a source to generate free radicals. Alterations in the functional substituents attached to the azo group provide a wide range of hydrophobicity or hydrophilicity. With gentle heating the C-N bond connected to the azo group cleaves and liberates nitrogen gas. In the process, a carbocation radical is formed. By picking the appropriate azo compound, site specific free radicals can be generated with little energy. Decomposition is unimolecular and carbon-centered free radicals can be generated without biological species. In addition, free radical generation occurs at a constant rate and many compounds are available that have a half-life of many days [208].

2,2'-Azobis(2-amidinopropane) dihydrochloride (AAPH) is one of the more commonly used azo-initiators. Because of its water solubility, and its ability to induce both nucleophilic and free radical oxidation, it has been thought to be a good candidate for replacing H_2O_2 as a model oxidant in antioxidant assays for both natural products and biological components [208]. In the presence of molecular oxygen, upon activation the free radical quickly reacts with O_2 to form peroxyl radicals. Due to formation of these biologically relevant radicals, AAPH has been used to study physiological phenomena such as lipid peroxidation [209].

The use of online continuous flow kinetics and electrospray ionization-ion trap-time of flight mass spectrometry (ESI-IT-TOF MS) has been previously demonstrated to provide detailed time-resolved measurements of the oxidative degradation of flavonols, using quercetin as a model analyte [11, Chapter 4]. These studies followed the degradation of quercetin by thermally-accelerating its autoxidation and by

hydrogen peroxide-induced oxidation. In both studies, quercetin was shown to undergo initial oxidation with formation of semiquinone and *o*-quinone structures, as well as participate in nucleophilic attack that led to cross-ring cleavage and production of smaller molecular weight phenolic acids.

In this study, the azo-initiated peroxyl radical-induced oxidative degradation of quercetin was characterized by using an in-house built continuous flow kinetic mixing device which was modified to fit the inlet of a mass spectrometer. This device (inspired by Wilson and Konermann [87]) provided the ability to adjust the reaction volume and, therefore, allowed for adjustment of the reaction time between 5 and 22 minutes. To mimic common conditions used in antioxidant capacity assays, measurements were made both at room temperature and at 37 ℃ by dippi ng the device into a water bath. The hybrid IT-TOF (MS) system provided high mass accuracy and multi-stage fragmentation (MS^n), yielding an in-depth study of the mechanisms and pathways of oxidative degradation by azo-induced peroxyl radicals. This novel approach of online and mass spectrometry based evaluation of degradation by azo-initiated free radicals has not been previously conducted on flavonoid compounds.

5.3 Methods and Equipment

5.3.1 Reagents and Solution

Ammonium acetate buffer was prepared by diluting ammonium acetate (Sigma-Aldrich, St. Louis, MO, USA) in enough LCMS-grade water ((Burdick and Jackson, Muskegon, MI, USA) to make a concentration of 1 mM and was adjusted to a pH of 7.4 by addition of sodium hydroxide (J. T. Baker, Phillipsburg, NJ, USA). A stock solution of quercetin was prepared by dissolving quercetin (100 mg; Sigma-Aldrich) into dimethyl sulfoxide (100 mL, Sigma-Aldrich). Aqueous solutions of quercetin (65 µM) were prepared by diluting the stock solution into the ammonium acetate buffer. Fresh solutions were prepared at each measured time point. A 50 mM aqueous solution of AAPH was prepared by dissolving AAPH (500 mg; Sigma-Aldrich) in 1mM ammonium acetate buffer (50 mL).

5.3.2 AAPH Thermal Activation

Two kinetic studies were conducted that differed by how the AAPH was thermally activated. In one study, a 50 mL volumetric flask of AAPH was submerged in a water bath controlled at 80 ℃ for 10 minutes then removed. The solution was then cooled to room temperature and the solution was then

mixed with quercetin using the device described without any further heating. The second study consisted of mixing unheated AAPH solution with quercetin using the kinetic device described below, however, in this case, the tubing downstream of the mixer was submerged into a water bath at 37 ℃.

5.3.3 Kinetic Device

Kinetic measurements were performed using a continuous-flow device which was built in-house (Figure 5.2) and consisted of two concentric capillary tubes. Two 2.5 mL glass syringe (7.284 mm internal diameter (I.D.); Hamilton, Reno, Nevada, USA) were connected to a micro-mixing tee (IDEX, Lake Forest, Illinois, USA) via one foot lengths of polyetheretherketone (PEEK) tubing (1/16" O.D.; 0.005" I.D.). A five foot length of flourinated ethylene propylene (FEP) tubing (400 µm I.D.; 1000 µm O.D.) was connected to the outlet end of the mixing tee. The downstream end of the FEP tubing was inserted into a five foot length of PEEK tubing (100 µm I.D.; 360 µm outer diameter (O.D.)). A stainless steel union (0.052" thru-hole) was slid over the FEP tubing 2 inches from the downstream end of the outer capillary and tightened with a fitting and a ferrule to seal any leaks. The downstream outlet end of the PEEK tubing (outer capillary) was connected to a PDA which in turn was connected to the inlet of the ESI. The syringes were driven by two syringe pumps (NE-1010, New Era Pump Systems, Farmingdale, NY, USA).

By moving the inner capillary, the volume of the reaction region was controlled, which allowed the ability regulate the amount of reaction time after mixing. The aqueous solution of quercetin was pumped through one syringe at a flow rate of 10.0 µl/min. AAPH was introduced using the other syringe and was pumped at a flow rate of 1.0 µL/min. These conditions resulted in solutions that contained quercetin concentrations of 59 µM and 5 mM of AAPH.

Kinetic measurements were made by pulling the inner PEEK tubing out at 1 foot intervals. In the configuration in which the device had no extension (minimum dwell time), the total system volume was estimated to be 51 µL. At the combined flow rate of 11.0 µl/min, this allowed for measurements ranging from 5.1 to 22.1minutes of reaction time.

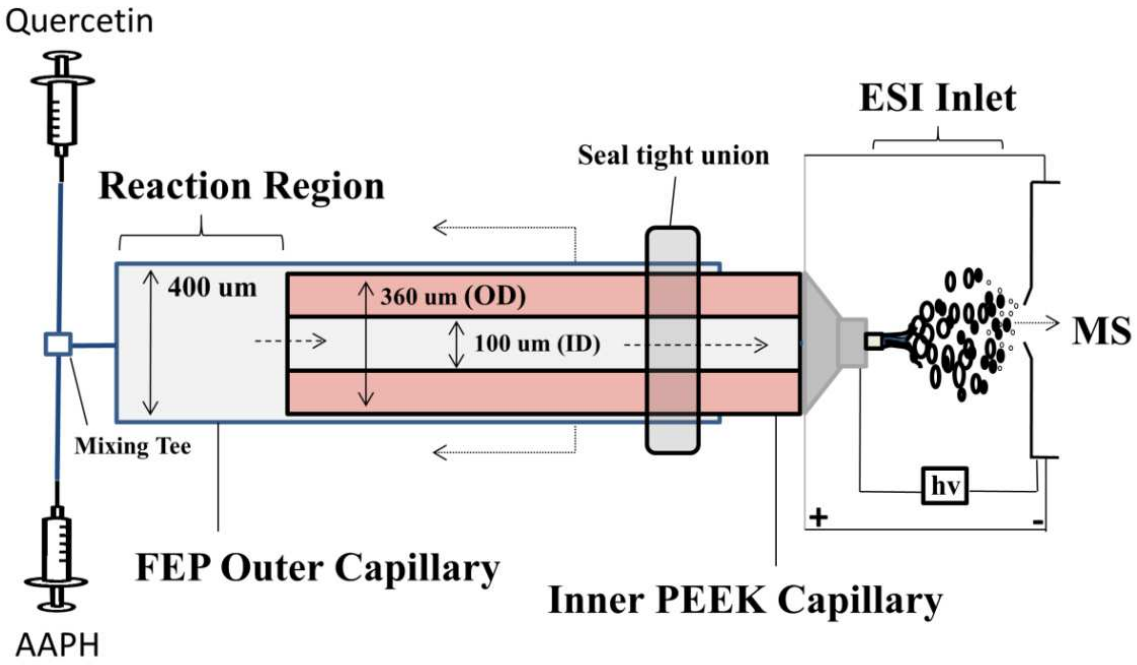

Figure 5.2: An online kinetic continuous flow device constructed from two concentric capillary tubes that interfaces with UV and MS detection.

5.3.4 Instrumentation

Negative ion MS spectra were obtained using an ion trap - time of flight mass spectrometer (IT-TOF-MS, Shimadzu Scientific Instruments, Inc., Kyoto, Japan) equipped with a conventional electrospray ionization (ESI) source. Analytical parameters for ionization, fragmentation, and detection were: interface voltage, -3.5 kV; nebulizing gas (N_2), 1.5 L/min; drying gas (N_2), 10 L/min; curved desolvation line, 250 ℃; detector voltage, 1.92 kV; ion accumulation tim e, 10 ms; precursor ion isolation width, 0.1 amu; collision gas (Ar), 50%; and frequency constant (q), 0.251. The estimated resolution of the instrument is 10,000 at m/z 1000. A scanning rate of 100 ms was used. The estimated duty cycle at MS^3 with these settings was < 0.5 seconds. The collision energy during collision-induced dissociation (CID) was adjusted at each tandem MS stage to determine the optimum parameters at which a maximum amount of signal information would be obtained. The IT-TOF was calibrated to < 5 ppm mass accuracy using a solution of sodium trifluoroacetate.

Data collection and analysis was carried out using *LCMS Solutions* version 3.4 software. The *Accurate Mass Calculator* and *Formula Predictor* software tools were used to support determination of theoretical *m/z* values and elemental formulas of observed fragments. The software was configured to eliminate formulaic possibilities based on the following requirements: 1-15 Carbons, 0-10 Oxygens, 0-15 Hydrogens, 0-1 Sodiums, 0-10 Nitrogens and within 25 ppm error. Isotopic ratios were also evaluated.

5.4 Results and Discussion

5.4.1 Evaluation of AAPH

Thermally activated solutions of AAPH were evaluated by heating the AAPH solution at 80 ℃ for 10 minutes and then directly infusing the solution into the mass spectrometer, and by flowing unheated AAPH solution through the fully extended capillary device which was submerged in a 37 ℃ water bath. Numerous species were observed in both the positive and negative modes, suggesting the compound underwent cleavage and continued through numerous side reactions.

Werber *et al.* used LC- UV and LC-MS to evaluate the thermal degradation pathway of AAPH [209]. Their studied demonstrated that with heating at pH 7, AAPH formed free radicals through release of N_2, and that numerous other side reactions were observed. Based on their results, they proposed that alkoxyl radicals were the predominant radical species. While the peroxyl radicals were not detected, they suggested that a tetroxide compound was formed from recombination of peroxyl radicals, and that cleavage of the tetroxide lead to alkoxyl radicals. Additionally, they concluded that free radicals from the initial AAPH cleavage recombined and underwent cyclization to form a cyclized structure (Figure 5.3).

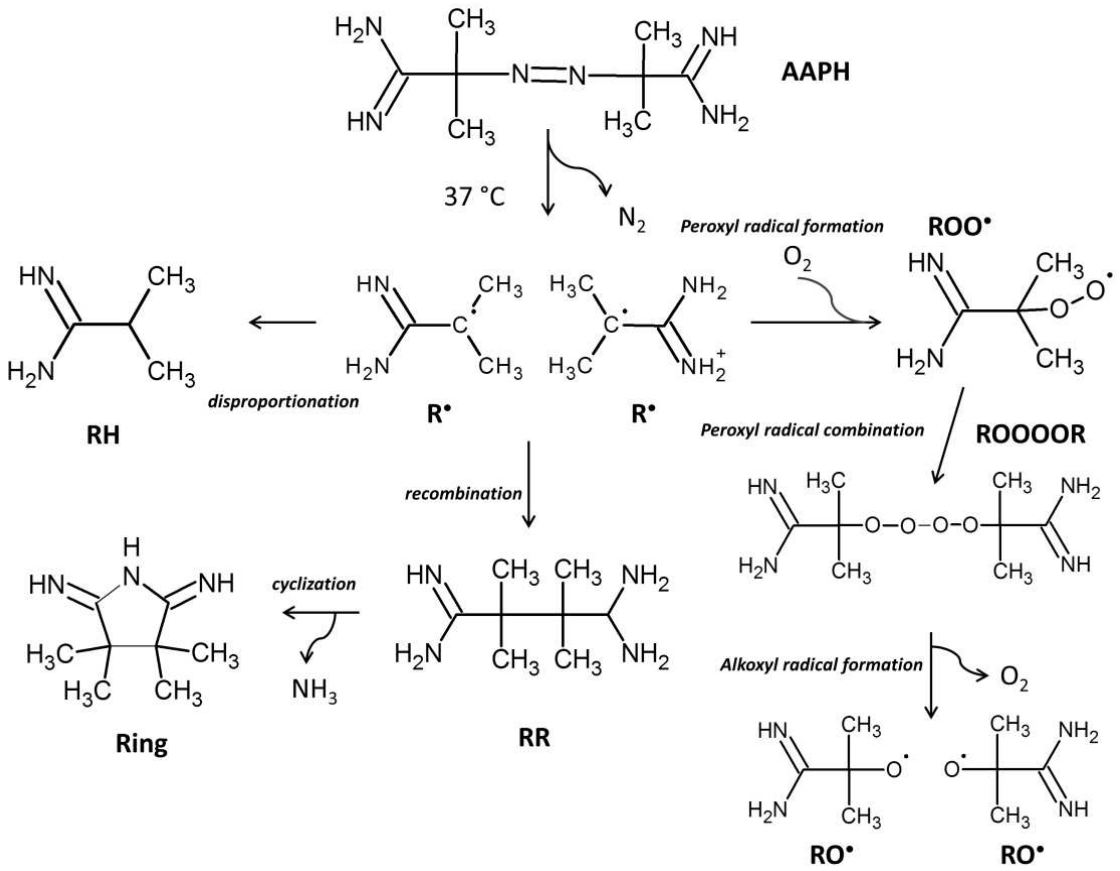

Figure 5.3: A proposed thermal degradation pathway for AAPH. Adapted from [209].

Comparison of both the heated solutions in the positive mode revealed an ion at m/z 154.1343 which corresponds to the ring structure described by Werber *et al.* (-2.6 ppm error). This ion was the base peak in the spectra for the 80 ℃ solution. In the 37 ℃ study, it was in similar intensity, however, the base peak in this solution was the ion m/z 199.1672, which represented the uncleaved ion $[AAPH+H]^+$ (-2.0 ppm). This ion was seen at a much lower intensity in the 80 ℃ solution suggesting that it underw ent significant cleavage at that temperature. Interestingly, the intermediate recombined free radical structure $[RR+H]^+$ (-2.3 ppm) was observed in the 37 ℃ but was not seen at 80 ℃. Additionally, a few other unidentified peaks were observed in the positive mode, along with many others in the negative mode, but efforts are currently being made to identify them (refer to Figure 5.4).

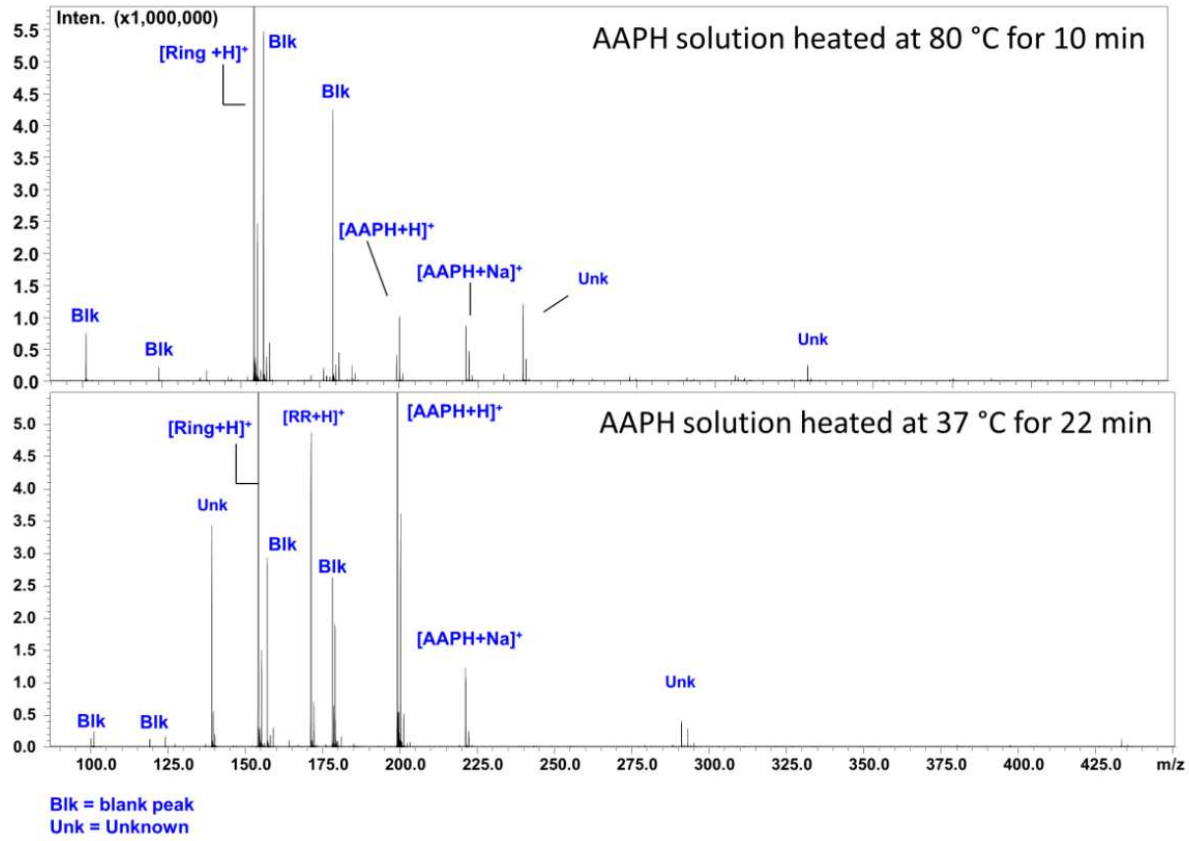

Figure 5.4: Thermally activated solutions of AAPH observed by ESI in the positive mode.

5.4.2 Exaggerated Degradation of Quercetin by AAPH

To determine the potential degradation products that may be observed during the kinetic study, a solution of 65 µM quercetin at pH 7.4 was mixed with a 1 mM AAPH at a ratio of 10:1 and heated at 80 °C for 10 minutes. The solution was directly infused at a flow rate of 50 ul/min. An averaged spectra from the negative mode can be seen in Figure 5.5.

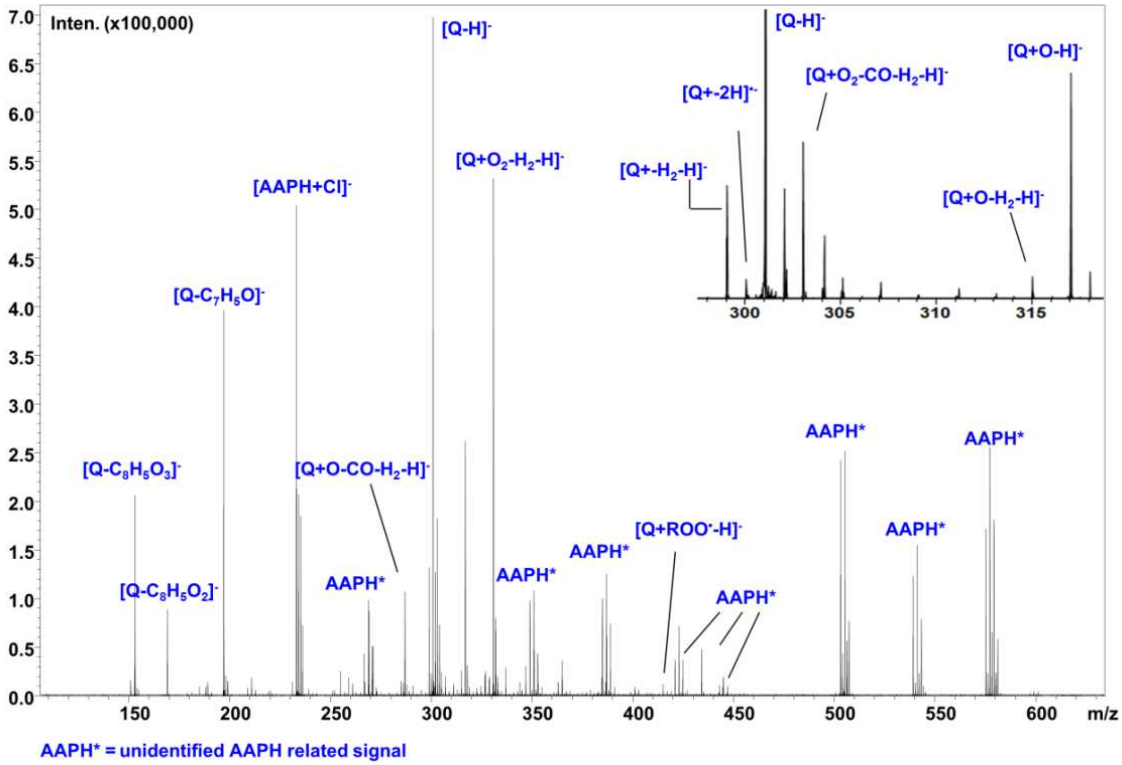

Figure 5.5: An averaged spectrum of a directly infused mixture of quercetin and AAPH (65 µM:1 mM, 10:1) that had been heated at 80 ℃ for 10 minutes.

As can be noted from the spectra, numerous degradation products and a significant number of AAPH related signals were observed. The common phenolic acid degradation products $[Q\text{-}C_8H_5O_3]^-$, $[Q\text{-}C_8H_5O_2]^-$, $[Q\text{-}C_7H_5O]^-$ (m/z 153.0193, 169.0142 and 197.0192, respectively) were observed, which were also observed in the thermal degradation and hydrogen peroxide-induced degradation of quercetin [11, Chapter 4]. The $[Q+O\text{-}H]^-$ (m/z 317.0303) was also noted, however, it is normally observed in room temperature solutions of quercetin. Two interesting signals noted were at m/z 331.0090 and 417.0918 which correspond to $[Q+O_2\text{-}H_2\text{-}H]^-$ and $[Q+ROO\text{-}H]^-$ with -1.5 ppm and -5.3 error, respectively. The $[Q+O_2\text{-}H_2\text{-}H]^-$ ion had not been previously observed before in either thermal of H_2O_2 degradation, however, its saturated counterpart, $[Q+O_2\text{-}H]^-$, was proposed as an intermediate in the H_2O_2 pathway (refer to Chapter 4). No ions related to quercetin with a nucleophilic addition of an alkoxyl radical were noted.

5.4.3 Kinetic Degradation of Quercetin

As expected the kinetic degradation of quercetin showed that the intensity of the $[Q\text{-}H]^-$ ion decreased over time (Figure 5.6). The 37 ℃ study resulted in a greater rate of de gradation than the study at room temperature (RT). The $[Q+O\text{-}H]^-$ was the most intense degradation product observed at early time points and was seen at significant higher relative intensities in the 37 ℃ study than the RT study. Continued heating of the AAPH may be generating alkoxyl radicals which undergo nucleophilic attack with quercetin at the C2 carbocation, however, no signals corresponding to nucleophilic attack of quercetin by alkoxyl signal was observed. Cleavage of the R group through the C-O bond could result in the increased $[Q+O\text{-}H]^-$ signal. Although, disproportionation of the azo free radicals could lead to increased levels of hydroxyl radicals, which could form $[Q+O\text{-}H]^-$.

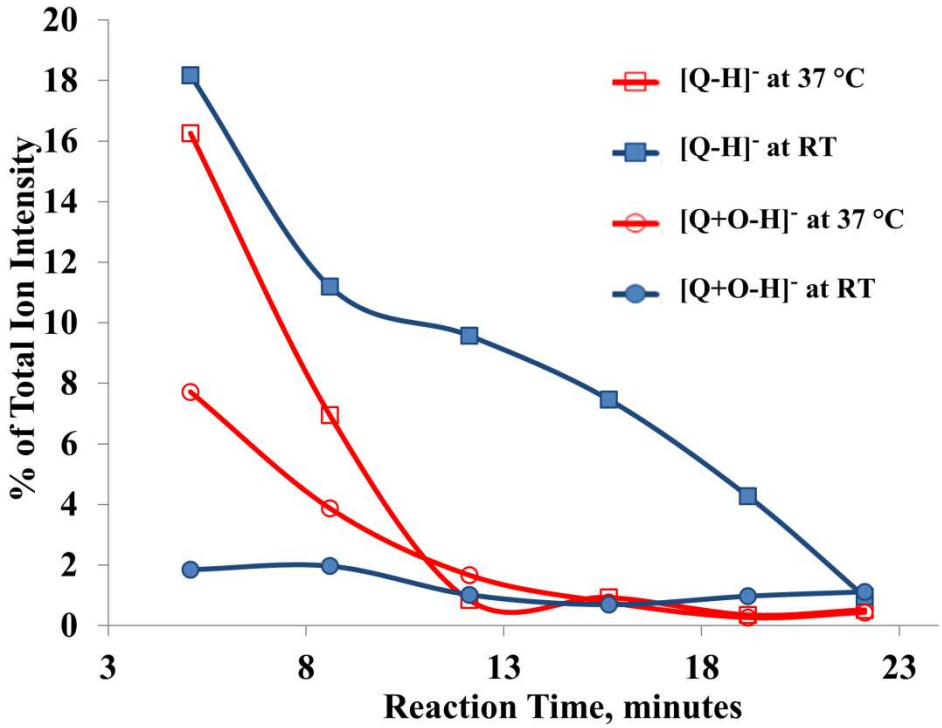

Figure 5.6: A kinetic plot of percent total ion intensity as a function of time for the [Q-H]- and [Q+O-H]- ions observed during the 37 ℃ and RT study.

The degradation product ion representing nucleophilic attack of quercetin by the peroxyl radical, $[Q+ROO\text{-}H]^-$, m/z 417.0940 was observed throughout the 37 ℃ study but was not seen in the 80 ℃

study. This ion stayed at a consistent relative intensity throughout, suggesting it was an intermediate structure. Fragmentation of the ion supports the proposed structure (refer to Table 5.1 and Figure 5.7).

Table 5.1: The degradation product ions observed during the 37 ℃ kinetic study ex pressed as % of total ion intensity.

Degradation Product, m/z	5.1 min	8.6 min	12.1 min	15.6 min	19.2 min	22.1 min
417.0940 $[Q+ROO-H]^-$	0.6%	0.2%	0.1%	0.2%	0.1%	0.1%
331.0095 $[Q+O_2-H_2-H]^-$	1.3%	1.0%	0.3%	0.4%	0.3%	0.1%
197.0092 $[Q-C_7H_5O]^-$	0.7%	0.9%	0.6%	0.7%	0.9%	3.2%
169.0142 $[Q-C_8H_5O_2]^-$	0.3%	0.3%	0.1%	0.2%	0.2%	0.6%
153.0193 $[Q-C_8H_5O_3]^-$	0.3%	0.2%	0.1%	0.2%	0.2%	0.7%

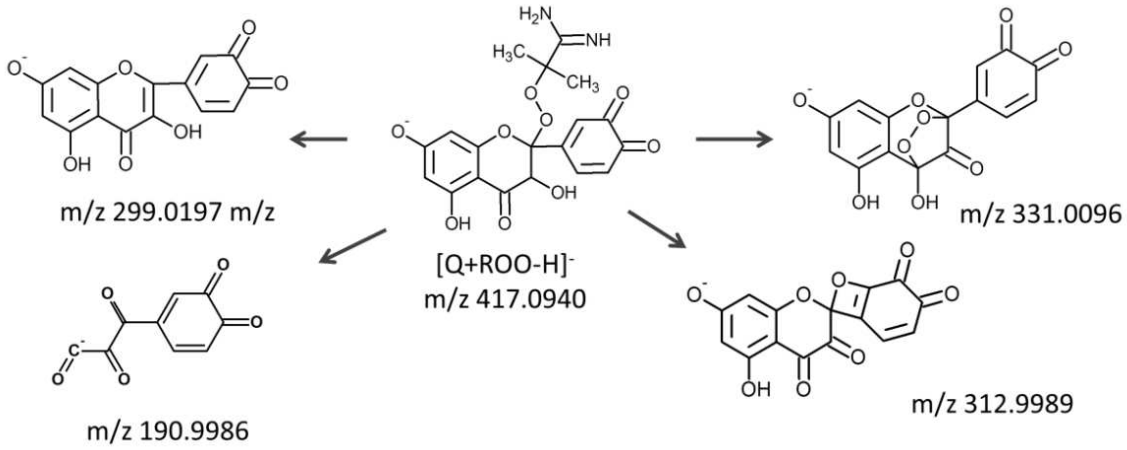

Figure 5.7:Proposed fragmentation product ions of m/z 417.0940.

The $[Q+O_2-H_2-H]^-$ was observed consistently throughout the 37 ℃ study, however, it was also observed in the RT study at a similar level. Fragmentation of this ion justified the proposed structure (refer to Figure 5.8). Zhou and Sadik observed fragmentation of a signal at m/z 331 which the demonstrated to have fragment ions similar to what was observed here (m/z 299, 313, 287, 271, 179). They describe the m/z 331 structure to be a methoxylated species, but based on high mass accuracy this would have a very high error. They only observed this degradant product during oxidation of quercetin with azobisisobutyronitrile [168].

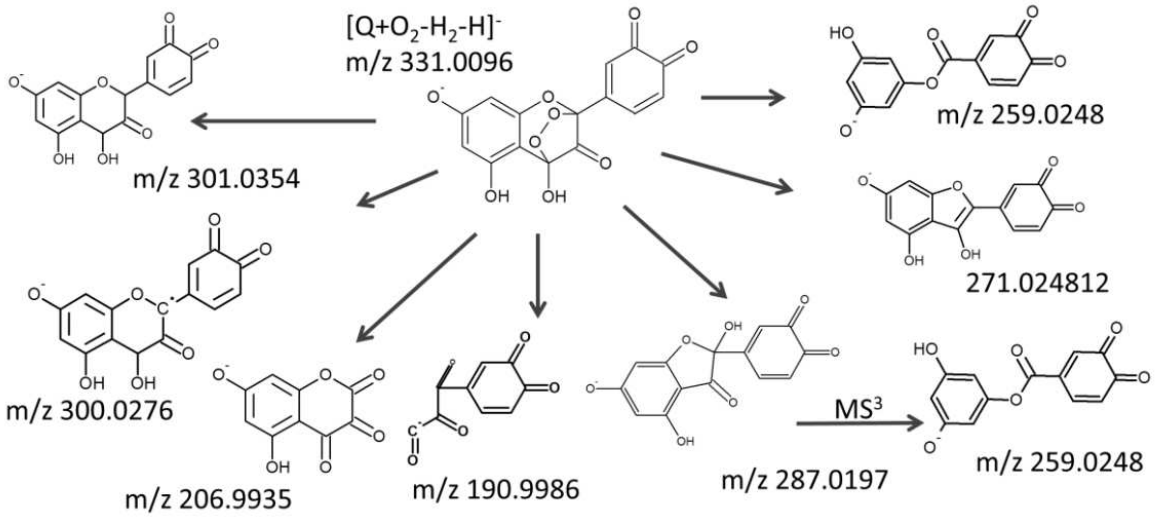

Figure 5.8: Proposed structures for fragmentation product ions of $[Q+O_2-H_2-H]^-$

Finally, the phenolic acid degradation products $[Q-C_8H_5O_3]^-$, $[Q-C_8H_5O_2]^-$, $[Q-C_7H_5O]^-$ (m/z 153.0193, 169.0142 and 197.0192, respectively) were observed in both studies at low concentrations, but significantly increased near the last time points (Table 5.1). In the 37 ℃ study, the $[Q-C_7H_5O]^-$ was the base peak in the spectra and appeared to be the favored degradation pathway for phenolic acid formation, but considering the level of noise in the spectra at that time, it amounted to only 3% of total ion intensity.

5.5 Conclusion

Degradation of deprotonated quercetin was observed to decrease when mixed with aqueous solutions of AAPH. The degradation pathway appeared to follow a similar pathway as observed for thermally-accelerated autoxidation and for hydrogen peroxide-induced oxidation.

Different intermediate structures were observed, compared to thermal and H_2O_2 degradation, further supporting the mechanism that quercetin may break free radical chain reactions by trapping them. Observation of an azo-generated peroxyl radical adduct (confirmed by MS/MS) demonstrated that biological relevant peroxyl radicals are being produced when AAPH is thermally degraded.

5.6 Acknowledgements

The authors gratefully acknowledge Shimadzu Scientific Instruments, Inc. for their support of instrumentation through the Shimadzu Equipment Grants for Research Program.

Chapter 6

Future Work and Conclusions

6.1 Oxidative Degradation of Flavonoids

As terrestrial plants emerged from the ocean millions of years ago, they evolved by producing antioxidants such as ascorbic acid and polyphenols to adapt to the destructive ROS produced from photosynthesis and the oxygen rich atmosphere [210]. Humans are also subject to destructive ROS from respiration and the environment, and may be able to combat the effects by taking advantage of the antioxidant defenses developed by plants through dietary intake. Since Denham Harman proposed the free radical theory of aging in the 1950s [211], there has been increasing interest in understanding how to maintain an oxidative balance and how plant-based antioxidants can be used to achieve this. Epidemiological evidence exists that correlate a number of improved health conditions and diets rich in fruits and vegetables. However, due to the lack of definitive *in vivo* clinical data and the complexity of plant matrices, the related antioxidant mechanisms between ingested polyphenolics and their effects on ROS in the body are unclear.

As a result, many *in vitro* antioxidant assays have be developed to characterize the antioxidant power of substances, in hope to provide some additional insight into which food substances bear the most significant antioxidant power. Unfortunately, as the media frenzy around these super foods and magical plant compounds increase, scrutiny over the biological relevance of the antioxidant capacity assays have developed. This has left regulatory agencies with the need to reaffirm that more research into this area is needed before consumers can rely on the results of these bench tests to guide their dietary and supplemental intake. Combining innovative techniques along with advances in hyphenated mass spectrometry instrumentation may allow for the development of a more detailed picture of the reactivity of flavonoids and their metabolites.

Considering the amount of literature available on quercetin as an antioxidant and the evidence of its high antioxidant character, it was used as a model analyte to evaluate the various reactivity and degradative pathways induced by different ROS sources using an in-house built continuous flow kinetic device that allows for time-resolved analysis by UV/Vis and ESI-IT-TOF MS.

First, a study on the thermally-induced oxidative degradation of quercetin demonstrated that the same oxidative degradation pathway was observed for aqueous solutions at weakly acidic conditions and at physiological pH, however, acidic solutions were noted to have more stability. Upon heating the solution, oxidative degradation was accelerated and in addition to the initial oxidation products from hydrogen transfer, cross-ring cleavage products were observed which increased over time.

Next, the kinetic device was further used to study the H_2O_2-induced oxidative degradation of quercetin and the results demonstrated that quercetin can neutralize free radicals through two mechanisms, 1.)donating a proton from one of its hydroxyl groups and 2.) capturing ROS upon nucleophilic attack at the carbocationic C2 position. It was proposed from the second mechanism that nucleophilic attack by water lead to an energetically favored C-ring opening at O1-C2, while capture of hydroperoxyl radicals lead to C-ring opening due to a cyclic addition of the peroxyl at C2-C4, followed by loss of C3-OH, and cleavage of the peroxy bond. Further interaction of these intermediates with ROS then leads to formation of smaller molecular weight phenolic acids, of which the ratios of formation are different between thermal degradation and H_2O_2-induced degradation.

Lastly, the kinetic device was used to evaluate degradation of quercetin with azo-initiated peroxyl radicals. The study demonstrated that quercetin degradation was observed, however, the AAPH solution introduced a large amount of side reactions which significantly increased the spectral noise and inherently complicated the analysis. Nonetheless, quercetin degradation products could be detected, and different nucleophilic intermediates were observed compared to thermal and H_2O_2-induced degradation pathways.

These studies have demonstrated that oxidative degradation of flavonoid involves multiple interrelated mechanisms and that flavonoids may be effective at quenching both radical and non-radical sources of reactive oxygen species. The first step in degradation is based on an electron transfer reaction, presumably through quenching or reduction of a radical, and is independent of the radical source. The rate of this step however, may be governed by the nature of the flavonoid and free radical. The second step in the degradation pathway involves capture of a non-radical nucleophilic species via nucleophilic attack of the quinone methide formed after the electron transfer steps.

In consideration of this, evaluation of the degradation of an antioxidant flavonoid species or the evaluation of the electron transfer step alone is insufficient in characterizing it's antioxidant character because since it can be assumed that the intermediate degradation products are also reacting with ROS in solution. Many antioxidant capacity assays, such as DPPH, would only measure the electron transfer step in the degradation pathway. Therefore, to truly evaluate the antioxidant capacity of flavonoids, the consumption of the ROS source must be measured, although this may not be easily accomplished.

Some advantages of the ORAC method are that it follows the reaction of antioxidant and radical through completion and it measures the protection of a marker by an antioxidant against free radical degradation. However, the use of AAPH limits the assay to evaluation of flavonoid reactions with peroxyl radicals. Based on the results presented here, degradation of quercetin with AAPH does not result in the same degradation pathway as observed in autoxidation or reactivity with hydrogen peroxide. Additionally, the AAPH created numerous side reactions which may lead to unexpected interferences and artificial results.

6.2 Advantages and Disadvantages of the Continuous Flow Device

Use of the concentric capillary continuous flow device has led the author to determine a few advantages of using the device which should be considered for any future use. First, the device allows for kinetic mode measurements of specific ion abundances which can be monitored while increasing the reaction volume, and at the same time, monitor for transient intermediates by scanning the entire spectra. Second, changes in the reaction time can be made without changing the flow rate, which with ESI analysis would otherwise significantly affect the signal intensity. Adjustments to the tubing length can be made quite quickly (< 1 minute) and do not require disconnecting the device from the ESI inlet, which can also affect the signal intensity due to unintentional movements of the ESI inlet. Finally, the device is relatively cheap to construct (<$100).

It should also be noted there are many disadvantages of using this device with this application. First, due to the small diameter, the PEEK tubing and FEP tubing are prone to crimping when sliding the inner tube into the outer tubing. Excessive crimping weakens the strength of the tubing, which eventually leads to the inability to further guide the inner tubing farther into the outer tubing. Crimping could also

lead to blocked flow and high back pressure which could exceed the rating of some syringe pumps. Second, due to the relatively insoluble nature of quercetin in aqueous conditions, precipitants easily formed which clogged the device tubing and could potentially clog the ESI capillary. The device required regular cleaning with a wide range of solvents to keep the device functioning properly. Finally, measurements had to be made manually and were time consuming since the flowing solutions required long equilibration times in between tubing length adjustments.

6.3 Future Work

It can be assumed that future work in evaluating the interaction of AAPH, trolox, fluorescein and antioxidant substances (components of the ORAC method) using the kinetic device in conjunction with ESI-IT-TOF MS would greatly benefit this area of research by providing details of the intermediate and degradation products produced which may depend on the antioxidant of interest. The addition of an in-line fluorescence detector would help overcome the qualitative limitations and would provide direct correlation to many of the current antioxidant capacity assays.

Further, studies of the degradative pathways generated by other ROS and ROS sources, such as superoxide and transition metals, is warranted. One such study could be conducted to evaluate the metal-catalyzed degradation of quercetin by mixing quercetin with sources of Fe(II) and Cu(II) and infusing them with the continuous flow device. Considering the transparency of the FEP tubing used in the device, a host of photo-initiated studies could be conducted as well, including photodegradation and photo-catalyzed production of hydroxyl radicals from hydrogen peroxide. Although it may be quite complex, experiments with combinations of flavonoids and other antioxidants, such as ascorbic acid, could be planned to ascertain synergistic effects.

Finally, computational modeling offers the researcher further justification of proposed intermediate and degradation products for observed ion signals. One particular computational study of interest may be to evaluate the energetics of the pathways that lead to the semi-quinone, quinone and quinone methide of flavonoids.

References

[1]P. D. Mascio et al. Am. J. Clin. Nutr. 1991, 53:194S-200S.

[2]B. Uttara,et al. Curr. Neuropharmacol. 2009, 7:65–74.

[3] K. Apel, H. Hirt. Annu. Rev. Plant Biol. 2004,55:373-99.

[4]G. Miller et al. Plant, Cell Environ. 2010, 33:453–467.

[5]K. Scharffetter-Kochanek et al. Biol. Chem. 1997,378:1247-1257.

[6]J. M. McCord Clin. Biochem.1993, 26: 351–357.

[7]R. L. Prior, et al. J. Agric. Food Chem., 2005, 53:4290-4302.

[8]K. Ishige et al. Free Radical Biol. Med. 2001, 30:433-446.

[9]J. S. Barnes, Analytical Characterization Of Anthocyanins From Natural Products By Reverse-phase Liquid Chromatography-photodiode Array-electrospray Ionization-ion Trap-time Of Flight Mass Spectrometry, Thesis, University of Texas at Arlington, 2010.

[10]L. Konermann J. Phys. Chem. A 1999, 103:7210-7216.

[11]J. S. Barnes et al. Amer. Soc. Mass Spectrom. 2013, 24:1513-1522.

[12]A. D. Romano et al. J. Nephrol.2010, 23:S29-36.

[13]T. Finkel, N. J. Holbrook, Nature 2009, 408:239-247.

[14]B. N. Ames et al. Proc. Natl. Acad. Sci. USA 1993, 90:7915-22.

[15]B. Frei Amer. J. Med. 1994, 97:5S-13S.

[16]C. L. Quinlan et al. J. Biol. Chem. 2012, 287:27255-27264.

[17]A. Boveris et al. Biochem. J. 1972, 128:617-30.

[18]A. W. Segal Int. J. Biochem. Cell Biol. 2008, 40:604-618.

[19]M. B. Hampton et al. Blood 1998, 92:3007–3017.

[20]E. P. Reeves et al. Nature 2002, 416:291–297.

[21]L. D. Martin et al. In Oxygen/Nitrogen Radicals and Cellular Injury pp. 1197-1204, Environmental Health Perspectives Supplements, 1998.

[22]C. Pucciariello et al. Plant Physiol. Biochem.2012, 59:3–10.

[23]P. D. Ray et al. Cell. Signal.2012, 24:981–990.

[24]C. Leloup et al. Diabetes 2006, 55:2084-2090.

[25]J. E. McEwen et al. Curr. Opin. Cardiol. 2005, 20:399-406.

[26]I. Dalle-Donne et al. Trends Mol. Med., 2003, 9:169-176.

[27]D. Huang et al. J. Agric. Food Chem. 2005, 53:1841-1856.

[28]I. Fernandes et al. J. Agric. Food Chem. 2010, 58:3785-3792.

[29]M. Hamalainen et al. Mediators Inflamm. 2007, 2007:45673.

[30]D. Ghosh, T. Konishi, Asia Pac. J. Clin. Nutr. 2007,16: 200-208.

[31]G. K. Jayaprakasha Analysis of Antioxidant-Rich Phytochemicals, Wiley-Blackwell, 2012.

[32]J. Harborne Phytochemical Methods: A Guide to Modern Techniques of Plant Analysis 3rd ed, Chapman & Hall, London, 1998.

[33]K. M. M. Inderjit et al. Principles and Practices in Plant Ecology: Allelochemical Interactions CRC Press, 1999.

[34]J. B. Harborne The Flavonoids, Advances in Research Since 1986. 1994, Chapman & Hall, London.

[35]C. A. Williams, R. J. Grayer, Nat. Prod. Rep., 2004, 21:539–573.

[36]M. J. Cho, et al. J. Sci. Food Agric. 2005, 85:2149–2158.

[37]M. Matgorzata Pol. J. Food Nutr. Sci. 2008, 58:407-413.

[38]F. Shahidi, M. Naczk, Phenolics in Food and Nutraceuticals Taylor and Francis e-Library, 2006.

[39]T. N. Ly et al. J. Agric. Food Chem.2005, 53:8183-8189.

[40]A. J. Dick et al. J. Agric. Food Chem.1987,35:529–531.

[41]P. C. H Hollman et al. FEBS Letters 1997, 418:152–156.

[42]K. Murota, J. Terao Arch. Biochem. Biophys. 2003, 417:12–17.

[43]P. C. H. Hollman et al. Cancer Letters1997, 114:139–140.

[44]P. C. Hollman et al. Am J Clin Nutr. 1995, 62:1276-1282.

[45]C. Morand et al. BioFactors 2000, 12:169–174.

[46]C. Morand et al.Am. J. Physiol.1998, 275R212-219.

[47]J. P. E. Spencer et al. Biochem. J. 2003, 372:173–181.

[48]D. R. Goughand, T. G. Cotter Cell Death Disease 2011 2: e213.

[49]R. M. Han et al. Molecules 2012, 17:2140-2160.

[50]S. V. Jovanovic et al. J. Am. Chem. Soc. 1994,116: 4846-4851.

[51]S. V. Jovanovic et al. In Flavonoids in health and disease Marcel Dekker Inc, New York, 1998.

[52]C A. Rice-Evans, Free Rad. Biol. Med. 1996, 20: 933–956.

[53]M. Medvidovic-Kosanovic et al. Croat. Chem. Acta, 2010, 83:197–207.

[54]K. E. Heim et al. J. Nutr. Biochem. 2002, 13:572–584.

[55]W. Bors et al. In Free Radicals and the Liver, Springer, Berlin, 1992.

[56]W. Bors et al. In Free Radicals, Birkhäuser, 1993.

[57]D. Metodiewa et al. Free Rad. Biol. Med. 1999, 26:107-116.

[58]T. Tu et al. Chem. Res. Toxicol. 2011, 24:1527-1539.

[59]B. A. Bohm, An Introduction to Flavonoids. Harwood Academic Publishers, Amsterdam, 1998.

[60]. L. Singleton, J. A. Rossi. Am. J. Enol. Vitic. 1965, 16, 144-158.

[61]M. C. Hanlon D. W. Seybert Free Rad. Biol. Med. 1997, 23:712–719.

[62]N. A. Porter et al. J. Am. Chem. Soc. 1981, 103:6447–6455.

[63]B. Ou et al. J. Agric. Food Chem. 2001, 49: 4619-4626.

[64]E. Cadenas, H. Sies Free Rad. Res.1998, 28:601-609.

[65]Oxygen Radical Absorbance Capacity (ORAC) of Selected Foods, Release 2 (2010), http://www.ars.usda.gov/services/docs.htm?docid=15866, Last Modified: 05/16/2012, accessed 11/1/13.

[66]Y. L. Ma et al. Rapid Comm. in Mass Spectrom. 1997, 11:1357-1364.

[67]E. D. Rijke et al. J. Chromatogr. A. 2006, 1112:31-63.

[68]R. March, J. Brodbelt, J Mass Spectrom. 2008, 43:1581-1617.

[69]P. M. Mayer, C. Poon, The mechanism of collisional activation of ions in mass spectrometry, Mass Spectrom. Reviews, Wiley Interscience, 2009.

[70]R. E. March, J. Mass Spectrom. 1997, 32:351-369.

[71]P. T. Kasper et al. Rapid Commun. Mass Spectrom. 2012, 26:2275–2286.

[72]F. Rasche, et al. Anal. Chem. 2011, 83:1243–1251.

[73]F. Cuyckens, M. Claeys, J. Mass Spectrom. 2005, 40:364-372.

[74]G. C. Kite, N. C Veitch, Rapid Commun. Mass Spectrom. 2009, 23:3125-3132.

[75]M. Giusti et al. J. Agric. Food Chem. 1999, 47:4657-4664.

[76]N. Fabre et al. Amer. Soc. Mass Spec. 2001, 12:707-715.

[77]J. S. Barnes, K. A. Schug Int. J. Mass Spectrom. 2011, 38, 71-80.

[78]T. Kind, O. Fiehn BMC Bioniformatics 2007, 8:1–20.

[79]J. S. Barnes et al. J. Chromatogr. A 2009, 1216:4728–4735.

[80]L. Zhaolin et al. BioResources 2012, 7:1405-1418.

[81]H. An et al. J. Pharma Biomed. Anal., 2013, 85:295-304.

[82]E. Sommella et al. J. Sep. Science 2013, 36:3351-3355.

[83]L. Tedmon et al. J. Am. Soc. Mass Spectrom. 2013, 24:399-409.

[84]Z. Chen et al. J. Chin. Pharm. Sci. 2013, 319-328.

[85]P. Dugo et al. J. Sep. Science 2009, 32:3627-3634.

[86]J. Liang et al. Biomed. Chromatogr. 2013, doi:10.1002/bmc.3034.

[87]D. J. Wilson, L. Konermann Anal. Chem. 2003, 75, 6408-6414.

[88]D. J. Wilson, L. Konermann Anal. Chem., 2004, 76:2537-2543.

[89]O. O. Sogbein et al. J. Am. Soc. Mass Spectrom. 2000, 11:312–319.

[90]V. W. S. Lee et al. Anal. Chem.1999, 71:4154–4159.

[91]L. Konermann et al. Biochemistry 1997, 36:5554–5559.

[92]S. Fiorucci et al. J. Agric. Food Chem. 2007, 55:903-911.

[93]P. Trouillas et al. Food Chem. 2006, 97:679-688.

[94]Z. S. Markovic et al. Theor. Chem. Acc. 2010, 127:69-80.

[95]A. M. Mendoza-Wilson, D. Glossman-Mitnik J. Mol. Struc.: THEOCHEM 2005, 716:67-72.

[96]Z. Dhaouadi et al. J. Mol. Struc.: THEOCHEM 2009, 904:35-42.

[97]C. Aliaga, E. A. Lissi Can. J. Chem. 2004, 82:1668-1673.

[98]G. C. Justino, A. J. S. C. Vieira J. Mol. Model 2010, 16:863-876.

[99]R. E. March, E. G. Lewars Rapid Commun. Mass Spectrom. 2007, 21:1669–1679.

[100]J. S. Barnes, K. A. Schug Int. J. Mass Spectrom. 2011, 308:71–80.

[101]S. Maini et al. J. Agric. Food Chem. 2012, 60:6966-6976.

[102]J. H. Von Elbe, S. J. Schwartz Colorants in Food Chemistry, 3rd Ed., New York, 1996.

[103]I. Irina, G. Mohamed In Advances in Applied Biotechnology, ISBN: 978-953-307-820-5, 2012.

[104]J. T. Chien et al. Int. J. Mol. Sci. 2010, 11:2805–2820.

[105] D. P. Makris, J. T. Rossiter J. Agric. Food Chem. 2000, 48:3830–3838.

[106]N. Buchner, et al. Rapid Commun. Mass Spectrom. 2006, 20:3229–3235.

[107]I. G. Zenkevich et al. Molecules 2007, 12:654-672.

[108]A. Zhou, O. A. Sadik, J. Agric. Food Chem. 2008, 56:12081–12091.

[109]A. K. Timbola et al. Braz. Chem. Soc. 2006, 17:139–148.

[110]A. Zhou et al. Electrochem. Commun. 2007, 9:2246–2255.

[111]V. Krishnamachari et al. J. Agric. Food Chem. 2002, 50:4357-4363.

[112]E. Hvattum et al. J. Mass Spectrom. 2004, 39:1570–1581.

[113]K. Kano et al. J. Chem. Soc., Chem. Commun. 1994, 593–594.

[114]D. P. Makris, J. T. Rossiter, Food Chem. 2002, 77:177-185.

[115]S. V. Jovanovic et al. J. Chem.Soc., Perkin Trans. 1996, 2:2497-2504.

[116]S. B. Brown et al. Biochem J. 1982, 205:239-244.

[117]D. P. Makris, J. T. Rossiter, J. Food Comp. Anal. 2002, 15:103-113.

[118]P. Knekt et al. Am. J. Clin. Nutr. 2002, 76:560-568.

[119]P. J. Mink et al. Am. J. Clin. Nutr. 2007, 85:895-909.

[120]H. D. Sesso et al. Am. J. Clin. Nutr. 2003, 77:1400-1408.

[121]A. Cassidy et al. Stroke 2012, 43:946-951.

[122]L. Pourcel et al. Trends Plant Sci. 2007, 12:29-36.

[123]M. Zhang, et al. Lebensm. Wiss. Technol. 2010, 43:181–185.

[124]B. Xu, S. K. C. Chang. J. Agric. Food Chem. 2009, 57:4754–4764.

[125]R. Pulido et al. J. Agric. Food Chem. 2000, 48:3396-3402.

[126]I. F. F. Benzie, J. J. Strain, Anal. Biochem. 1996, 239:70–76.

[127]C. López-Alarcón, A. Denicola Anal. Chim. Acta 2013, 763:1–10.

[128]M. Pinelo et al. Food Chem. 2004, 88:201-207.

[129]D. J. Clarke et al. Anal. Chem. 2010, 82:1897-904.

[130]D. B. Northrop, F. B. Simpson Bioorg. Med. Chem. 1997, 5:641–644.

[131]H. Orsnes et al. Anal. Chem. 1998, 70:4751-4754.

[132]B. M. Kolakowski, et al. Rapid Commun. Mass Spectrom. 2000, 14:772-776.

[133]B. M. Kolakowski, L. Konermann Anal. Biochem. 2001, 292:107–114.

[134]K. Lemanska et al. Free Radical Research, 2004, 38:639-647.

[135]G. Wang, R. B. Cole Org. Mass Spectrom. 1994, 29:419-427.

[136]K. A. Schug, H. M. McNair J. Chromatgr. A, 2003, 985:531-539.

[137]S. V. Gudkov et al. Biophysics, 2012, 57:1–8.

[138]L. V. Jørgensen et al. Free Radic Res. 1998, 29:339-350.

[139]M. Yonekawa et al. Tetrahedron, 2013, 69:4076-4080.

[140]J. R. Mecinovic et al. Angew. Chem. Int. Ed. 2009, 48:2796 –2800.

[141]H. H. Wasserman, J. Parr Acc. Chem. Res. 2004, 37:687-701.

[142]C. Tournaire Tetrahedron, 1994, 50:9303-9314.

[143]Day, A. J.; Williamson, G. In Flavonoids in Health and Disease, 2nd ed., Rice-Evans, C. A.; Packer, L., Ed.; CRC Press 2010, pp 391-412.

[144]M. G. Hertog et al. Arch. Intern. Med,. 1995, 155:381-386.

[145]T. Guardia et al. Il Farmaco, 2001, 56:683–687.

[146]A. P. Rogerio et al. Inflamm. Res. 2007, 56:402-408.

[147]M. Comalada et al. Eur. J. Immunol., 2005, 35:584–592.

[148]A. W. Boots et al. Europ. J. Pharmaco., 2008, 585:325-337.

[149]A. E. Mitchell et al. J. Agric. Food Chem. 2007, 55:6154-6159.

[150]N. Buchner et al. Rapid Commun. Mass Spectrom. 2006, 20:3229-3235.

[151]D. P. Makris, J. T. Rossiter J. Food Comp. Anal., 2002, 15:103-113.

[152]E. Wiberg et al. Inorganic Chemistry, Academic Press, 2001.

[153]B. Halliwella et al. FEBS Letters, 2000, 486:10-13.

[154]P. I. Branemark et al. Bone Joint Surg Am. 1967, 49:48-62.

[155]G. M. Sapers, J.E. Sites, J. Food Science, 2003, 68:1793–1797.

[156]S. J. Duthie et al. Mutat. Res.-Gen. Tox. En., 1997, 393:223–231.

[157]C. A. Musonda, J. K. Chipman Carcinogenesis, 1998, 19:1583-1589.

[158]M. K. Johnson, G. Loo Mutat. Res.-DNA Repair, 2000, 459:211-218.

[159]S. A. Aherne, N. M. O'Brien Nutr. Cancer,1999, 34:160-166.

[160]S. R. Husain et al. Phytochemistry, 1987, 26:2489-2491.

[161]Y. H. Miura et al. Biol. Pharm. Bull., 1998, 21:93-96.

[162]P. Pignatelli et al. Am. J. Clin. Nutr., 2000, 72:1150-1155.

[163]A. Zhou et al. Electrochem. Commun., 2007, 9:2246–2255.

[164]D. P. Makris, J. T. Rossiter Food Chem., 2002, 77:177-185.

[165]C. Aliaga, E. A. Lissi Can. J. Chem, 2004, 82:1668-1673.

[166]S. Jo et al. Int. J. Appl. Res. Nat. Prod., 2009, 2:52-60.

[167]E. Hvattum et al. Mass Spectrom., 2004, 39:1570–1581.

[168]A. Zhou, O. A. Sadik J. Agric. Food Chem., 2008, 56:12081–12091.

[169]J. S. Barnes, K. A. Schug Int. J. Mass Spectrom., 2011, 38:71-80.

[170]L. Tedmon et al. J. Am. Soc. Mass Spectrom., 2013, 24:399-409.

[171]D. J. Wilson, L. Konermann Anal. Chem., 2003, 75:6408-6414.

[172]J. S. Barnes et al. J. Amer. Soc. Mass Spectrom., 2013, 24:1513-1522.

[173]S. Fiorucci et al. J. Agric. Food Chem., 2007, 55:903-911.

[174]P. Trouillas et al. Food Chem., 2006, 97:679-688.

[175]Z. S. Markovic et al. Theor. Chem. Acc., 2010, 127:69-80.

[176]A. M. Mendoza-Wilson, D. Glossman-Mitnik J. Mol. Struc.: THEOCHEM, 2005, 716:67-72.

[177]Z. Dhaouadi, et al. J. Mol. Struc.: THEOCHEM, 2009, 904:35-42.

[178]G. C. Justino, A. J. S. C. Vieira J. Mol. Model, 2010, 16:863-876.

[179]Gaussian 03, Revision C.02, M. J. Frisch, G. W. Trucks, H. B. Schlegel, G. E. Scuseria, M. A. Robb, J. R. Cheeseman, J. A. Montgomery, Jr., T. Vreven, K. N. Kudin, J. C. Burant, J. M. Millam, S. S. Iyengar, J. Tomasi, V. Barone, B. Mennucci, M. Cossi, G. Scalmani, N. Rega, G. A. Petersson, H. Nakatsuji, M. Hada, M. Ehara, K. Toyota, R. Fukuda, J. Hasegawa, M. Ishida, T. Nakajima, Y. Honda, O. Kitao, H. Nakai, M. Klene, X. Li, J. E. Knox, H. P. Hratchian, J. B. Cross, V. Bakken, C. Adamo, J. Jaramillo, R. Gomperts, R. E. Stratmann, O. Yazyev, A. J. Austin, R. Cammi, C. Pomelli, J. W. Ochterski, P. Y. Ayala, K. Morokuma, G. A. Voth, P. Salvador, J. J. Dannenberg, V. G. Zakrzewski, S. Dapprich, A. D. Daniels, M. C. Strain, O. Farkas, D. K. Malick, A. D. Rabuck, K. Raghavachari, J. B. Foresman, J. V. Ortiz, Q. Cui, A. G. Baboul, S. Clifford, J. Cioslowski, B. B. Stefanov, G. Liu, A. Liashenko, P. Piskorz, I. Komaromi, R. L. Martin, D. J. Fox, T. Keith, M. A. Al-Laham, C. Y. Peng, A. Nanayakkara, M. Challacombe, P. M. W. Gill, B. Johnson, W. Chen, M. W. Wong, C. Gonzalez, and J. A. Pople, Gaussian, Inc., Wallingford CT, 2004

[180]T. J. Mabry et al. The Systematic Identification of Flavonoids, Springer: London, 2012.

[181]J. B. He et al. Anal. Sciences, 2009, 25:373-377.

[182]K. A. Schug, H. M. McNair J. Chromatgr. A, 2003, 985:531-539.

[183]K. A. Schug, H. M. McNair J. Sep. Science, 2002, 25:759–766.

[184]G. Wang, R. B. Cole Org. Mass Spectrom., 1994, 29:419-427.

[185]M. Medvidovic-Kosanovic et al. Croat. Chem. Acta, 2010, 83:197–207.

[186]S. V. Jovanovic et al. J. Am. Chem. Soc., 1994, 116:4846-4851.

[187]K. Lemanska et al. Free Radical Research, 2004, 38:639-647.

[188]V. Krishnamachari et al. J. Agric. Food Chem., 2002, 50:4357-4363.

[189]I. G. Zenkevich et al. Molecules, 2007, 12:654-672.

[190]S. Fiorucci et al. ChemPhysChem, 2004, 5:1726-1733.

[191A. Pekal et al. Biometals, 2011, 24:41-49.

[192]S. Dall'Acqua et al. Molecules, 2012,17:8898-8907.

[193]J. B. Zvezdanovic et al. J. Serb. Chem. Soc., 2012, 77:297–312.

[194]H. M. Merken, G. R. Beecher J. Agric. Food Chem., 2000, 48:577-599.

[195]M. Lodovici, E. Bigagli, J. Toxicol. 2011, 2011:487074.

[196]I. M. Møller Ann. Rev. Plant Phys. Plant Mol. Biol. 2001, 52:561-591.

[197]V. J. Thannickal, B. L. Fanburg Amer. J. Phys. Lung Cell. Mol. Phys. 2000, 279:L1005-L1028.

[198]D. Wulf Philos.Trans. R. Soc Lond. B. Biol. Sci. 2005, 360:235-2372.

[199]M. S. Cooke et al. FASEB J. 2003, 17:1195-1214.

[200]C. M. Bergamini et al. Curr. Pharm. Des.2004, 10:1611-1626.

[201]B. Halliwell, S. Chirico Am. J. Clin. Nutr., 1993, 57:715S-724S.

[202]P. G. Pietta J. Nat. Prod. 2000, 63:1035-1042.

[203]B. Ou et al. J. Agric. Food Chem. 2001, 49:4619-4926.

[204]A. J. Day, G. Williamson, Absorption of Quercetin Glycosides, Flavonoids in Health and Disease, Second Edition, CRC Press, 2010.

[205]I. Kreft et al. Food Chem. 98, 2006, 3:508–512.

[206]E. Frankel, A. S. Meyer J. Sci. Food Agric. 2000, 80:1925-1941.

[207]G. Cao et al. Free Rad. Biol. Med. 1993, 14:303–311.

[208]Y. Yoshida et al. Free Radical Research, 2004, 38:375–384.

[209]H. Estebauer et al. Free Rad. Biol. Med. 1992, 13:341-390.

[209]J. Werber et al. J. Pharm. Sci. 2011,100:3307–3315.

[210]I. F. F. Benzie Comp. Biochem. Physiol. Part A 2003, 136:113-126.

[211] D. Harman Biogerontology. 2009;10:773-81

Biographical Information

Jeremy was born in 1979 and grew up on a small ranch in Mansfield, Texas with his father and older brother. He spent most of his time with his brother, playing video games and exploring nature. He earned an Associates' Degree in Liberal Arts from Tarrant County College in 1999, a Bachelor's in Science (Biology) from the University of Texas-Arlington in 2002, and a Master's in Science (Chemistry) from the University of Texas-Arlington in 2010. He is happily married, enjoys American Football, and will not know what to do with his life after retiring from academics.